Relative importance of the Anti-Apoptotic versus Apoptosis-Unrelated Functions of MCL-1 *in vivo*

Kerstin Brinkmann[*1,2], Kate McArthur[3‡], Shezlie Malelang[1,2‡], Leonie Gibson[1], Annli Tee[1,2], Sheik Nadeem Elahee Doomun[4], Caitlin L Rowe[3], Philip Arandjelovic[1,2], Julia M Marchingo[1,2], Damian D'Silva[1,2], Annabell Bachem[5], Simon Monard[1], Lauren G Wheelan[1], Grant Dewson[1,2], Tracy L Putoczki[1,2], Philippe Bouillet[1,2], Nai Yang Fu[1,2,6], Kristin K Brown[7,8,9], Andrew J Kueh[1,2,10,11], Verena C Wimmer[1,2], Marco J Herold[1,2,10,11†], Tim Thomas[1,2†], Anne K Voss[1,2†], Andreas Strasser[*1,2†]

[1] The Walter and Eliza Hall Institute of Medical Research; Melbourne, Australia.

[2] Department of Medical Biology, University of Melbourne; Melbourne, Australia.

[3] Department of Biochemistry and Molecular Biology, Biomedicine Discovery Institute, Monash University; Melbourne, Australia.

[4] Metabolomics Australia, Bio21 Institute, University of Melbourne; Melbourne, Australia

[5] Department of Microbiology and Immunology, Peter Doherty Institute, University of Melbourne; Melbourne, Australia

[6] Cancer and Stem Cell Biology Program, Duke-NUS Medical School; Singapore.

[7] Peter MacCallum Cancer Centre, Melbourne, Australia

[8] The Sir Peter MacCallum Department of Oncology, University of Melbourne, Melbourne, Australia

[9] Department of Biochemistry and Pharmacology, University of Melbourne, Melbourne, Australia

[10] Olivia Newton-John Cancer Research Institute; Melbourne, Australia.

[11] School of Cancer Medicine, La Trobe University; Melbourne, Australia

*Corresponding author. Email: strasser@wehi.edu.au; brinkmann.k@wehi.edu.au

‡ These authors contributed equally to this work

† These senior authors contributed equally to this work

Abstract: The anti-apoptotic protein MCL-1 (myeloid cell leukemia-1) is essential for embryogenesis and the survival of many cell types that tolerate loss of its relatives, BCL-XL and BCL-2. Apoptosis-unrelated roles of MCL-1 in metabolism may contribute to this requirement, though their relevance for embryogenesis and postnatal life remains unclear. We hypothesized that BCL-XL and BCL-2 may substitute MCL-1's anti-apoptotic but not its apoptosis-unrelated functions. Replacing MCL-1 with BCL-XL or BCL-2 supported embryo development by rescuing the *Mcl-1*$^{-/-}$ preimplantation lethality. *Mcl-1*$^{Bcl\text{-}xL/Bcl\text{-}xL}$ but not *Mcl-1*$^{Bcl\text{-}2/Bcl\text{-}2}$ mice were born on a mixed background, though they showed metabolic defects. Thus MCL-1's apoptosis-unrelated functions appear critical in later development, with BCL-XL, but not BCL-2, partially compensating. These findings clarify MCL-1's distinct physiological roles, critically informing MCL-1 inhibitor development as cancer therapeutics.

Apoptotic cell death is essential for morphogenesis and tissue homeostasis (*1, 2*), with defects in apoptosis promoting cancer, autoimmune disorders and degenerative diseases (*3, 4*). Apoptosis is regulated by three BCL-2 protein family subgroups (*5, 6*). Anti-apoptotic proteins (BCL-2, BCL-XL, MCL-1, A1, BCL-W) prevent apoptosis by neutralizing BH3-only proteins (e.g., tBID, BIM, PUMA, NOXA) and effectors BAX and BAK (*5, 7, 8*) (fig. S1A). Activated BAX and BAK cause mitochondrial outer membrane permeabilization (MOMP), initiating the caspase cascade that dismantles the cell (*9, 10*).

MCL-1 is critical for cell survival. Its removal or inhibition causes death of many cell types that are not affected by loss or inhibition of other anti-apoptotic BCL-2 proteins (*11, 12*). MCL-1-deficient embryos die around embryonic day E3.5 (*13*). BCL-XL-deficient embryos die at ~E13.5 due to erythroid and neuronal cell death (*14*). BCL-2-deficient mice die ~4 weeks after birth from polycystic kidney disease (*15, 16*). Removal of A1 or BCL-W causes only minor defects (*17*) (fig. S1B). Anti-apoptotic BCL-2 proteins differ in binding to their pro-apoptotic relatives, turnover, and localization (fig S1A,C,D) (*18-20*). Some anti-apoptotic BCL-2 proteins reportedly also exert functions unrelated to apoptosis (*21*). Proteolytically processed MCL-1 (*22-25*) and BCL-XL (*26, 27*), but not BCL-2 (*28*), are found in the inter-mitochondrial membrane space regulating mitochondrial dynamics and ATP production through oxidative phosphorylation (OXPHOS). MCL-1 also controls mitochondrial fatty acid oxidation (FAO) through interaction with ACSL1 (acyl-CoA synthetase long-chain family member 1) on the outer mitochondrial membrane (*29, 30*).The physiological importance of apoptosis-unrelated roles of MCL-1 (and other BCL-2 proteins) is unclear. Notably, dying *Mcl-1*$^{-/-}$ blastocysts reportedly lacked apoptosis hallmarks (*13*), prompting the hypothesis that implantation failure results from loss of an apoptosis-unrelated role of MCL-1 (*22*). Moreover, cardiomyocytes reportedly require both the anti-apoptotic and apoptosis-unrelated function(s) of MCL-1 to maintain heart function (*25, 31*).

MCL-1 inhibitors can block both MCL-1 functions (*29, 30*) and, in some cases (AMG-176, AZD5991) cause cardiotoxicity in patients (*32*). To advance MCL-1 inhibitors for cancer therapy, we need to know if their efficacy and toxicity stem solely from inhibiting the anti-apoptotic or also apoptosis-unrelated functions of MCL-1 (*32, 33*). To address this and to investigate functional redundancies and differences with other anti-apoptotic BCL-2 proteins, we generated mice in which *Mcl-1* coding sequences were replaced by sequences encoding BCL-XL, BCL-2 or A1.

Validation of *Mcl-1* gene-replacement strategy

MCL-1 would only be fully substituted by another BCL-2 family member if it has no unique essential apoptosis-unrelated function. To test this, we used cDNA sequences encoding human BCL-2 (hBCL-2; termed *Mcl-1*$^{Bcl-2}$ mice), FLAG-tagged mouse BCL-XL (*Mcl-1*$^{Bcl-xL}$) or FLAG-tagged mouse A1 (*Mcl-1*^{A1}) to replace the *Mcl-1* coding exons and introns in C57BL/6 mice (Fig. 1A). This strategy maintained the 5' and 3' untranslated regions of the *Mcl-1* gene. As a control for loss of *Mcl-1* introns, we used a cDNA encoding human MCL-1 (hMCL-1). Heterozygous *Mcl-1*$^{hMcl-1/+}$, *Mcl-1*$^{Bcl-xL/+}$, *Mcl-1*$^{Bcl-2/+}$ and *Mcl-1*$^{A1/+}$ mice were viable and reached adulthood (fig. S2A,B). The expression of hMCL-1, FLAG-BCL-XL, hBCL-2 and FLAG-A1 proteins was confirmed by Western blotting in E10.5 embryo lysates (Fig. 1B), mouse embryonic fibroblasts (MEFs) (fig. S2C,D), and by flow cytometry in bone marrow cells from heterozygous gene-replacement mice (fig. S2E). Endogenous mouse MCL-1 (mMCL-1) was discriminated from the knock-in hMCL-1 by differences in molecular weight (*34*). Endogenous mouse BCL-2 (mBCL-

2) was discriminated from the knock-in hBCL-2 using species-specific monoclonal antibodies. The knock-in BCL-XL and A1 were FLAG-tagged to allow discrimination from the endogenous proteins. We observed the expected reduction in endogenous MCL-1 in *Mcl-1*$^{Bcl\text{-}xL/+}$, *Mcl-1*$^{Bcl\text{-}2/+}$ and *Mcl-1*$^{A1/+}$ embryo lysates and MEFs (Fig. 1B,G, fig. S2C,D). There were no major changes in the abundance of other BCL-2 family proteins, with the exception of a reduction in BCL-XL in lysates from *Mcl-1*$^{Bcl\text{-}2/+}$ and *Mcl-1*$^{Bcl\text{-}2/Bcl\text{-}2}$ E10.5 embryos as well as *Mcl-1*$^{Bcl\text{-}2/+}$ MEFs (Fig. 1B,G, fig. S2C,D,F,G).

For functional validation we treated mitogen-activated B cells from heterozygous *Mcl-1* gene-replacement mice with BH3 mimetic drugs (Fig. 1C). Cells from *Mcl-1*$^{hMcl\text{-}1/+}$ mice were more susceptible to the MCL-1 inhibitor S63845 than were wild-type cells, consistent with the higher affinity of S63845 for hMCL-1 than mMCL-1 (*35*). B cells from *Mcl-1*$^{Bcl\text{-}xL/+}$ or *Mcl-1*$^{Bcl\text{-}2/+}$ mice expressed higher total amounts of BCL-XL (mBCL-XL plus FLAG-BCL-XL) or BCL-2 (mBCL-2 plus hBCL-2) and less MCL-1 compared to those of wild-type cells, and thus were more susceptible to the BCL-XL inhibitor A1331852 or the BCL-2 inhibitor ABT-199/Venetoclax, respectively. B cells from *Mcl-1*$^{A1/+}$ mice were more susceptible to BH3 mimetic drugs compared to wild-type B cells, presumably due to the low abundance of A1 (Fig. 1B,C). These findings demonstrate the expression and functionality of the knock-in proteins.

Intercrosses of *Mcl-1*$^{hMcl\text{-}1/+}$ mice yielded *Mcl-1*$^{hMcl\text{-}1/hMcl\text{-}1}$ offspring at the expected Mendelian frequency (Fig. 1D) and they displayed normal appearance, weight and survival (Fig. 1E, fig. S3A). Histological analysis of the liver, kidney and heart revealed no abnormalities (fig. S3B-D). MEFs from *Mcl-1*$^{hMcl\text{-}1/+}$ and *Mcl-1*$^{hMcl\text{-}1/hMcl\text{-}1}$ mice showed normal responses to apoptotic stimuli (fig. S3E). These findings demonstrate that the function of the mouse *Mcl-1* gene locus can be replaced by a cDNA encoding human MCL-1; i.e., absence of introns of the *Mcl-1* gene does not have deleterious impact.

Apoptosis-unrelated functions of MCL-1 are dispensable for early embryogenesis

We examined whether the E3.5 lethality caused by MCL-1 loss could be rescued by replacing MCL-1 with hBCL-2, FLAG-BCL-XL or FLAG-A1. Intercrosses of *Mcl-1*$^{A1/+}$ mice did not produce homozygous *Mcl-1*$^{A1/A1}$ embryos at E10.5 or later stages (Fig. 1F, fig. S4A), possibly due to low amounts of FLAG-A1 (Fig. 1B). Examination of pre-implantation embryos (E2.5-E3.5) showed that, like *Mcl-1*$^{-/-}$ embryos, *Mcl-1*$^{A1/A1}$ embryos died before E3.5 (fig. S4B-D). In contrast, *Mcl-1*$^{Bcl\text{-}xL/Bcl\text{-}xL}$ and *Mcl-1*$^{Bcl\text{-}2/Bcl\text{-}2}$ embryos expressing hBCL-2 or FLAG-BCL-XL instead of MCL-1 were present at E10.5 at the expected Mendelian frequency (Fig. 1F), with no compensatory changes in expression of other BCL-2 family proteins detected (Fig. 1G, fig. S4E). Early embryonic development stages include E0-E7.5, with critical developmental patterning events that result in the formation of the three germ layers, requiring precise gene regulation, occurring during gastrulation (E6–E8)(*36*). Neuronal development during early embryogenesis includes neurulation (E8.0-E8.5) and neuronal tube closure (E9.0-E9.5)(*36*). Thus, *Mcl-1*$^{Bcl\text{-}xL/Bcl\text{-}xL}$ and *Mcl-1*$^{Bcl\text{-}2/Bcl\text{-}2}$ embryos underwent pre-implantation, implantation, gastrulation, and embryonic patterning without MCL-1. The presence of the forebrain, midbrain, hindbrain, and spinal cord indicated successful neurulation and neural tube patterning (Fig. 1H). Embryos had a detectable heartbeat and were within the expected size range (crown-rump length ~2.5–3.5 mm at E10.5)(*36*), although *Mcl-1*$^{Bcl\text{-}2/Bcl\text{-}2}$ embryos appeared slightly smaller than wild-type (ANOVA: $p<10^{-4}$) but remained within normal developmental limits (fig. S2H). However, some embryos showed head region anomalies, including collapsed ventricles and ridged

neuroepithelium (Fig. 1H). These findings demonstrate that BCL-2 and BCL-XL can replace MCL-1 during the pre-implantation state when all *Mcl-1*$^{-/-}$ embryos die. Unlike MCL-1 and BCL-XL, BCL-2 does not localize to the mitochondrial inter-membrane space (*28*) and does not interact with ASCL1 (*30*). Therefore, the development of *Mcl-1*$^{Bcl\text{-}2/Bcl\text{-}2}$ embryos to E10.5 demonstrates that the reported apoptosis-unrelated functions of MCL-1(*22, 29, 30*) are not critical for early embryogenesis.

Comparison of *Mcl-1*$^{Bcl\text{-}2/Bcl\text{-}2}$ *vs Mcl-1*$^{Bcl\text{-}xL/Bcl\text{-}xL}$ mouse development

Among offspring of inter-crosses of heterozygotes, *Mcl-1*$^{Bcl\text{-}xL/Bcl\text{-}xL}$ fetuses were under-represented from E13.5 (Fig. 2A), whereas *Mcl-1*$^{Bcl\text{-}2/Bcl\text{-}2}$ embryos were already under-represented from E12.5 (Fig. 2B). At E14.5, 10% of offspring were *Mcl-1*$^{Bcl\text{-}xL/Bcl\text{-}xL}$, but no *Mcl-1*$^{Bcl\text{-}2/Bcl\text{-}2}$ fetuses were detected (Fig. 2A, B). No viable *Mcl-1*$^{Bcl\text{-}xL/Bcl\text{-}xL}$ or *Mcl-1*$^{Bcl\text{-}2/Bcl\text{-}2}$ embryos were found at E15.5, and none survived to weaning on a C57BL/6 background (Fig. 2A, B). From E11.5 to E12.5, significantly higher percentages (Chi-square: $p<10^{-4}$) of abnormal *Mcl-1*$^{Bcl\text{-}xL/Bcl\text{-}xL}$ and *Mcl-1*$^{Bcl\text{-}2/Bcl\text{-}2}$ embryos were observed compared to those of wild-type littermates (Fig. 2C-E, fig. S4F, table S1). Some homozygous embryos were small and abnormal (7% *Mcl-1*$^{Bcl\text{-}xL/Bcl\text{-}xL}$; 11% *Mcl-1*$^{Bcl\text{-}2/Bcl\text{-}2}$), whereas others died (3% and 48%, respectively; Fig. 2C-E, fig. S4F, table S1). Anomalies included exencephaly (9% *Mcl-1*$^{Bcl\text{-}2/Bcl\text{-}2}$), other cranial abnormalities (10% *Mcl-1*$^{Bcl\text{-}xL/Bcl\text{-}xL}$; 2% *Mcl-1*$^{Bcl\text{-}2/Bcl\text{-}2}$; collapsed lateral and 4th ventricles, ridged neuroepithelium) and cranial blood accumulation, consistent with hemorrhages (17% *Mcl-1*$^{Bcl\text{-}xL/Bcl\text{-}xL}$; 7% *Mcl-1*$^{Bcl\text{-}2/Bcl\text{-}2}$; Fig. 2C-E, fig. S4F, table S1). Whole mount 3D imaging (*37*) of intact E12.5 embryos, with staining of endothelial cells and inherent blood auto-fluorescence, revealed no major differences in vital organs including the heart, fetal liver, or vascularization between genotypes (Fig. 2F, Movies S1-3). From E11.5-E12.5 a considerably smaller proportion of living *Mcl-1*$^{Bcl\text{-}2/Bcl\text{-}2}$ embryos was observed compared to that of *Mcl-1*$^{Bcl\text{-}xL/Bcl\text{-}xL}$ embryos (Chi-square: $p<10^{-4}$) (Fig. 2C-E, fig. S4F, table S1), indicating that BCL-XL compensates for MCL-1 loss more effectively than does BCL-2.

Apoptosis signaling in embryos

The defects in *Mcl-1*$^{Bcl\text{-}xL/Bcl\text{-}xL}$ and *Mcl-1*$^{Bcl\text{-}2/Bcl\text{-}2}$ embryos at later stages may result from reduced apoptosis, as both BCL-2 or BCL-XL proteins have a longer half-life than the replaced MCL-1. Accordingly, *Mcl-1*$^{Bcl\text{-}xL/+}$ or *Mcl-1*$^{Bcl\text{-}2/+}$ MEFs and mitogen-activated B cells were significantly more resistant to apoptotic stimuli than were wild-type cells (Fig. 3A, fig. S5A). *Mcl-1*$^{Bcl\text{-}xL/+}$ and *Mcl-1*$^{Bcl\text{-}2/+}$ females displayed an increased incidence of vaginal septa, indicating failure of normal apoptotic septum regression during development (Fig. 3B). Potentially consistent with this, E9.5 *Mcl-1*$^{Bcl\text{-}2/+}$ embryos exhibited reduced TUNEL^{+} cells compared to wild-type controls. Homozygous *Mcl-1*$^{Bcl\text{-}2/Bcl\text{-}2}$embryos exhibited increased TUNEL positive cells (fig S5B), possibly due to cell death associated with their developmental abnormalities (Fig. 2C-E).

Histological analysis revealed that some E11.5-E12.5 *Mcl-1*$^{Bcl\text{-}xL/Bcl\text{-}xL}$ and *Mcl-1*$^{Bcl\text{-}2/Bcl\text{-}2}$ embryos exhibited folding of the neuroepithelium in several areas of the developing brain (fig. S5C,D), likely due to the collapse of the lateral and fourth brain ventricles. No defects in neural tube closure were observed in *Mcl-1*$^{Bcl\text{-}xL/Bcl\text{-}xL}$ embryos, but 8% of *Mcl-1*$^{Bcl\text{-}2/Bcl\text{-}2}$ embryos showed exencephaly (Fig. 2C-E, fig. S4F), a phenotype common in mice with apoptosis defects (*2*). At E11.5, neuronal differentiation has begun in the hindbrain, whereas the cortex has few

differentiated cells. Proliferating cells are located in the ventricular zone (VZ), and differentiating neurons migrate to the marginal zone (MZ). The VZ to MZ proportion and the percentage of cells in these zones did not differ between genotypes (fig. S5E). The dorsal telencephalon, the precursor to the cerebral cortex, mainly consists of proliferating neural precursor cells at E11.5, with minimal cell death. No significant differences in percentages of mitotic or pyknotic nuclei were found between genotypes (fig. S5F). However, cell density was significantly reduced in the E11.5 *Mcl-1*$^{Bcl\text{-}2/Bcl\text{-}2}$ dorsal telencephalon (fig. S5F), indicating cell death or reduced proliferation at an earlier developmental stage.

The inhibition of intrinsic apoptosis during development by substituting BCL-XL or BCL-2 for MCL-1 extended survival until E14.5 at most (Fig. 2A,B). In contrast, *Bax*$^{-/-}$*Bak*$^{-/-}$*Bok*$^{-/-}$ triple knock-out (TKO) fetuses, which cannot undergo intrinsic apoptosis due to lacking all apoptosis effectors, develop until E18.5, with 1.8% even reaching weaning (Fig. 3C) (*38*). Hence, the lethal developmental abnormalities observed in *Mcl-1*$^{Bcl\text{-}xL/Bcl\text{-}xL}$ and *Mcl-1*$^{Bcl\text{-}2/Bcl\text{-}2}$ fetuses are not due to impaired developmental apoptosis, supporting an apoptosis-unrelated function of MCL-1 at later developmental stages that cannot be substituted by BCL-XL or BCL-2.

Impact of potential apoptosis-unrelated roles of BCL-2 and BCL-XL

Apoptosis-unrelated functions have been reported for BCL-2 and BCL-XL, and their excess may contribute to defects in *Mcl-1*$^{Bcl\text{-}2/Bcl\text{-}2}$ and *Mcl-1*$^{Bcl\text{-}xL/Bcl\text{-}xL}$ embryos. The early lethality of *Mcl-1*$^{-/-}$ and *Mcl-1*$^{Bcl\text{-}2/Bcl\text{-}2}$ embryos limit the analysis of these processes *in vivo*. To explore potential impact of apoptosis-unrelated functions of excess BCL-2 and BCL-XL, we created mice with one floxed *Mcl-1* allele and the other expressing FLAG-BCL-XL or hBCL-2, using *Mcl-1*$^{fl/fl}$ mice as controls. All contained the *Rosa26-CreERT2* transgene for tamoxifen-inducible *Mcl-1*^{fl} deletion (*39*). PCR and Western blot analysis in MEFs confirmed *Mcl-1*^{fl} deletion upon tamoxifen treatment and expression of the gene-swap encoded proteins, producing *Mcl-1*$^{del/del}$ (control), *Mcl-1*$^{Bcl\text{-}xL/del}$ and *Mcl-1*$^{Bcl\text{-}2/del}$ MEFs (fig. S6A,B).

BCL-XL and BCL-2 allegedly control calcium flux through various mechanisms (*21*). However, no differences in calcium flux peak amplitude were observed between genotypes in MEFs (fig. S6C). BCL-2 may inhibit cell proliferation by delaying the G1-to-S phase transition of the cell cycle (*40, 41*). Consistently, we observed slightly reduced proliferation rates of *Mcl-1*$^{Bcl\text{-}2/fl}$ MEFs compared to those of controls (ANOVA: $p=0.046$) (Fig. 3D,E). CreERT2-induced *Mcl-1*^{fl} deletion significantly reduced proliferation across all lines, particularly in *Mcl-1*$^{del/del}$ MEFs (ANOVA: $p<10^{-4}$) (Fig. 3D,E). *Mcl-1*$^{Bcl\text{-}xL/del}$ MEFs had higher proliferation rates than did *Mcl-1*$^{Bcl\text{-}2/del}$ MEFs (ANOVA: $p<10^{-4}$), indicating greater efficacy of BCL-XL in compensating for MCL-1 loss. The proliferation rate of *Mcl-1*$^{Bcl\text{-}2/del}$ MEFs was not significantly different than that of *Mcl-1*$^{del/del}$ MEFs, indicating that in the absence of MCL-1, inhibitory effects of BCL-2 on proliferation are negligible.

These results indicate that excess apoptosis-unrelated functions of BCL-2 and BCL-XL do not contribute to the observed phenotypes in *Mcl-1*$^{Bcl\text{-}2/Bcl\text{-}2}$ and *Mcl-1*$^{Bcl\text{-}xL/Bcl\text{-}xL}$ embryos but support the notion that BCL-XL is a more effective substitute for MCL-1 than is BCL-2.

Mixed genetic background *Mcl-1*$^{Bcl\text{-}xL/Bcl\text{-}xL}$ pups

One *Mcl-1*$^{Bcl\text{-}xL/Bcl\text{-}xL}$ pup (C57BL/6 background) developed to E18.5 appeared normal (Fig. 3F) with no major anomalies in brain architecture (Fig. 3G). However, specific features that might have been slightly abnormal, such as the area of the subventricular neurogenic zone and the size of the lateral ventricles, could not be statistically assessed. Because animals with mixed genetic backgrounds often better tolerate genetic mutations (*42-44*), we crossed *Mcl-1*$^{Bcl\text{-}2}$ and *Mcl-1*$^{Bcl\text{-}xL}$ mice to FVBxBALB/c F1 hybrids.

MCL-1 loss also caused pre-implantation lethality on this background. E2.5 *Mcl-1*$^{-/-}$ embryos were compromised and rarely reached the morula stage (Fig. S4B,C). They failed to produce inner cell mass outgrowths in culture and none developed to the E3.5 blastocyst stage (Fig. S4B,C). TUNEL^{+} cells were detected in a dying *Mcl-1*$^{-/-}$ E2.5 morula (fig. S7A-C), indicating that the lethality was caused by aberrant apoptosis, contrary to a previous report (*13*) but consistent with our finding that replacement of MCL-1 with BCL-2 or BCL-XL allowed development until at least E10.5.

Many *Mcl-1*$^{Bcl\text{-}xL/Bcl\text{-}xL}$ mice were born alive on the mixed genetic background and 11% reached weaning (Fig. 4A). In contrast, no *Mcl-1*$^{Bcl\text{-}2/Bcl\text{-}2}$ mice on a mixed background were present at E19.5 or weaning (Fig. 4B). These findings further demonstrate that an apoptosis-unrelated function of MCL-1, which can be partially replaced by BCL-XL, but not by BCL-2, is critical for fetal development and survival after birth.

BCL-XL cannot fully replace MCL-1 in pups

Mcl-1$^{Bcl\text{-}xL/Bcl\text{-}xL}$ pups on a mixed genetic background were abnormally small, had a hunched posture, and displayed a domed head (Fig. 4C). All died within 31 days postnatally (Fig. 4D). Histological examination revealed that the total depth of the frontal cortex and individual cortical layers showed no genotype differences (fig. S8A-F). However, *Mcl-1*$^{Bcl\text{-}xL/Bcl\text{-}xL}$ pups had a significantly larger subventricular zone neurogenic region compared to wild-type controls (fig. S8B) and 1 out of 5 displayed enlarged lateral ventricles (fig. S8C).

In *Mcl-1*$^{Bcl\text{-}xL/Bcl\text{-}xL}$ pups, severe disruption of hepatic architecture, reticulin network and marked steatosis were observed (Fig. 4E-G, fig. S9A,B). However, *Mcl-1*$^{Bcl\text{-}xL/Bcl\text{-}xL}$ pups did not show increased concentration of serum ALT (alanine transaminase) (Fig. 4H) or immune cell infiltration in the liver (fig. S9B), indicating that the hepatocytes were not rupturing. However, *Mcl-1*$^{Bcl\text{-}xL/Bcl\text{-}xL}$ pups had significantly increased concentrations of serum AST (aspartate transaminase) and creatine kinase (Fig. 4I, fig. S9C), possibly due to damage in other tissues (fig. S9D-F). The small intestine showed disorganized crypts with abnormally low cell numbers (fig. S9D) whereas kidney damage included degeneration of proximal renal tubular cells and glomeruli (fig. S9E). Cardiomyocytes appeared to undergo degeneration (fig. S9F). Staining for activated caspase-3 (Fig. 4E bottom row, fig. S9D-G) and TUNEL in the liver (fig. S9H) revealed no increase in apoptosis. No hepatic (fig. S9B) or cardiac fibrosis (fig. S10A) were detected, a phenotype driven by BAX or BAK-mediated apoptosis with cardiomyocyte-specific MCL-1 deletion (*25*). This indicates that the observed defects result from the loss of an apoptosis-unrelated function of MCL-1.

Mcl-1$^{Bcl\text{-}xL/Bcl\text{-}xL}$ pups exhibited a phenotype similar to that of *Vdac2*$^{-/-}$ pups, which also die shortly after birth with swelling hepatocytes and liver damage (*45*) (fig. S10B). Due to the role of VDAC2 in ATP export from mitochondria, this phenotype was linked to metabolic defects (*45, 46*). Thus, *Mcl-1*$^{Bcl\text{-}xL/Bcl\text{-}xL}$ pups might exhibit similar metabolic defects. Congruently, serum

glucose concentrations were abnormally reduced (Fig. 4J), suggesting dysregulation of glucose metabolism pathways.

RNAseq analysis of livers from *Mcl-1*$^{Bcl\text{-}xL/Bcl\text{-}xL}$ pups revealed significantly altered expression of metabolic genes (Fig. 4K,L), with upregulation of glycolysis-related genes and downregulation of lipid metabolism genes (Fig. 4M). Several genes involved in fatty acid omega-oxidation, a compensatory process in the endoplasmic reticulum triggered by defects in mitochondrial beta-oxidation (*47*), were also upregulated. Differential gene expression analysis in mouse embryonic fibroblasts (MEFs) (fig. S11A), revealed that *Mcl-1*$^{del/del}$ and *Mcl-1*$^{Bcl\text{-}2/del}$ MEFs exhibited substantially greater overlap in upregulated (but not downregulated) metabolic genes than did *Mcl-1*$^{del/del}$ and *Mcl-1*$^{Bcl\text{-}xL/del}$ MEFs (Chi-square: $p=5x10^{-6}$ and $p=0.3$, respectively; fig. S11B, table S2). This indicates that BCL-XL compensates for the loss of MCL-1 in the regulation of metabolism better than BCL-2 does.

Metabolic defects in *Mcl-1*$^{Bcl\text{-}xL/Bcl\text{-}xL}$ pups

MCL-1 controls mitochondrial morphology and OXPHOS by regulating complex IV assembly and activity (*22, 25*). No defects in complex IV, or any other electron transport chain complexes, were observed in liver extracts from *Mcl-1*$^{Bcl\text{-}xL/Bcl\text{-}xL}$ pups (Fig. 5A). Complex IV defects were only observed in *Mcl-1*$^{-/-}$ MEFs cultured without MCL-1 long-term, whereas acute or medium-term induced deletion of *Mcl-1* in *Mcl-1*$^{del/del}$, *Mcl-1*$^{Bcl\text{-}2/del}$ or *Mcl-1*$^{Bcl\text{-}xL/del}$ MEFs did not affect complex IV formation or activity (fig. S12A-D). Thus, complex IV defects may be secondary to prolonged loss of MCL-1. No complex IV defects were observed in *Mcl-1*$^{Bcl\text{-}xL/Bcl\text{-}xL}$ MEFs (fig. S12E). *Mcl-1*$^{del/del}$ and *Mcl-1*$^{Bcl\text{-}2/del}$ MEFs showed fragmented mitochondria whereas *Mcl-1*$^{Bcl\text{-}xL/del}$ MEFs had normal mitochondrial structure (Fig. 5B,C). Electron microscopy confirmed these findings, however normal cristae organization was seen in intact mitochondria from *Mcl-1*$^{del/del}$, *Mcl-1*$^{Bcl\text{-}2/del}$, *Mcl-1*$^{Bcl\text{-}xL/del}$ MEFs and *Mcl-1*$^{Bcl\text{-}xL/Bcl\text{-}xL}$ MEFs (fig. S13A,B). Thus, in MEFs and hepatocytes, BCL-XL can at least partially replace the function of MCL-1 in electron transport chain assembly and mitochondrial morphology.

MCL-1 loss, akin to treatment with certain drugs (*48*), causes defects in fatty acid oxidation (FAO) (*29, 30*), and this may underly the defects observed in *Mcl-1*$^{Bcl\text{-}xL/Bcl\text{-}xL}$ pups. To explore this, we conducted metabolomic analyses on liver extracts from *Mcl-1*$^{Bcl\text{-}xL/Bcl\text{-}xL}$ pups and wild-type littermates (Fig. 5D-G fig. S14A-D). This revealed significant dysregulation in key metabolic pathways (Fig. 5D). Amounts of tricarboxylic acid cycle (TCA) intermediates malic and fumaric acid (Fig. 5E, fig. S14A) and the metabolites aspartic and glutamic acid (Fig. 5F) were increased, indicating dysregulation of mitochondrial metabolic pathways. Depletion of glucose and early glycolytic intermediates suggests dysregulation of glucose metabolism pathways (Fig. 5F, fig. S14B). Increased abundance of ketone bodies (e.g. 2-HB, fig. S14C) indicate activation of alternative ketogenesis pathways. Increased long chain fatty acid (LCFA) levels and dodecanoic acid accumulation (fig. S14D) point to defects in FAO.

Together with the RNAseq analysis (Fig. 4K-M), these findings indicate that defects in FAO are associated with metabolic adaptations, including increased glycolysis in *Mcl-1*$^{Bcl\text{-}xL/Bcl\text{-}xL}$ pups. Steatosis in *Mcl-1*$^{Bcl\text{-}xL/Bcl\text{-}xL}$ pups is likely caused by loss of MCL-1 function in regulating FAO that cannot be replaced by BCL-XL.

Role of MCL-1 in FAO

Supporting the hypothesis that MCL-1 regulates FAO, we observed proliferation defects and reduced ATP production in *Mcl-1*$^{del/del}$, *Mcl-1* $^{Bcl\text{-}2/del}$ and *Mcl-1* $^{Bcl\text{-}xL/del}$ MEFs when cultured in galactose to promote aerobic energy production (Fig. 5H, fig. S14E). No differences were observed in *Mcl-1* $^{Bcl\text{-}2/del}$ or *Mcl-1* $^{Bcl\text{-}xL/del}$ MEFs when compared to *Mcl-1*$^{del/del}$ MEFs, thus neither BCL-2 nor BCL-XL appears to compensate for MCL-1 under non-glycolytic conditions.

Seahorse analysis revealed significant reduction in maximal respiration and spare respiratory capacity in *Mcl-1*$^{del/del}$, *Mcl-1*$^{Bcl\text{-}2/del}$ and *Mcl-1*$^{Bcl\text{-}xL/del}$ MEFs compared to those of control MEFs (*Mcl-1*$^{fl/fl}$, *Mcl-1*$^{Bcl\text{-}2/fl}$, *Mcl-1*$^{Bcl\text{-}xL/fl}$, wild-type, and *RosaCreERT2*$^{+/Ki}$, fig. S14F). No significant further reduction was observed in *Mcl-1*$^{del/del}$, *Mcl-1*$^{Bcl\text{-}2/del}$ and *Mcl-1*$^{Bcl\text{-}xL/del}$ MEFs upon treatment with the carnitine palmitoyltransferase 1 (CPT1a) inhibitor etomoxir (inhibiting FAO), unlike in wild-type and *RosaCreERT2*$^{+/Ki}$ MEFs (Fig. 5I), suggesting a metabolic shift from FAO to alternative pathways. No significant differences were seen between *Mcl-1*$^{del/del}$ *vs. Mcl-1*$^{Bcl\text{-}2/del}$ and *Mcl-1*$^{Bcl\text{-}xL/del}$ MEFs, indicating that the primary metabolic role of MCL-1 is regulating FAO, with no compensation from BCL-2 or BCL-XL. Notably, CPT1a and ACSL1 expression was detected by Western blotting in liver and heart lysates from heterozygous *Mcl-1*$^{hMcl\text{-}1/+}$, *Mcl-1*$^{Bcl\text{-}2/+}$ and *Mcl-1*$^{Bcl\text{-}xL/+}$mice (fig. S15A-B) and homozygous E10.5 *Mcl-1*$^{hMcl\text{-}1/hMcl\text{-}1}$, *Mcl-1*$^{Bcl\text{-}xL/Bcl\text{-}xL}$, *Mcl-1*$^{Bcl\text{-}2/Bcl\text{-}2}$ embryos (fig. S15C) as well as by IHC in liver and heart tissues from mixed background homozygous *Mcl-1*$^{Bcl\text{-}xL/Bcl\text{-}xL}$ pups (fig. S15D,E).

Collectively, these findings show that in various tissues and cells during late development and post-birth, MCL-1 is essential not only for inhibiting apoptosis but also for regulating critical apoptosis-unrelated processes. BCL-XL, but not BCL-2, can substitute for MCL-1 in regulating the mitochondrial electron transport chain, but neither can replace MCL-1 in controlling FAO.

Discussion

Our study using *Mcl-1* gene-replacement mice resolved the physiological importance of the anti-apoptotic versus apoptosis-unrelated function(s) of MCL-1 in pre- and post-natal development. Although *Mcl-1*$^{-/-}$ blastocysts were reported to fail implantation without apoptosis (*13*), we observed apoptotic DNA fragmentation in a *Mcl-1*$^{-/-}$ E2.5 embryo, indicating aberrant apoptosis. Congruently, replacing MCL-1 with BCL-2 or BCL-XL supported embryogenesis until E13.5. Although both MCL-1 and BCL-XL may regulate mitochondrial OXPHOS (*26, 29, 30, 49*), BCL-2 does not, as it lacks inter-mitochondrial membrane localization (*28, 50*). Recently, MCL-1 was shown to regulate FAO by binding to ACSL1, thereby faciltating long chain fatty acid import into mitochondria (*30*). BCL-2 does not interact with ACSL1 and thus cannot replace any of the reported metabolic functions of MCL-1 (*30*). Collectively, these findings demonstrate that only the anti-apoptotic but no apoptosis-unrelated function of MCL-1 is essential for early embryogenesis.

At later developmental stages and post-natally, the role of MCL-1 in regulating mitochondrial metabolism was essential for normal cell function and survival. *Mcl-1*$^{Bcl\text{-}xL/Bcl\text{-}xL}$ and *Mcl-1*$^{Bcl\text{-}2/Bcl\text{-}2}$ fetuses died significantly earlier than *Bax*$^{-/-}$*Bak*$^{-/-}$*Bok*$^{-/-}$ fetuses lacking all apoptotic executioners (*38*), indicating developmental defects unrelated to apoptosis. BCL-XL proved more effective than BCL-2 in compensating for MCL-1 loss, although it, too, could not fully replace the metabolic role of MCL-1. *Mcl-1*$^{Bcl\text{-}xL/Bcl\text{-}xL}$ embryos developed one day further on a C57BL/6 background and only *Mcl-1*$^{Bcl\text{-}xL/Bcl\text{-}xL}$, but not *Mcl-1*$^{Bcl\text{-}2/Bcl\text{-}2}$ mice, were born alive on a mixed genetic background. We propose that these differences are due to the ability of BCL-XL, but not BCL-2, to sustain OXPHOS (*26, 49*). Consistently, we found no defects in the assembly of the

electron transport chain in *Mcl-1*$^{Bcl\text{-}xL/Bcl\text{-}xL}$ pups. However, *Mcl-1*$^{Bcl\text{-}xL/Bcl\text{-}xL}$ mixed genetic background pups suffered from severe metabolic defects due to impaired FAO, presumably owing to the loss of the interaction of MCL-1 with ACSL1 (*30*). A weak interaction between BCL-XL and ACSL1 has been observed (*30*); however, our data indicate that this is insufficient for effective FAO needed for the survival of cells with high energy demand (e.g. hepatocytes).

In conclusion, our findings show that both the anti-apoptotic and apoptosis-unrelated roles of MCL-1 are essential for pre- and post-natal development, with their importance varying by developmental stage and cell type. This information has implications for the efficacy and tolerability of MCL-1 inhibitors in cancer therapy.

References and Notes

1. A. Glucksmann, Cell deaths in normal vertebrate ontogeny. *Biol Rev Camb Philos Soc* **26**, 59-86 (1951).
2. A. K. Voss, A. Strasser, The essentials of developmental apoptosis. *F1000Res* **9**, (2020).
3. A. Strasser, L. O'Connor, V. M. Dixit, Apoptosis signaling. *Annu Rev Biochem* **69**, 217-245 (2000).
4. C. B. Thompson, Apoptosis in the pathogenesis and treatment of disease. *Science* **267**, 1456-1462 (1995).
5. P. E. Czabotar, G. Lessene, A. Strasser, J. M. Adams, Control of apoptosis by the BCL-2 protein family: implications for physiology and therapy. *Nat Rev Mol Cell Biol* **15**, 49-63 (2014).
6. R. Singh, A. Letai, K. Sarosiek, Regulation of apoptosis in health and disease: the balancing act of BCL-2 family proteins. *Nat Rev Mol Cell Biol* **20**, 175-193 (2019).
7. D. R. Green, G. Kroemer, The pathophysiology of mitochondrial cell death. *Science* **305**, 626-629 (2004).
8. X. Luo, K. L. O'Neill, K. Huang, The third model of Bax/Bak activation: a Bcl-2 family feud finally resolved? *F1000Res* **9**, (2020).
9. G. S. Salvesen, V. M. Dixit, Caspases: intracellular signaling by proteolysis. *Cell* **91**, 443-446 (1997).
10. G. S. Salvesen, V. M. Dixit, Caspase activation: the induced-proximity model. *Proc Natl Acad Sci U S A* **96**, 10964-10967 (1999).
11. K. Brinkmann, A. P. Ng, C. A. de Graaf, A. Strasser, What can we learn from mice lacking pro-survival BCL-2 proteins to advance BH3 mimetic drugs for cancer therapy? *Cell Death Differ* **29**, 1079-1093 (2022).
12. J. T. Opferman, A. Kothari, Anti-apoptotic BCL-2 family members in development. *Cell Death Differ* **25**, 37-45 (2018).
13. J. L. Rinkenberger, S. Horning, B. Klocke, K. Roth, S. J. Korsmeyer, Mcl-1 deficiency results in peri-implantation embryonic lethality. *Genes & development* **14**, 23-27 (2000).
14. N. Motoyama *et al.*, Massive cell death of immature hematopoietic cells and neurons in Bcl-x-deficient mice. *Science* **267**, 1506-1510 (1995).
15. P. Bouillet, S. Cory, L. C. Zhang, A. Strasser, J. M. Adams, Degenerative disorders caused by Bcl-2 deficiency prevented by loss of its BH3-only antagonist Bim. *Dev Cell* **1**, 645-653 (2001).
16. D. J. Veis, C. M. Sorenson, J. R. Shutter, S. J. Korsmeyer, Bcl-2-deficient mice demonstrate fulminant lymphoid apoptosis, polycystic kidneys, and hypopigmented hair. *Cell* **75**, 229-240 (1993).

17. R. L. Schenk *et al.*, Characterisation of mice lacking all functional isoforms of the pro-survival BCL-2 family member A1 reveals minor defects in the haematopoietic compartment. *Cell Death Differ* **24**, 534-545 (2017).
18. K. W. Adams, G. M. Cooper, Rapid turnover of mcl-1 couples translation to cell survival and apoptosis. *J Biol Chem* **282**, 6192-6200 (2007).
19. M. J. Herold *et al.*, The stability and anti-apoptotic function of A1 are controlled by its C terminus. *J Biol Chem* **281**, 13663-13671 (2006).
20. U. Maurer, C. Charvet, A. S. Wagman, E. Dejardin, D. R. Green, Glycogen synthase kinase-3 regulates mitochondrial outer membrane permeabilization and apoptosis by destabilization of MCL-1. *Mol Cell* **21**, 749-760 (2006).
21. A. Gross, S. G. Katz, Non-apoptotic functions of BCL-2 family proteins. *Cell Death Differ* **24**, 1348-1358 (2017).
22. R. M. Perciavalle *et al.*, Anti-apoptotic MCL-1 localizes to the mitochondrial matrix and couples mitochondrial fusion to respiration. *Nat Cell Biol* **14**, 575-583 (2012).
23. M. L. Rasmussen *et al.*, A Non-apoptotic Function of MCL-1 in Promoting Pluripotency and Modulating Mitochondrial Dynamics in Stem Cells. *Stem Cell Reports* **10**, 684-692 (2018).
24. M. L. Rasmussen *et al.*, MCL-1 Inhibition by Selective BH3 Mimetics Disrupts Mitochondrial Dynamics Causing Loss of Viability and Functionality of Human Cardiomyocytes. *iScience* **23**, 101015 (2020).
25. X. Wang *et al.*, Deletion of MCL-1 causes lethal cardiac failure and mitochondrial dysfunction. *Genes & development* **27**, 1351-1364 (2013).
26. K. N. Alavian *et al.*, Bcl-xL regulates metabolic efficiency of neurons through interaction with the mitochondrial F1FO ATP synthase. *Nat Cell Biol* **13**, 1224-1233 (2011).
27. S. B. Berman *et al.*, Bcl-x L increases mitochondrial fission, fusion, and biomass in neurons. *J Cell Biol* **184**, 707-719 (2009).
28. T. Lithgow, R. van Driel, J. F. Bertram, A. Strasser, The protein product of the oncogene bcl-2 is a component of the nuclear envelope, the endoplasmic reticulum, and the outer mitochondrial membrane. *Cell Growth Differ* **5**, 411-417 (1994).
29. M. S. Prew *et al.*, MCL-1 is a master regulator of cancer dependency on fatty acid oxidation. *Cell Rep* **41**, 111445 (2022).
30. T. Wright *et al.*, Anti-apoptotic MCL-1 promotes long-chain fatty acid oxidation through interaction with ACSL1. *Mol Cell* **84**, 1338-1353 e1338 (2024).
31. R. L. Thomas *et al.*, Loss of MCL-1 leads to impaired autophagy and rapid development of heart failure. *Genes & development* **27**, 1365-1377 (2013).
32. S. T. Diepstraten *et al.*, The manipulation of apoptosis for cancer therapy using BH3-mimetic drugs. *Nat Rev Cancer* **22**, 45-64 (2022).
33. J. Montero, A. Letai, Why do BCL-2 inhibitors work and where should we use them in the clinic? *Cell Death Differ* **25**, 56-64 (2018).
34. M. S. Brennan *et al.*, Humanized Mcl-1 mice enable accurate preclinical evaluation of MCL-1 inhibitors destined for clinical use. *Blood* **132**, 1573-1583 (2018).
35. A. Kotschy *et al.*, The MCL1 inhibitor S63845 is tolerable and effective in diverse cancer models. *Nature* **538**, 477-482 (2016).
36. K. Takaoka, H. Hamada, Cell fate decisions and axis determination in the early mouse embryo. *Development* **139**, 3-14 (2012).
37. N. Renier *et al.*, iDISCO: a simple, rapid method to immunolabel large tissue samples for volume imaging. *Cell* **159**, 896-910 (2014).

38. F. F. S. Ke *et al.*, Embryogenesis and Adult Life in the Absence of Intrinsic Apoptosis Effectors BAX, BAK, and BOK. *Cell* **173**, 1217-1230 e1217 (2018).
39. J. Seibler *et al.*, Rapid generation of inducible mouse mutants. *Nucleic Acids Res* **31**, e12 (2003).
40. Y. M. Janumyan *et al.*, Bcl-xL/Bcl-2 coordinately regulates apoptosis, cell cycle arrest and cell cycle entry. *EMBO J* **22**, 5459-5470 (2003).
41. G. P. Linette, Y. Li, K. Roth, S. J. Korsmeyer, Cross talk between cell death and cell cycle progression: BCL-2 regulates NFAT-mediated activation. *Proc Natl Acad Sci U S A* **93**, 9545-9552 (1996).
42. M. Bonyadi *et al.*, Mapping of a major genetic modifier of embryonic lethality in TGF beta 1 knockout mice. *Nat Genet* **15**, 207-211 (1997).
43. H. M. McRae *et al.*, Downregulation of the GHRH/GH/IGF1 axis in a mouse model of Borjeson-Forssman-Lehman syndrome. *Development* **147**, (2020).
44. H. M. McRae *et al.*, PHF6 regulates hematopoietic stem and progenitor cells and its loss synergizes with expression of TLX3 to cause leukemia. *Blood* **133**, 1729-1741 (2019).
45. H. S. Chin *et al.*, VDAC2 enables BAX to mediate apoptosis and limit tumor development. *Nat Commun* **9**, 4976 (2018).
46. M. Y. Liu, M. Colombini, Regulation of mitochondrial respiration by controlling the permeability of the outer membrane through the mitochondrial channel, VDAC. *Biochim Biophys Acta* **1098**, 255-260 (1992).
47. Y. Miura, The biological significance of omega-oxidation of fatty acids. *Proc Jpn Acad Ser B Phys Biol Sci* **89**, 370-382 (2013).
48. S. K. Satapathy, V. Kuwajima, J. Nadelson, O. Atiq, A. J. Sanyal, Drug-induced fatty liver disease: An overview of pathogenesis and management. *Ann Hepatol* **14**, 789-806 (2015).
49. Y. B. Chen *et al.*, Bcl-xL regulates mitochondrial energetics by stabilizing the inner membrane potential. *J Cell Biol* **195**, 263-276 (2011).
50. S. Krajewski *et al.*, Investigation of the subcellular distribution of the bcl-2 oncoprotein: residence in the nuclear envelope, endoplasmic reticulum, and outer mitochondrial membranes. *Cancer Res* **53**, 4701-4714 (1993).
51. A. J. Kueh *et al.*, An update on using CRISPR/Cas9 in the one-cell stage mouse embryo for generating complex mutant alleles. *Cell Death Differ* **24**, 1821-1822 (2017).
52. T. Thomas, M. P. Dixon, A. J. Kueh, A. K. Voss, Mof (MYST1 or KAT8) is essential for progression of embryonic development past the blastocyst stage and required for normal chromatin architecture. *Mol Cell Biol* **28**, 5093-5105 (2008).
53. J. Seibler *et al.*, Rapid generation of inducible mouse mutants. *Nucleic Acids Res* **31**, e12 (2003).
54. I. Vikstrom *et al.*, Mcl-1 is essential for germinal center formation and B cell memory. *Science* **330**, 1095-1099 (2010).
55. A. K. Voss, T. Thomas, P. Gruss, Germ line chimeras from female ES cells. *Exp Cell Res* **230**, 45-49 (1997).
56. A. K. Voss *et al.*, Taube nuss is a novel gene essential for the survival of pluripotent cells of early mouse embryos. *Development* **127**, 5449-5461 (2000).
57. B. E. Sleebs *et al.*, Discovery of potent and selective benzothiazole hydrazone inhibitors of Bcl-XL. *J Med Chem* **56**, 5514-5540 (2013).
58. Y. Liao, G. K. Smyth, W. Shi, The R package Rsubread is easier, faster, cheaper and better for alignment and quantification of RNA sequencing reads. *Nucleic Acids Res* **47**, e47 (2019).

59. M. E. Ritchie *et al.*, limma powers differential expression analyses for RNA-sequencing and microarray studies. *Nucleic Acids Res* **43**, e47 (2015).
60. M. D. Robinson, D. J. McCarthy, G. K. Smyth, edgeR: a Bioconductor package for differential expression analysis of digital gene expression data. *Bioinformatics* **26**, 139-140 (2010).
61. M. D. Robinson, A. Oshlack, A scaling normalization method for differential expression analysis of RNA-seq data. *Genome Biol* **11**, R25 (2010).
62. C. W. Law, Y. Chen, W. Shi, G. K. Smyth, voom: Precision weights unlock linear model analysis tools for RNA-seq read counts. *Genome Biol* **15**, R29 (2014).
63. A. T. L. Lun, G. K. Smyth, No counts, no variance: allowing for loss of degrees of freedom when assessing biological variability from RNA-seq data. *Stat Appl Genet Mol Biol* **16**, 83-93 (2017).
64. R. Liu *et al.*, Why weight? Modelling sample and observational level variability improves power in RNA-seq analyses. *Nucleic Acids Res* **43**, e97 (2015).
65. H. M. Johnston *et al.*, Utilising fluorescent reporters to probe the mode of action of norbornen-7-one CO releasing molecules. *Org Biomol Chem* **20**, 5812-5819 (2022).
66. M. McKenzie, M. Lazarou, D. R. Thorburn, M. T. Ryan, Analysis of mitochondrial subunit assembly into respiratory chain complexes using Blue Native polyacrylamide gel electrophoresis. *Anal Biochem* **364**, 128-137 (2007).
67. N. Renier *et al.*, iDISCO: a simple, rapid method to immunolabel large tissue samples for volume imaging. *Cell* **159**, 896-910 (2014).

Acknowledgments: The authors thank WEHI Bioservices, particularly Giovanni Siciliano, Jaclyn Gilbert, Tracey Baldwin, Louise Spencer, Leanne Johnson, Tom Kitson and Katie Franks for animal husbandry and help with experiments using mice; Bruno Helbert, Rainbow Chan and Natalie Coleman for genotyping; the WEHI Histology Centre, particularly Ellen Tsui, Emma Pan and Andrew Spence; Michelle Clark, Göknur Giner, Nishika Kapuruge and Alex Garnham for experimental advice; Joseph Opferman for sharing critical reagents and discussions; Gemma Kelly, Adam Rose, Luke Formosa and Michael Lazarou for their help with data interpretation and discussions; and Lachlan Whitehead for imaging data processing. The generation of the gene-swap mice used in this study was supported by Phenomics Australia and the Australian Government through the National Collaborative Research Infrastructure Strategy (NCRIS) program.

Funding:

National Health and Medical Research Council (NHMRC) program grant #101671 (AS, PB)

National Health and Medical Research Council (NHMRC) investigator grant #1020363 (AS)

National Health and Medical Research Council (NHMRC) investigator grant #1176789 (AKV)

National Health and Medical Research Council (NHMRC) fellowship #2017971 (MJH)

National Health and Medical Research Council (NHMRC) ideas grant #2021510 (KB, KMcA)

National Health and Medical Research Council (NHMRC) project grant #1160618 (TT)

National Health and Medical Research Council (NHMRC) ideas grant #2010711 (TT)

Cancer Council Grant's in Aid 2024 (AS, KB)

Victorian Cancer Agency MCR fellowship #23020 (KB)

Leukemia Foundation Research Scholarship (DdS)

Viertel Senior Medical Research Fellowship (TLP)

NMRC OF-IRG #MOH-000614 (NF)

Bodhi Education Fund Fellowship (GD)

Author contributions:

Conceptualization: KB, MJH and AS

Methodology: KB, KMcA, AJK, AT, LG, AB, DBdS, LGW, CR, ShM, SNED, SiM,VCW, PA, KKB,TT, AKV

Investigation: KB, KMcA, MJH, JMM, TT, GD, KKB, TLP, NF, PB, AKV, AS

Visualization: KB, ShM, AT, LG, SiM, SNED, JMM, VCW, PA, AS, AKV

Funding acquisition: KB, KMcA, AS, MJH, AKV

Project administration: KB, AS

Supervision: KB, AS, MJH, AKV, TT, KMcA

Writing – original draft: KB, AS, MJH, AKV, TT, KMcA

Writing – review & editing: all co-authors

Diversity, equity, ethics, and inclusion [optional]: This study has been conducted by researchers of a broad range of backgrounds, including early, mid and late career researchers from 11 different nationalities.

Competing interests: KB, AK, AT, ShM, KMcA, LGW, DBdS, SiM, JMM, VW, LG, PA, NF, TLP, GD, PB, AKV, TT, MJH and AS are, or were for some time, employees of the Walter and Eliza Hall Institute. The Walter and Eliza Hall Institute receives milestone payments and royalties from the sale of Venetoclax, parts of which are distributed to current and former employees. MJH and AS collaborated with Servier on the development of MCL-1 inhibitors and received financial support for some of their research. ShM, SNED, AB, KKB and CR declare no conflict of interest.

Data and materials availability: RNAseq data presented in this study can be accessed through https://www.ncbi.nlm.nih.gov/geo. Metabolomics LCMS data presented in this study can be accessed through https://www.ebi.ac.uk/metabolights. All other data are available in the main text or the supplementary materials.

Supplementary Materials

Materials and Methods

Figs. S1 to S15

Tables S1 to S5

References *#51–#67* only included in Supplementary Material

Movies S1 to S3

Main Figure Legends

Fig. 1. Essential function of MCL-1 in pre-implantation development replaced by BCL-XL or BCL-2 but not by A1. (**A**) Schematic of the *Mcl-1* gene-targeting strategy. (**B**) Representative (from n≥2 repeats) western blot of wild-type (wt), *Mcl-1*$^{hMcl\text{-}1/+}$, *Mcl-1*$^{Bcl\text{-}xL/+}$, *Mcl-1*$^{Bcl\text{-}2+/}$ and *Mcl-1*$^{A1/+}$ E10.5 embryo lysates (n=2 per genotype) detecting the indicated proteins. (**C**) Survival (as %AnnexinV-PI-) of mitogen-activated B cells from wild-type (wt), *Mcl-1*$^{hMcl\text{-}1/+}$, *Mcl-1*$^{Bcl\text{-}xL/+}$, *Mcl-1*$^{Bcl\text{-}2/+}$ and *Mcl-1*$^{A1/+}$ mice treated with indicated drugs for 24 h. Data shown as mean ± SEM from ≥2 experiments each performed in triplicates. Two-way ANOVA with Tukey's multiple comparison; p-values shown. (**D**) Offspring genotype frequencies at weaning from intercrosses of *Mcl-1*$^{hMcl\text{-}1/+}$ mice. (**E**) Representative images of a wild-type (wt) and a *Mcl-1*$^{hMcl\text{-}1/hMcl\text{-}1}$ mouse aged 50 days (top) and whole-body weights of 50-60 days old wild-type (wt; n=7), *Mcl-1*$^{hMcl\text{-}1/+}$ (n=12) and *Mcl-1*$^{hMcl\text{-}1/hMcl\text{-}1}$ (n=7) males (bottom). One-way ANOVA with Dunnet's multiple comparison. No significant differences were observed. (**F**) Offspring genotype frequencies at E10.5 from homotypic intercrosses of *Mcl-1*$^{hMcl\text{-}1/+}$, *Mcl-1*$^{Bcl\text{-}xL/+}$, *Mcl-1*$^{Bcl\text{-}2/+}$ or *Mcl-1*$^{A1/+}$ mice. (**D, F)** Genotype distributions analyzed using cumulative binomial probability (p-values and n indicated). (**G**) Representative (from n≥2 repeats) western blot of wild-type (wt), *Mcl-1*$^{hMcl\text{-}1/hMcl\text{-}1}$, *Mcl-1*$^{Bcl\text{-}xL/Bcl\text{-}xL}$ and *Mcl-1*$^{Bcl\text{-}2/Bcl\text{-}2}$ E10.5 embryo lysates (n=2 per genotype) detecting the indicated proteins. (**H**) Representative images of E10.5 wild-type (wt), *Mcl-1*$^{hMcl\text{-}1/hMcl\text{-}1}$, *Mcl-1*$^{Bcl\text{-}xL/Bcl\text{-}xL}$ and *Mcl-1*$^{Bcl\text{-}2/Bcl\text{-}2}$ embryos. **Labeling**: 1a, 1b, maxillary and mandibular portion of the 1st pharyngeal arch; 2 second pharyngeal arch; FL, forelimb bud; HB, hindbrain; He, heart, here beneath the tail; HL, hindlimb bud; MB, midbrain; OV, otic vesicle; T, tail; Te, telencephalon. White arrowhead and white arrow: areas of the lateral ventricles in the telencephalon and the 4th ventricle in the hindbrain, respectively, that appeared collapsed; black arrowhead: blood accumulation; black arrows: neuroepithelium forming ridges in the telencephalon and hindbrain.

Fig. 2. *Mcl-1*$^{Bcl\text{-}xL/Bcl\text{-}xL}$ and *Mcl-1*$^{Bcl\text{-}2/Bcl\text{-}2}$ embryos are more likely to exhibit abnormalities compared to wild-type embryos. (A, B) Offspring genotype frequencies at indicated embryonic days from homotypic intercrosses of (**A**) *Mcl-1*$^{Bcl\text{-}xL/+}$ or (**B**) *Mcl-1*$^{Bcl\text{-}2/+}$ mice, analyzed using cumulative binomial probability (p-values and n indicated). E10.5 data from Fig. 1F are included for comparison. Representative images showing wild-type (wt; n=2), *Mcl-1*$^{Bcl\text{-}xL/Bcl\text{-}xL}$ (n=8) (**C**) and *Mcl-1*$^{Bcl\text{-}2/Bcl\text{-}2}$ (n=11) (**D**) embryos at E11.5. (**E**) Summary frequencies of the phenotypes from E11.5-E12.5 of wild-type (wt; n=73), *Mcl-1*$^{Bcl\text{-}xL/Bcl\text{-}xL}$ (n=30) and *Mcl-1*$^{Bcl\text{-}2/Bcl\text{-}2}$ (n=44) embryos; percentages shown per genotype. Full breakdown in table S1. Statistical significance assessed using cumulative binomial probability (normal *Mcl-1*$^{Bcl\text{-}xL/Bcl\text{-}xL}$ and *Mcl-1*$^{Bcl\text{-}2/Bcl\text{-}2}$ embryos *vs* wild-type embryos); p-values shown. (**F**) Representative (from n ≥ 2 embryos per genotype) whole-mount images (iDISCO) showing a wild-type (wt), a *Mcl-1*$^{Bcl\text{-}xL/Bcl\text{-}xL}$ and a *Mcl-1*$^{Bcl\text{-}2/Bcl\text{-}2}$ E12.5 embryo (vasculature (CD31/PCAM1): purple; blood cells (autofluorescence): white). Higher magnifications highlight (1) heart and liver, (2) cephalic vasculature. **Labeling**: ACA, anterior cerebral artery; BA, basilar artery; DA, descending aorta; E, eye; e, ear; FB, forebrain; FL, forelimb (forelimb bud, E11.5 and E12.5); HB, hindbrain; He, heart; HL, hindlimb (hindlimb bud, E11.5 and E12.5); JLS, jugular lymph sac, here blood filled; Li, liver; MCA, middle cerebral artery; MB, midbrain; OA, olfactory artery; PA, pharyngeal

arches; PCA, posterior communicating artery; Te, telencephalon; UV, umbilical vein; VA, vertebral artery.

Fig. 3. Lethality of *Mcl-1*$^{Bcl\text{-}xL/Bcl\text{-}xL}$ and *Mcl-1*$^{Bcl\text{-}2/Bcl\text{-}2}$ embryos caused not only by aberrant apoptosis. (**A**) Survival (as %AnnexinV-PI-) of mitogen activated B cells from wild-type (wt; n=4), *Mcl-1*$^{Bcl\text{-}xL/+}$ (n=4), *Mcl-1*$^{Bcl\text{-}2/+}$ (n=4) and *Mcl-1*$^{A1/+}$ (n=4) mice treated with cytarabine for 24 h. Data shown as mean ± SEM from ≥3 independent experiments each performed in triplicates. Two-way ANOVA with Tukey's test; p-values shown. (**B**) Representative images of vaginal septa in wild-type, *Mcl-1*$^{Bcl\text{-}xL/+}$ and *Mcl-1*$^{Bcl\text{-}2/+}$ females (top row) and incidence of non-perforate vaginal septa in wild-type (wt; n=258), *Mcl-1*$^{Bcl\text{-}xL/+}$ (n=109) and *Mcl-1*$^{Bcl\text{-}2/+}$ (n=74) females (bottom row). Chi-square test comparing observed *vs* expected frequencies; p-values shown. (**C**) Schematic of developmental lethality and survival of *Mcl-1*$^{-/-}$, *Mcl-1*$^{hMcl\text{-}1/hMcl\text{-}1}$, *Mcl-1*$^{A1/A1}$, *Mcl-1*$^{Bcl\text{-}xL/Bcl\text{-}xL}$, *Mcl-1*$^{Bcl\text{-}2/Bcl\text{-}2}$ and *Bax*$^{-/-}$*Bak*$^{-/-}$*Bok*$^{-/-}$ mice. (**D**) Incucyte proliferation analysis of MEFs treated with 4-Hydroxytamoxifen (1 µM) over 150 h (to = 72 h post-treatment) (solid lines) or left untreated (dotted lines) (n≥8 each genotype and condition). (**E**) Growth curve slopes from (D) analyzed with two-way ANOVA with Tukey's multiple comparison; p-values shown. (**F**) Offspring genotype frequency at E18.5 from intercrosses of *Mcl-1*$^{Bcl\text{-}xL/+}$ mice (left panel) and images of a wild-type (wt), a *Mcl-1*$^{Bcl\text{-}xL/+}$ and a *Mcl-1*$^{Bcl\text{-}xL/Bcl\text{-}xL}$ embryo at E18.5 with whole-body weights indicated (right panel). Genotype distributions analyzed using cumulative binomial probability (p-values and n indicated). (**G**) Cresyl violet-stained coronal brain sections (E18.5) at the anterior commissure level, showing frontal cortex of wild-type (wt), *Mcl-1*$^{Bcl\text{-}xL/+}$ and *Mcl-1*$^{Bcl\text{-}xL/Bcl\text{-}xL}$ embryos (left panel) with morphometric analysis of cortical layers, subventricular zone (SVZ), and lateral ventricles (LV) (right). Circles represent the left and right side of the single brain per genotype. **Labeling**:AC, anterior commisure; CPig CPsg corteal plate, intrage, CPsg cortical plate, infragranular and supragranular part; Sp, subplate: WM, white matter; SVZ, subventricular zone.

Fig. 4. Requirement of apoptosis-unrelated function of MCL-1 for survival of mice after birth. (**A**) Offspring genotype frequency at weaning from *Mcl-1*$^{Bcl\text{-}xL/+}$ (n=177) intercrosses (FVBxBALB/cxC57BL/6) analyzed using cumulative binomial probability; p-values shown. (**B**) Offspring genotype frequency from *Mcl-1*$^{Bcl\text{-}2/+}$ intercrosses (FVBxBALB/cxC57BL/6) at weaning (n=69) and E19.5 (n=16) analyzed using cumulative binomial probability; p-values shown. (**C**) Representative images of a wild-type (wt) and a *Mcl-1*$^{Bcl\text{-}xL/Bcl\text{-}xL}$ mouse at post-natal day 21 (FVBxBALB/cxC57 BL/6, left panel), and body weights of wild-type (n=14), *Mcl-1*$^{Bcl\text{-}x/+}$ (n=46) and *Mcl-1*$^{Bcl\text{-}xL/Bcl\text{-}xL}$ (n=24) mice at post-natal day 21 (FVBxBALB/cxC57BL /6, male and female, right panel). One-way ANOVA with Dunnet's multiple comparison test; p-values shown. (**D**) Kaplan-Meyer survival curve of wild-type (wt; n=46), *Mcl-1*$^{Bcl\text{-}xL/+}$ (n=106) and *Mcl-1*$^{Bcl\text{-}xL/Bcl\text{-}xL}$ (n=46) mice (FVBxBALB/cxC57 BL/6). Log Rank (Mantle-Cox) test; p-values shown. (**E**) Representative (from n≥3 each genotype) H&E-stained liver sections (top row) and cleaved (activated) caspase-3-stained sections (bottom row) of wild-type (wt; left panel) and *Mcl-1*$^{Bcl\text{-}xL/Bcl\text{-}xL}$ mice (right panel) (FVBxBALB/cxC57BL/6). Black arrowheads: apoptotic (cleaved caspase-3 positive) cells. White arrowheads: swelling hepatocytes. (**F**) Representative OilRedO stained liver sections (detecting lipids) from wild-type (wt; left panel) and *Mcl-1*$^{Bcl\text{-}xL/Bcl\text{-}xL}$ pups (right panel) (FVBxBALB/cxC57BL/6). (**G**) Triglyceride content in liver extracts from wild-type (wt; n=5) and *Mcl-1*$^{Bcl\text{-}xL/Bcl\text{-}xL}$ (n=4) pups (FVBxBALB/cxC57BL/6). (**H-J**) Serum concentration of, (**H**) alanine aminotransferase (ALT), (**I**) aspartate aminotransferase (AST) (**J**) glucose from wild-type (wt; H: n=7, I-J: n=9) and *Mcl-1*$^{Bcl\text{-}xL/Bcl\text{-}xL}$ (H: n=9, I-J: n=19)

pups (FVBxBALB/cxC57BL/6). (**G-J**) Data shown as mean ± SEM analyzed by two-tailed t-test; p-values shown. (**K-M**) RNAseq analysis in liver extracts from wild type (wt; n=6) and *Mcl-1*$^{Bcl\text{-}xL/Bcl\text{-}xL}$ (n=4) pups (FVBxBALB/cxC57BL/6). (**K**) Heatmap showing differentially expressed genes. (**L**) Enrichment plot showing the top 25 deregulated pathways using KEGG analysis. (**M**) MA-plot showing deregulated genes within metabolic pathway determined by KEGG pathway analysis. Genes involved in glycolysis (*Pfkl*, *Pfkp*, *Pfkfb3*, *Tpi1*, *Aldoa*, *Gapdh*, *Pkm*, *Pgk*, *Pgam1*, *Pgm2*, *Pgm3*)*, lipid metabolism (*Acsl1*, *Acsl3*, *Acsl4*, *Eno1b*, *Elovl5*, *Acacb*, *Acaca*, *Elovl3*, *Alox12*)$^{\#}$, fatty acid omega oxidation (*Cyp4a32*, *Cyp4a10*, *Cyp4a14*)$^{\$}$ and other non-aerobic metabolic pathways that may be associated with liver damage (*Aldoart1*, *Gucy2c*, *Akrb7*, *Gpx3*, *Galk1*) are highlighted.

Fig. 5. The metabolic function of MCL-1 in fatty acid oxidation is critical for liver function. (**A**) Blue native PAGE and immunoblot analysis of respiratory complexes I-IV (CI-CIV) in mitochondria isolated from livers of wild-type and *Mcl-1*$^{Bcl\text{-}xL/Bcl\text{-}xL}$ pups. UQCRC1 and COX1 antibodies were used for CI-III and CIV detection, respectively. Coomassie-stained complex V (CV) serves as a loading control. (**B**) Representative immunofluorescent images of MEFs of the indicated genotypes showing mitochondria stained with *Mitotracker*^{TM} (red) and cell nuclei stained with DAPI (blue). (**C**) Quantification of mitochondrial count, area, and branching in MEFs of the indicated genotypes using ImageJ. Data shown as mean ± SEM from n=35 cells across 4 independent experiments. All data points shown with each experiment indicated by distinct symbols (e.g circle, square, diamond, triangle). One-way ANOVA with Dunnet's multiple comparison; p-values shown. (**D-G**) Metabolomics analysis in liver extracts from wild-type (wt; n=5) and *Mcl-1*$^{Bcl\text{-}xL/Bcl\text{-}xL}$ (n=4) pups (FVBxBALB/cxC57BL/6). (**D**) Metabolite pathway analysis (top) and heatmap showing the top 25 deregulated metabolites (bottom). Metabolite levels of (**E**) fumaric acid (FA), malic acid (MA), (**F**) glutamic acid (GA), aspartic acid (AA) and (**G**) glucose (Glu), glucose-6phosphate (G6P), fructose-6-phosphate (F6P) and pyruvic acid. Data shown as mean ± SEM, two-tailed t-test; p-values shown. (**H**) Incucyte proliferation analysis of MEFs cultured for 48 h in glucose (filled bars) or galactose (hollow bars). Data shown as mean ± SEM (n=3 independent experiments in triplicates, all data points shown). Two-way ANOVA with Tukey's multiple comparison; p-values shown. (**I**) Representative Seahorse analysis in MEFs of the indicated genotypes with (hollow bars) or without (filled bars) treatment with the CPT1a (carnitine palmitoyltransferase 1a) inhibitor etomoxir, showing maximal respiration (top) and spare respiratory capacity (bottom). Data shown as mean ± SEM from n ≥ 6 replicates. Two-way ANOVA with Tukey's multiple comparison; p-values shown.

Science
AAAS

Supplementary Materials for

Relative importance of the Anti-Apoptotic versus Apoptosis-Unrelated Functions of MCL-1 *in vivo*

Kerstin Brinkmann[*1,2], Kate McArthur[3‡], Shezlie Malelang[1,2‡], Leonie Gibson[1], Annli Tee[1,2], Sheik Nadeem Elahee Doomun[4], Caitlin L Rowe[3], Philip Arandjelovic[1,2], Julia M Marchingo[1,2], Damian D'Silva[1,2], Annabell Bachem[5], Simon Monard[1], Lauren G Wheelan[1], Grant Dewson[1,2], Tracy L Putoczki[1,2], Philippe Bouillet[1,2], Nai Yang Fu[1,2,6], Kristin K Brown[7,8,9], Andrew J Kueh[1,2,10,11], Verena C Wimmer[1,2], Marco J Herold[1,2,10,11†], Tim Thomas[1,2†], Anne K Voss[1,2†], Andreas Strasser[*1,2†]

Corresponding author: strasser@wehi.edu.au; brinkmann.k@wehi.edu.au

The PDF file includes:

Materials and Methods
Figs. S1 to S15
Tables S1 to S5
References *#51–#67* only included in Supplementary Material

Other Supplementary Materials for this manuscript include the following:

Movies S1 to S3

Materials and Methods

Mice

Mcl-1^{hMcl-1}*, Mcl-1*$^{Bcl-xL}$*, Mcl-1*$^{Bcl-2}$ *and Mcl-1*^{A1} mice were generated on a C57BL/6 J background by the MAGEC laboratory at The Walter and Eliza Hall Institute, using previously described methods (*51*). A mixture of 20 ng/μL Cas9 mRNA, 10 ng/μL single guide RNAs and 40 ng/μL donor template were injected into fertilized one-cell stage C57BL/6J embryos. Guide RNAs and targeting vector sequences are provide in table S3. Heterozygous knock-in mice were first backcrossed to C57BL/6J mice for 2 generations to eliminate potential off-target events. Mice were maintained on a C57BL/6J background unless stated otherwise in the text (see below).

Mcl-1^{Bcl-xL} and *Mcl-1*$^{Bcl-2}$ mice on a C57BL/6J background were bred to F1 hybrids of the FVBxBALB/c strains. This F1 hybrid was chosen because these mice are among the most genetically diverse laboratory mouse strains, which improves fertility and vigor, as described previously (*52*).

The *RosaCreERT2*$^{+/Ki}$ and *Mcl-1*$^{fl/fl}$ mice, both on a C57BL/6J background, have been described previously (*53, 54*). To activate CreERT2, mice were given 90 mg/kg body weight tamoxifen (Sigma-Aldrich, #10540-29-1) in peanut oil/10% ethanol each day for 2 consecutive days by oral gavage.

Mice were weaned between 19-23 days of age and deemed adult at 8 weeks of age. Male and female animals were both used as they became available or occurred during dissection of embryos and fetuses. No animals and no data were excluded. All animal experiments were performed with the approval of the Walter and Eliza Hall Institute Animal Ethics Committee and according to the Australian code of practice for the care and use of animals for scientific purposes.

For the genotyping of adult mice and embryos, ear clip samples or embryo tail clip samples, respectively, were lysed in Direct PCR (Tail) lysis buffer (Viagen, Biotech, #102-T) supplemented with 40 μg/mL Proteinase K (Sigma-Aldrich, #EO0491). Genotyping was performed in-house using specific oligonucleotides listed in Table S4.

Mouse serum analysis

Mouse serum was harvested via cardiac puncture, and levels of glucose, aspartate aminotransferase (AST), alanine aminotransferase (ALT), creatine kinase (CK) and triglyceride (TAG) were analyzed using the standard pipeline for patient samples of the Royal Melbourne Hospital.

Pre-implantation embryo handling and analysis

For timed matings, noon of the day on which the vaginal plug was first observed was defined as embryonic day 0.5 (E0.5). Pre-implantation embryos were recovered from the oviduct at E0.5, E2.5 and from the uterus at E3.5.

E0.5 embryos were cultured in embryo culture medium (EmbryoMax® Human Tubal Fluid, Sigma-Aldrich, # MR-070-D) under mineral oil for embryo culture (Sigma-Aldrich, # M5310) to observe pre-implantation development *ex vivo* and photographed daily (Nikon Diaphot 300) equipped with a digital camera (Zeiss).

The zonae pellucidae were removed from E2.5 and E3.5 embryos using Acid Tyrode's solution (0.8 g NaCl, 0.02 g KCl, 0.024 g $CaCl_2 \cdot 2H_2O$, 0.01 g $MgCl_2 \cdot 6H_2O$, 0.1 g glucose and 0.4 g polyvinylpyrrolidone dissolved in 100 mL of H_2O).

For direct genotyping, zona-less E2.5 and E3.5 embryos were placed into 10 µL of DNA lysis buffer (1X MyTaq Red Mix, Bioline, #25044) complemented with 0.2 µL of 10 mg/mL proteinase K (Sigma-Aldrich, # EO0491) and incubated at 55˚C for 2 h. The proteinase K was inactivated at 85˚C for 1 h, before conducting the genotyping PCR.

Inner cell mass (ICM) outgrowth cultures were performed as reported previously(*55*). In brief, E3.5 embryos were plated individually into gelatin-coated wells of 24-well plates in embryonic stem cell (ESC) medium (DMEM, high glucose 4500 mg/L (Gibco, Thermo Fisher, #11965,), 100 µM 2-mercapto-ethanol (Sigma-Aldrich, #M-7522), 1 x non-essential amino acids (Gibco, Thermo Fisher, #11140050), 1 x L-glutamine (Gibco, Thermo Fisher, # 25030-024), 1 x sodium pyruvate (Gibco, Thermo Fisher, #11360070,), 1000 IU LIF/mL (Sigma-Aldrich, #ESG1107) and 20% ESC-qualified fetal bovine serum (FBS; Gibco, Thermo Fisher, #26140079). Embryos were incubated at 37˚C in 5% (v/v) CO_2 in air and photographed daily using an inverted microscope (Nikon Diaphot 300) equipped with a digital camera (Zeiss). Cultures were lysed and genotyped after 7 to 9 days of culture.

Terminal deoxynucleotidyl transferase dUTP nick end labelling (TUNEL) staining of pre-implantation embryos was performed as reported previously(*56*). In brief, zona-less E2.5 embryos were immobilized on gelatin-coated microscope slides by fixation in 1% (w/v) paraformaldehyde (Sigma-Aldrich, #P6148) in PBS, washed, post-fixed in cooled ethanol:acetic acid (2:1) and stained using a TUNEL kit (ApopTag® Fluorescein In Situ Apoptosis Detection Kit, Merck Millipore, #S7110) according to the manufacturer's instructions. After photography using an upright microscope (Zeiss) and a digital camera (Zeiss), coverslips were removed by submerging slides in PBS, the embryos were individually scraped off the microscope slide using drawn-out glass pipettes (new pipette for each embryo) filled with 1X MyTaq Red mix (Bioline, #25044), aspirated and transferred into 10 µL of DNA lysis buffer and processed for genotyping as described above.

Post-implantation embryo handling and analysis

For timed matings, noon of the day on which the vaginal plug was first observed was defined as embryonic day 0.5 (E0.5). Mouse embryos and fetuses were recovered at E10.5, E11.5, E12.5, E13.5, E14.5, E15.5 and E18.5 and examined and scored before genotyping (i.e., blinded to genotype). Embryos were imaged using the SV11 stereomicroscope from Zeiss equipped with the ZEN software (Zeiss). Embryo images were further processed using the Adobe Photoshop software. For some images the healing brush spot tool was used to delete image parts of neighboring embryos from the background and scratches in the dish, but no such changes have been made to the embryos. Other changes, including level adjustment (black/white balance), brightness adjustment and exposure adjustment have been applied uniformly to the entire image. Embryos and data were only excluded when technical errors occurred (e.g., no clear genotyping result or damage during dissection).

Whole-mount embryo labeling and imaging

Mouse embryos were recovered at E12.5 and fixed in 4% (w/v) paraformaldehyde (Sigma-Aldrich, #P6148)/PBS at room temperature (RT) over night (ON). Antibody labeling and clearing were performed following the iDISCO protocol (https://www.cell.com/fulltext/S0092-8674(14)01297-5). In brief, embryos were washed 3x with PBS for 30 min and dehydrated with a methanol/H_2O series (20%, 40%, 60%, 80%, 100% (2x)) for 1 h for each dilution at room temperature. Embryos were incubated overnight in 66% dichloromethane (DCM, Sigma-Aldrich,

#75-09-2)/33% methanol at room temperature and washed 2x in 100% methanol at room temperature and then chilled at 4°C. Embryos were bleached in chilled fresh 5% H_2O_2 in methanol ON at 4°C and then rehydrated with a methanol/H_2O series (80%, 60%, 40%, 20%, PBS) for 1 h each at room temperature. Embryos were washed twice with PTx (PBS/0.2% Triton-X-100) for 1 h at room temperature, incubated with permeabilization buffer (PTx/20%DMSO/38 mg/mL glycine) for 1 day and blocking buffer (PTx / 10% DMSO/6% donkey serum) for 2 days. For immunolabelling embryos were washed 4 times with PTwH (PBS/0.2% Triton-X-100/10 µg/mL heparin (Stem cell Technologies, #07980)) for 1 h each at 37°C and incubated with primary antibody (PE-labeled rabbit anti-CD31/PCAM1 (1:100, cloneC31.7, Abcam, #ab215753) in PTwH/5% DMSO/3% Donkey Serum (Abcam, #7475) for 5 days at 37° C. For clearing, embryos were washed 4 times with PTwH for 1 h each at 37°C and then dehydrated with a methanol/H_2O series: 20%, 40%, 60%, 80%, 100% (2x); for 1 h each dilution at room temperature. On the next day, embryos were incubated in 66% DCM/33% methanol for 3 h at room temperature. Embryos were washed with 100% DCM 3x for 15 min at room temperature and incubated DiBenzyl Ether (DBE, Sigma-Aldrich, #103-50-4) for 15 min. Cleared and stained embryos were transferred into ethyl cinnamate (Sigma-Aldrich, #103-36-6). Light sheet imaging was performed using a Zeiss Z.1 Light sheet microscope equipped with a 5x/0.16 detection objective. 3D tiled image stacks of autofluorescence (excitation 405 nm, emission 505-545 nm) and PE fluorescence (excitation 561 nm; emission 575-615 nm) were acquired sequentially. Data sets were 3D reconstructed using Imaris v9.7.1 (Bitplane). Imaris version 9.7.1 (Bitplane) was used for image processing.

Cell lines and *in vitro* cell survival assays

Mouse embryonic fibroblasts (MEFs) were prepared from E11.5 embryos of the indicated genotypes. Briefly, the fetal liver and head were removed, and the remaining tissue was incubated for 5-10 min in 0.05% (w/v) trypsin to form a single cell suspension. Cells were washed with Dulbecco's Modified Eagle Medium (DMEM, Gibco, Thermo Fisher, #12491015) and seeded onto 0.1% gelatin-coated 6-well plates in DMEM supplemented with 10% fetal calf serum (Gibco, Thermo Fisher, #26140079) and 1x Glutamax (Gibco, Thermo Fisher, #35050061). Primary MEFs were cultured in a low oxygen (3%) incubator to prolong their lifespan. Where indicated, MEFs were immortalized with the SV40 Large T antigen. Cells were cultured in a 6-well plate and transfected with 10 µg of linearized plasmid expressing the SV40 Large T antigen using the FuGene Transfection Kit (Promega, #E2691) according to the manufacturer's instructions. Cells were then serially passaged, with complete immortalization observed at passages 8-10. Immortalized MEFs were cultured in DMEM supplemented with 10% fetal calf serum (Gibco, Thermo Fisher, #26140079), 1x Glutamax (Gibco, Thermo Fisher, #35050061), 50 µM 2-mercaptoethanol (Sigma-Aldrich, #M6250), and 100 mM asparagine (Sigma-Aldrich, #70-47-3). Cell survival assays were performed in 96-well flat bottom plates containing $5x10^4$ MEFs per well. Cells were treated with the ABT-199 (Active Biochem. #A-1231), A-1331852 (in house) (*57*), S-63845 (Active Biochem, #6044), Etoposide (Sigma-Aldrich, #33419-42-0), Thapsigargin (Sigma-Aldrich, #T9033), Nutlin 3-A (Selleckchem, #S8059) or Ionomycin (Sigma-Aldrich, #56092-82-1) at the concentrations indicated in the figures and figure legends for the indicated time periods. Cell viability was assessed by MTT assay (Roche, #11465007001) or Cell titer glow assay as indicated, according to the manufacturer's instructions.

Mitogen-activated B cells were generated from splenocytes isolated from adult mice. In brief, single cell suspension were generated by mashing the spleen through a 100 µm cell strainer. Cells were washed twice with PBS and $5x10^3$ cells/mL were plated in RPMI 1640 medium (Gibco, Thermo Fisher, #11965) supplemented with 10% fetal cave serum, 1x Glutamax (Gibco, Thermo Fisher, #35050061), 50 µM 2-mercaptoethanol (Sigma-Aldrich, #M6250), 100 mM asparagine (Sigma-Aldrich, #70-47-3), non-essential amino acids (Gibco, Thermo Fisher, #11140050). B cells were activated by adding 100 units/mL IL-4 (in house), 10 µg/mL rat anti-CD40 antibody (clone FGK45, in house) 10 ng/mL LPS (Lipopolysaccharides from *Escherichia coli*, Sigma-Aldrich, #L2630) to the culture for 48 h. Cell survival assays were performed in 96-well flay bottom plates containing $5x10^4$ cells per well. Cells were treated with the BCL-2 inhibitor ABT-199 (Active Biochem. #A-1231), the BCL-XL inhibitor A-1331852 (in house) (*57*), the MCL-1 inhibitor S-63845 (Active Biochem, #6044) or Cytarabine (Pfizer, #C587PB) at the concentrations indicated in the figures and figure legends and cell survival was assessed at the indicated time points post-treatment by flow cytometry (BD Fortessa X20) after staining with annexin V conjugated to Alexa Fluor plus 647 (Thermo Fisher, #P1304MP) and propidium iodide (PI, Thermo Fisher, #P1304MP)). Viable cells were identified as those negative for both annexin V and PI.

In vitro cell proliferation assays

To assess proliferation, cells were seeded into a 96-well plate at a density of 2000 cells per well in 200 µL of complete growth medium (RPMI containing 10% FCS, 1µM Asparagine, 1x Glutamax). The following day plates were placed in the Incucyte Live-Cell Analysis System at 37°C with 5% CO2. Phase-contrast images were captured every 6 h over 6 days. Proliferation was quantified as confluence using Incucyte software, and growth curves were generated from the data. Wells with medium only were used as background controls.

To assess proliferation under non-glycolytic conditions, cells were seeded into a 96-well plate at a density calculated to reach 100% confluency after 24 h, based on the specific proliferation rates of the cell lines assessed before. After 24 h, the medium was replaced with either complete medium (RPMI containing 10% FCS, 1 µM Asparagine, 1x Glutamax) or glucose-free medium. Plates were then placed in the Incucyte Live-Cell Analysis System at 37°C with 5% CO2, and phase-contrast images were captured every 12 h for 2 days. Proliferation was quantified as confluence using Incucyte software, and growth curves were generated. Wells containing medium only served as background controls.

In vitro ATP production assays

Cells were seeded into a white opaque 96-well plate at 10,000 cells/well and incubated overnight in complete growth medium (RPMI containing 10% FCS, 1 µM Asparagine, 1x Glutamax). The following day, the medium was replaced with either full medium or galactose medium. After 48 h, CellTiter-Glo reagent (Promega, #G9681) was added to each well, and luminescence was measured after a 10 min incubation. Background luminescence from medium-only wells was subtracted, and ATP levels were used to assess metabolic activity under the different conditions.

Western blot analysis

Total cell lysates were generated from E10.5 embryos using CHAPS buffer (10 mM HEPES, pH 7.4, 150 mM NaCl, 1% CHAPS plus complete protease inhibitor cocktail (Roche,

#11697498001). After determining the protein concentration of each sample using the Protein Assay Dye Reagent Concentrate (Biorad, #50000002), 30 µg of lysate was resolved on 10%-14% NuPage Bis-Tris-polyacrylamide gels (Invitrogen) and proteins were then transferred onto PVDF/nitrocellulose membranes (Amersham) using the Invitrogen iBlot 2 system (Biorad). Blots were then incubated with blocking buffer (Tris Buffered Saline, 0.1% Tween20, 5% milk) for 1 h at room temperature and probed with the primary antibodies at 4°C ON. A list of the antibodies used is provided in Table S5. Incubation with HRP-conjugated secondary antibodies was subsequently performed for at least 1 h, and protein bands were visualized on the ChemiDoc Touch Imaging System (Biorad) using the Luminata Forte enhanced chemiluminescence reagent (Millipore, #RPN2209) or Immobilon Forte Western HRP Substrate (Millipore, #WBLUF). Western blot images were initially analyzed using the ImageLab software (Biorad) and further processed using the Adobe Photoshop software, including image cropping and brightness adjustment that were applied uniformly to the entire image.

Flow cytometric analysis

Bone marrow cells were harvested, and single-cell suspensions were prepared. Intracellular staining was performed using the eBioscience FoxP3 Transcription Factor Staining Buffer Set (Thermo Fisher, #00-5523-00) according to the manufacturer's instructions. Single-cell suspensions were incubated with fluorochrome-conjugated monoclonal antibodies detecting hBCL-2 (BD Biosciences, #551051) or FLAG (Sigma Aldrich, #F3165) for 30 min on ice in buffered saline supplemented with 5% fetal bovine serum and 10% 24G2 hybridoma supernatant (antibody against FcγR) to block nonspecific antibody binding. After staining, cells were washed twice with buffered saline supplemented with 5% fetal bovine serum and analyzed in the same buffer supplemented with propidium iodide (PI, 2 µg/ml). Flow cytometric analysis was performed using a FortessaX20 flow cytometer (BD Biosciences). Cell doublets and dead cells were identified and gated out using FSC-H/FSC-A and PI staining analysis, respectively. Changes in median fluorescence intensity (MFI) were determined after normalizing values (absolute MFI of the samples/background MFI of an unstained control). Data are presented as fold change to average MFI in cells from a C57BL/6 wild-type mouse.

Calcium flux analysis

Cells were seeded into a 12-well plate at 400,000 cells/well and incubated overnight in complete growth medium. The following day, cells were loaded with the Abcam Calcium Flux Assay Kit (Abcam # ab233472) according to the manufacturer's protocol. After incubation with the calcium indicator dye, cells were washed and resuspended in assay buffer.

Baseline calcium levels were recorded using flow cytometry. After 10 sec, ionomycin (4 ng/mL) was added to release stored calcium. Flow cytometric analysis was then performed to track changes in calcium levels. Baseline and peak calcium levels were calculated by averaging the timepoints of the baseline and maximum release recordings. The peak amplitude is calculated by determining the difference between the maximum calcium level observed after ionomycin addition (the peak) and the baseline calcium level before ionomycin treatment.

RNAseq analysis in MEFs and liver tissues

RNAseq analysis in MEFs was performed using 5 replicates for each genotype. RNAseq analysis in liver tissue was performed in samples from wild-type (n=6) and (n=5) *Mcl-1*$^{Bcl\text{-}xL/Bcl\text{-}xL}$ mice. Total RNA was extracted from cell pellets or liver tissues with Direct-zol RNA MicroPrep kit (Zymo research, #R2060) according to the manufacturer's instructions. RNA was quantified and quality verified using Agilent Bioanalyzer 2100.

An input of 100 ng of total RNA was prepared and indexed for illumina sequencing using the TruSeq RNA sample Prep Kit v2 (illumina, #RS-122-2001) according to the manufacturer's instructions. The library was quantified using the Agilent Tapestation and the Qubit™ RNA assay kit for Qubit 2.0® Fluorometer (Thermo Fisher, # Q32852). The indexed libraries were then prepared and diluted to 750pM for paired end (2x 66 base) sequencing on a NextSeq2000 instrument using the P2 100 cycle kit using v3 chemistry (illumina, # 20100981) according to the manufacturer's instructions. The base calling and quality scoring were determined using Real-Time Analysis on board software v2.4.6, while the FASTQ file generation and de-multiplexing utilized bcl2fastq conversion software v2.15.0.4.

The samples from each dataset were aligned to the mm39 build of the mouse genome using the align function from the Rsubread package v2.18.0(*58*). For all samples at least 97% of fragments (read pairs) were successfully mapped. Fragments mapping to genes were then summarized using Rsubread's feature Counts function. Genes were identified using RefSeq annotation to the mm39 genome. Differential gene expression analyses between experimental groups were then conducted using the limma v3.60.6 (*59*)and edgeR v4.2.2 (*60*) software packages. Each data set was analyzed independently.

MEFs: Prior to analysis, all genes without official gene symbols were removed, and lowly expressed genes were filtered using edgeR's filterByExpr function with default parameters. Sample composition was then normalized using the TMM method (*61*) implemented in limma's normLibSizes function. Following filtering and normalization, the data were transformed to $\log_2$-counts per million (CPM) with associated precision weights using voom (*62*). Linear models were then fit to each gene and differential expression was assessed using robust empirical bayes moderated t-statistics (robust limma-voom pipeline). To increase precision the linear models incorporated two surrogate variables calculated using limma's wsva function.

Liver samples: Prior to analysis all genes without official gene symbols were removed together with sex-lined genes. This included the Xist gene and those unique to the Y-chromosome. Sex-linked genes were removed to avoid sex biases in the analysis. Lowly expressed genes were then filtered using edgeR's filterByExpr function with default parameters. Sample composition was then normalized using the TMMwsp method to accommodate for samples with a higher proportion of exact zero counts. Following filtering and normalization, the data were transformed to $\log_2$-CPM with associated precision weights using voom. This was implemented using limma's voomLmFit function to assist samples with a high proportion of exact zeros (*63*). Included in this process was a calculation for correlation between samples from the same pool, and a sample weights calculation (*64*). Linear models were then fit to each gene and differential expression between the wild-type and *Mcl-1*$^{Bcl\text{-}xL/Bcl\text{-}xL}$ groups was assessed using robust empirical Bayes moderated t-statistics (robust limma-voomLmFit pipeline).

For both data sets the false discovery rate was controlled below 5% using the Benjamini and Hochberg method. Pathway analyses were carried out using limma's goana and kegga functions. Heatmaps were drawn using the pheatmap software package. Mean-difference plots were

generated using limma's plotMD function. Pathway enrichment plots were created using the ggplot2 software package.

Metabolomics GC-MS (Gas Chromatography-Mass Spectrometry) analysis

The liver samples (~20 mg) were cryomilled in 600 µL of 3:1 MeOH/Milli-Q water containing 2 nmol of $^{13}C_5{}^{15}N$ valine and $^{13}C_6$ sorbitol, using a Bertin Technologies Precellys bead mill coupled to a Cryolys cooling unit. The homogenates were incubated at 4°C for 10 min with continuous agitation (950 rpm) using an Eppendorf Thermomixer C. The samples were centrifuged at 4°C for 10 min at 16,000 *g* using an Eppendorf centrifuge 5430 R. The supernatant was transferred into a fresh 1.5 mL Eppendorf tube. A 30 µL aliquot of each sample was pooled to create the pooled biological quality control (PBQC). A total of 30 µL of each study sample and the PBQC were transferred into HPLC inserts and evaporated at 30 °C to complete dryness, using a CHRIST RVC 2-33 CD plus speed vacuum. To limit the amount of moisture present in the insert, 30 µL 100% methanol (LCMS grade) was added to each insert and evaporated using a speed vacuum.

Dried samples for targeted analysis were derivatized online using the Shimadzu AOC6000 autosampler robot. Derivatization was achieved by the addition of 25 µL methoxamine hydrochloride (30 mg/mL in pyridine, Merck) followed by shaking at 37°C for 2 h. Samples were then derivatized with 25 µL of N,O-bis (trimethylsilyl)trifluoroacetamide with trimethylchlorosilane (BSTFA with 1% TMCS, Thermo Fisher) for 1h at 37°C. The sample was allowed to equilibrate at room temperature for 1 h before 1 µL was injected onto the GC column using a hot needle technique. Split (1:10) injections were performed for each sample.

The GC-MS system used comprised of an AOC6000 autosampler, a 2030 Shimadzu gas chromatograph and a TQ8050NX triple quadrupole mass spectrometer (Shimadzu, Japan) with an electron ionization source (-70eV). The mass spectrometer was tuned according to the manufacturer's recommendations using tris-(perfluoro butyl)-amine (CF43). GC-MS was performed on a 30 m Agilent DB-5 column with 0.25 mm internal diameter column and 1 µm film thickness. The injection temperature (inlet) was set at 280°C, the MS transfer line at 280°C and the ion source adjusted to 200°C. Helium was used as the carrier gas at a flow rate of 1 mL/min and argon gas was used in the collision cell to generate the MRM product ion. The analysis of the derivatized samples was performed under the following oven temperature program; 100°C start temperature, hold for 4 min, followed by a 10°C/min oven temperature ramp to 320°C with a following final hold for 11 min.

Samples were analyzed in a randomized order, with a pooled biological quality control sample added after every 5 samples. The pooled biological quality control was used to monitor downstream sample stability and analytical reproducibility. Approximately 625 targets were collected using the Shimadzu Smart Metabolite Database, where each target comprised a quantifier MRM along with a qualifier MRM, which covers approximately 420 unique endogenous metabolites and multiple stable isotopically labeled internal standards. Resultant data were processed using Shimadzu LabSolutions Insight software, where peak integrations were visually validated and manually corrected where required.

The dataset was normalized by median and log10 transformed. PCA and heatmaps were generated using MetaboAnalyst 6.0.

Mitochondrial isolation and blue native-page analysis

Crude mitochondria were isolated from cultured cells as previously described (*65*). MEFs were seeded onto 150 mm tissue culture dishes (Corning, #CLS430599) and cultured to confluency in DMEM (Gibco, #11885084; Thermo Fisher) supplemented with 10% fetal calf serum, 1 x penicillin/streptomycin (Sigma-Aldrich; #P4458),1x GlutaMAX (Life Technologies; #35050061) and 100 mM L-asparagine (Sigma-Aldrich; #A4159). Cells were dissociated from culture dishes using PBS + 2 mM EDTA and centrifuged at 800g for 5 min at 4ºC. Supernatants were aspirated and cell pellets washed in cold PBS and centrifuged at 800g for 5 min at 4ºC. Supernatants were aspirated and cell pellets frozen at -80ºC for at least 30 min. To isolate the crude mitochondrial fraction, thawed cell pellets from MEFs and primary hepatocytes were resuspended in Isolation Buffer A (20 mM HEPES-KOH pH 7.6, 220 mM mannitol, 70 mM sucrose, 1 mM EDTA, 0.5 mM PMSF and 2 mg/mL BSA) and lysed using 20 strokes of a Dounce glass homogenizer. Cell lysates were centrifuged at 800g for 5 min at 4ºC to pellet nuclei and remaining intact cells. Supernatants containing mitochondria were transferred into clean tubes and centrifuged at 13,000g for 10 min at 4ºC. Supernatants were aspirated and the remaining mitochondrial pellets were resuspended in Isolation Buffer B (20 mM HEPES-KOH pH 7.6, 220 mM mannitol, 70 mM sucrose, 1 mM EDTA and 0.5 mM PMSF) and centrifuged again at 13,000*g* for 10 min at 4ºC. Supernatants were aspirated and mitochondrial pellets were resuspended in 500 µL Isolation Buffer B if used immediately or in 500 µL Sucrose Buffer (10 mM HEPES pH 7.6 and 0.5 M sucrose) if aliquoted and frozen for later use.

Protein concentration was determined by using the bicinchoninic assay (BCA; Thermo Fisher, #23223). BN-PAGE was performed as previously described (*66*) with continuous 4%-13% gels made using a gradient mixer, the separating gels composed of acrylamide/bis-acrylamide solutions made in BN gel buffer (66 mM ε-amino n-caproic acid, 50 mM Bis-Tris pH 7.0) with 13% acrylamide/bis-acrylamide and 20% (w/v) glycerol or 4% acrylamide/bis-acrylamide alone) and the stacker gel composed of 4% acrylamide/bis-acrylamide in BN gel buffer and layered onto the separating gel. Crude mitochondria were pelleted from the solution at 13,000g, 10 min at 4ºC, with supernatants subsequently removed and the remaining mitochondrial pellets solubilized in digitonin detergent buffer (20 mM Bis-Tris pH 7.0, 50 mM NaCl, 10% (w/v) glycerol and 1% digitonin) for 10 min on ice, followed by centrifugation at 13,000g for 10 min at 4ºC. The supernatants containing solubilized mitochondrial complexes were then transferred into a clean tube containing one-tenth the volume of 10X BN-PAGE loading dye (5% (w/v) Coomassie blue G250, 500 mM ε-amino n-caproic acid, 100 mM Bis-Tris pH 7.0) prior to gel loading.

Gel electrophoresis was performed using BN-PAGE blue cathode buffer (50 mM tricine, 15 mM Bis-Tris, 0.02% (w/v) Coomassie blue G250), which was replaced with BN-PAGE clear cathode buffer (50 mM tricine, 15 mM Bis-Tris) once the dye front has migrated halfway through the gel, and BN-PAGE anode buffer (50 mM Bis-Tris pH 7.0). Transfer to PVDF membranes (Merck, #IPVH00010) was performed using an Invitrogen Power Blotter System (Thermo Fisher) according to the manufacturer's instructions. Primary antibodies, sources and associated dilutions are listed in Table S5. Anti-mouse IgG (Sigma-Aldrich, #A9044) or anti-rabbit IgG (Sigma-Aldrich; A0545) antibodies conjugated to horseradish peroxidase were used as secondary reagents at a dilution of 1:10,000. Clarity Western ECL chemiluminescent substrate (BioRad; #1705061) was used for detection on a BioRad ChemiDoc XRS+ imaging system according to the manufacturer's instructions.

In gel activity assays of OXPHOS complexes

Isolated mitochondria were solubilized in 1% digitonin in solubilization buffer (20 mM Bis-Tris pH 7.0, 50 mM NaCl, 10% (vol/vol) glycerol) for 10 min on ice, then centrifuged at 10,000 x *g* for 10 min at 4°C. The supernatant was transferred into a new tube containing 10x BN loading dye (500 mM ε-amino n-caproic acid, 100 mM Bis-Tris pH 7.0, 5% (wt/vol) Coomassie Brilliant Blue G-250) to a final 1x concentration and loaded into 4-13% BN-PAGE gels. Upon completion of BN-PAGE gel run, gels were extracted and incubated for 15-30 min or until color developed in either Complex I buffer (5 mM Tris-HCl, 0.1mg/mL NADH, 2.5 mg/mL nitrotetrazolium blue), Complex II buffer (5 mM Tris–HCl pH 7.4, 0.2 mM phenazine methasulfate, 20 mM succinate, 2.5 mg/mL nitrotetrazolium blue), Complex IV buffer (50 mM 3:30-Diamidobenzidine tetrahydrochloride (in 50 mM phosphate buffer (0.169 g sodium dihydrogen orthophosphate, 1.01 g disodium hydrogen orthophosphate, pH 7.4 and make up to 100 mL with distilled water)), 2 µg/mL catalase (in 50mM phosphate buffer), 1 mg/mL cytochrome *c*, 75 mg/mL sucrose) or Complex V buffer (35 mM Tris, 270 mM glycine, 14 mM MgSO4, 0.2% (w/v) Pb(NO3)2, 8 mM ATP pH 7.8). Once color developed, gels were transferred to fixing solutions (50% (v/v) methanol, 10% (v/v) acetic acid for Complex I, II and IV or 50% methanol (v/v) for Complex V). Post fixation, gels were imaged on either a scanner (Complex I, II or IV) or ChemiDoc™ XRS+ system (Bio-Rad).

Mitochondrial respiration analysis using the Seahorse Mito Stress Test

Mitochondrial respiration was analyzed using the Seahorse XF Cell Mito Stress Test Kit (Agilent #103015-100). Cells were plated at 20,000 cells per well (35,000 for *Mcl-1*$^{del/del}$ MEFs to account for proliferation defects) in Seahorse XF 96-well plates (cat# 103794-100) and incubated overnight at 37°C under normoxic conditions. The sensor cartridge was hydrated with 180 µL Seahorse XF Calibrant per well and incubated overnight at 37°C in a non-CO2 incubator.

On the day of the assay, Seahorse XF RPMI assay medium was prepared by supplementing RPMI with 1 mM pyruvate, 2 mM glutamine, and 10 mM glucose. The medium in the plates was replaced with 180 µL of the prepared assay medium, and plates were incubated at 37°C in a non-CO2 incubator for 45–60 min. Drug working solutions, including Etomoxir (50 µM final), Oligomycin (1.5 µM final), FCCP (2 µM final), and Rotenone/Antimycin A (0.5 µM final), were prepared and loaded into the sensor cartridge injection ports.

The Seahorse Mito Stress Test was conducted using the standard protocol to measure basal respiration, ATP production, maximal respiration, and non-mitochondrial respiration after the sequential injection of the prepared compounds. Following the assay, normalization to protein concentration was performed using a BCA assay. Data were analyzed with Seahorse Wave software.

Immunofluorescence analysis of adult liver sections

Liver samples were harvested, fixed and embedded in paraffin. Histological sections (5 µm) on slides were de-waxed and heat-induced epitope retrieval was performed using Tris-EDTA (10 mM Tris, 1 mM EDTA) pH 9.0 retrieval buffer. Slides were washed 2-3 times with tap water followed by 2 washes with PBS containing 0.1% Triton X-100 ("0.1% PBS-T"). Next, sections were blocked for 1 h at room temperature using 10% horse serum (Thermo Fisher, # 26050088) and 2% mouse-on-mouse (M.O.M) IgG blocking reagent (Vector Labs) diluted in 0.1% PBS-T. Sections were washed 3 times with PBS containing 0.01% Triton X-100 ("0.01% PBS-T"). This was followed by the application of primary antibodies (diluted in 0.01% PBS-T containing 1%

horse serum), which were incubated overnight at 4°C. The following primary antibodies were used: mouse anti-Glutamine Synthetase (1:200), rabbit anti-MCL-1 (1:100) (details for primary antibodies are listed in Table S5). The next morning, sections were washed 3 times with 0.01% PBS-T before incubating for 1 h at room temperature with secondary antibodies (also diluted in 0.01% PBS-T containing 1% horse serum). The following secondary antibodies were used: donkey anti-mouse IgG conjugated to AlexaFluor plus 488 (1:500, Thermo Fisher, #32766), donkey anti-rabbit IgG conjugated to AlexaFluor plus 647 (1:500, Thermo Fisher, #A32795). After incubation with secondary antibodies, sections were washed 3 times with 0.01% PBS-T and DAPI (Sigma-Aldrich, #28718-90-3) nuclear stain, diluted in PBS, was applied for 15-20 min at room temperature. Subsequently, sections were washed 3 times with 0.01% PBS-T, mounted with Fluoromount-G (Thermo Fisher, #00-4958-02) mounting medium and stored in the dark at 4°C until ready for imaging. Sections were imaged on a Zeiss LSM 980 confocal microscope and images processed using FIJI (v2.9.0).

Immunofluorescence analysis of MEFs

Cells were plated on coverslips at 80% confluency and stained with 200 nM MitoTracker Deep Red FM (Thermo Fisher, #M22426) in serum-free MEF medium for 30 min at 37°C. After incubation, cells were washed twice with serum-free medium and once with PBS. Cells were fixed with 4% paraformaldehyde at room temperature for 20 min, protected from light, and rinsed with PBS.

DAPI stain (1:500) in PBS was added to the cells for 5 min at room temperature, followed by three washes with PBS. Coverslips were removed, excess water wiped off, and 20 µL of anti-fade mounting oil was applied to a microscope slide. The coverslip was placed onto the slide, avoiding air bubbles, and the slide was imaged using a Zeiss LSM 980 confocal microscope and images processed using FIJI (v2.9.0).

Electron microscopy

Cells were fixed in 2.5% glutaraldehyde in 0.1 M cacodylate buffer for 1 h at room temperature followed by 3 x 10 min rinse in 0.1 M cacodylate buffer. Cells were osmicated in 1% osmium tetroxide in 0.1 M cacodylate buffer for 30 min at room temperature which was then reduced with 1.5% potassium ferrocyanide in 0.1 M cacodylate buffer for 30 min at room temperature. After rinsing with mQH_2O (3x10 min at room temperature) the cells were stained with 2.5% uranyl acetate (aqueous) overnight at 4°C. Cells were then rinsed as previously (mQH_2O for 3x10 mins at room temperature) and scrapped and pelleted for embedding in agarose (4% low melting point agarose, aqueous). Agarose blocks were de-hydrated with increasing concentrations of ethanol before final dehydration with 100% acetone (ethanol: 20%, 50%, 70%, 90%, 2 x 100%; acetone: 2 x 100%), aided by a microwave regime for 40 sec for each step (150 W, no vacuum, Pelco Biowave). Agarose blocks were then infiltrated with increasing concentrations of epon resin in acetone for 3 min for each step (25%, 50%, and 75%, 2 x 100%). Samples were left in fresh 100% resin overnight. After being transferred into silicone molds, blocks were polymerized in the oven at 60°C for 48 h. Sections of 70 nm were cut on a Leica UC7 ultramicrotome with a diamond knife (Diatome) and 150 mesh hexagonal copper grids. Transmission electron microscopy imaging was acquired on a Jeol JEM 1400-Plus at 80 kv. A combination of single snapshots and image montages were collected of cells using Jeol acquisition software (TEM Centre).

Histology

Whole embryos and fetuses were sacrificed and placed into 4% (w/v) paraformaldehyde (Sigma-Aldrich, #P6148)/PBS (E10.5-E14.5) or Bouin's fixative (Australian Biostain, #ABF2.5l) (E18) and subsequently embedded in paraffin. E10.5-E13.5 Embryos were embedded in 4% low-melting point agarose (Sigma-Aldrich, #A9414) before paraffin embedding. 5 µm serial transverse sections were obtained and stained with hematoxylin and eosin (H&E). Stained slides were scanned using a 20x brightfield slide scanner (Polaris) and examined and imaged using the CaseViewer Software (3DHISTECH) or the QuPath software.

To examine tissues from pups and mice, samples of the brain, heart, kidney, liver, small intestine, large intestine, caecum and colon were dissected, fixed in 10% formalin and embedded in paraffin. Histological sections (5 µm) were subsequently stained with H&E or cresyl violet acetate (Sigma-Aldrich, #C5042). Immunohistochemistry to detect activated (cleaved) caspase-3 was performed using an antibody detecting cleaved caspase-3 (Asp175, Cell Signaling, #9661). TUNEL assays were performed using the TUNEL detection kit (Abcam, #ab206386) according to the manufacturer's instructions. To detect fibrosis, formalin-fixed heart sections were stained with Masson's trichrome (Sigma-Aldrich, #HT15). To visualize the reticulin network, lymphocytes and macrophages formalin-fixed liver sections were stained with antibodies detecting reticulin (Sigma-Aldrich, #HT102A), CD45 (CST#70251) and F4/80 (CST#D2S9R), respectively.

To detect lipid accumulation, frozen sections were stained with OilRedO (Sigma-Aldrich, #1320-06-5). Stained slides were scanned using a 20x brightfield slide scanner (Polaris) and examined and imaged using the CaseViewer Software (3DHISTECH) or the QuPath software.

Triglyceride (TAG) measurement in liver tissues

Triglyceride levels were measured using the TAG assay kit (Abcam, # ab65336) according to the manufacturer's instructions. Briefly, samples were prepared and mixed with the assay reagents in a 96-well plate. The reactions were incubated at 37°C, and absorbance was measured at 570 nm wavelength using a microplate reader. TAG concentrations were calculated based on a standard curve generated with known concentrations of the provided standard.

Quantification and statistical analysis

Genotype distributions were analyzed by computing the cumulative binomial probability of being less or equal to the expected value (pbinom) using R (version 4.2.2, 2022-10-31, The R Foundation for Statistical Computing).

Kaplan Meyer mouse survival curves were analyzed by Log-Rank (Mantel Cox) test using statistics software (Prism 9 for Mac, version 9.4.1; GraphPad).

For *in vitro* cell survival and proliferation analysis, comparison of the percentages of cell survival and confluency, respectively, between different genotypes and treatments were analyzed using two-way ANOVA with subsequent Tukey's multiple comparison analysis (comparing to the wild-type samples) using statistics software (Prism 9 for Mac, version 9.4.1; GraphPad).

Mouse body weight data were compared using one-way ANOVA with subsequent Dunnet's multiple comparison analysis (comparing to the wild-type samples) using statistics software (Prism 9 for Mac, version 9.4.1; GraphPad).

Oxygen consumption rates (Seahorse) and ATP production rates (CTG) were analyzed using two-way ANOVA with subsequent Tukey's multiple comparison analysis (comparing to the wild-type samples) using statistics software (Prism 9 for Mac, version 9.4.1; GraphPad).

Serum AST, ALT, glucose, creatinine kinase and hepatic TAG levels as well as metabolite levels in the liver were analyzed using two-tailed, unpaired t-tests, with Welch's correction applied when variance equality was violated (based on F-test results) as indicated, using statistics software (Prism 9 for Mac, version 9.4.1; GraphPad).

For each experimental approach, the number of replicates (n) is defined as number of mice examined or repeat experiments performed and this is stated in the figures and/or figure legends. Data are presented as mean ±SEM as indicated in the figure legends.

Western blots were quantified using densitometry in Bio-Rad Image Lab software to measure band intensities, enabling the relative assessment of protein expression levels.

Quantification of activated (i.e. cleaved) caspase-3 (CC3) positive cells in histology sections was performed upon manually counting CC3 positive cells in n≥9 image frames from n≥3 samples each genotype.

Quantification of mitochondrial branching, mitochondrial count and mitochondrial area in immunofluorescent images was performed using the *MitochondriaAnalyser* plugin in Image J and analyzed using one-way ANOVA with subsequent Dunnet's multiple comparison analysis (comparing to the wild-type samples) using statistics software (Prism 9 for Mac, version 9.4.1; GraphPad).

Fig. S1

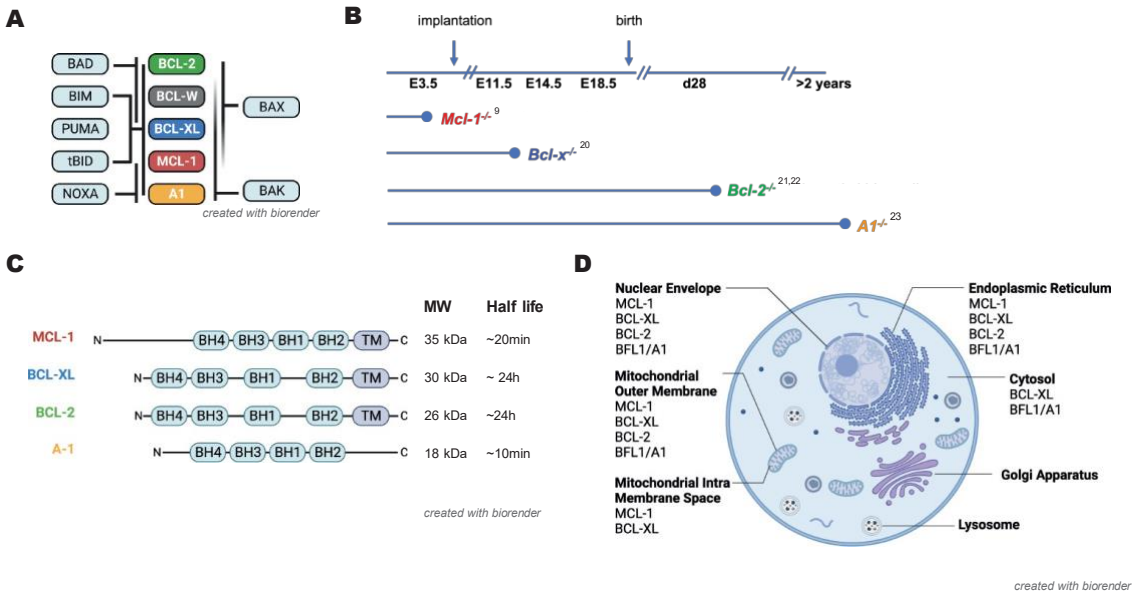

Fig. S1. Similarities and differences of the anti-apoptotic members of the BCL-2 protein family. (**A**) Schematic of the reported interactions of pro-apoptotic and anti-apoptotic members of the BCL-2 protein family. (**B**) Schematic of developmental lethality and survival of *Mcl-1*$^{-/-}$, *Bcl-x*$^{-/-}$, *Bcl-2*$^{-/-}$ and *A1*$^{-/-}$ mice. (**C**) Schematic presentation of the protein domains of the anti-apoptotic BCL-2 family members, BCL-2, BCL-XL, MCL-1 and A1. Respective molecular weights (MW) and half-lives of these proteins are indicated. (**D**) Schematic of the subcellular localization of the anti-apoptotic BCL-2 proteins, BCL-2, BCL-XL, MCL-1 and A1.

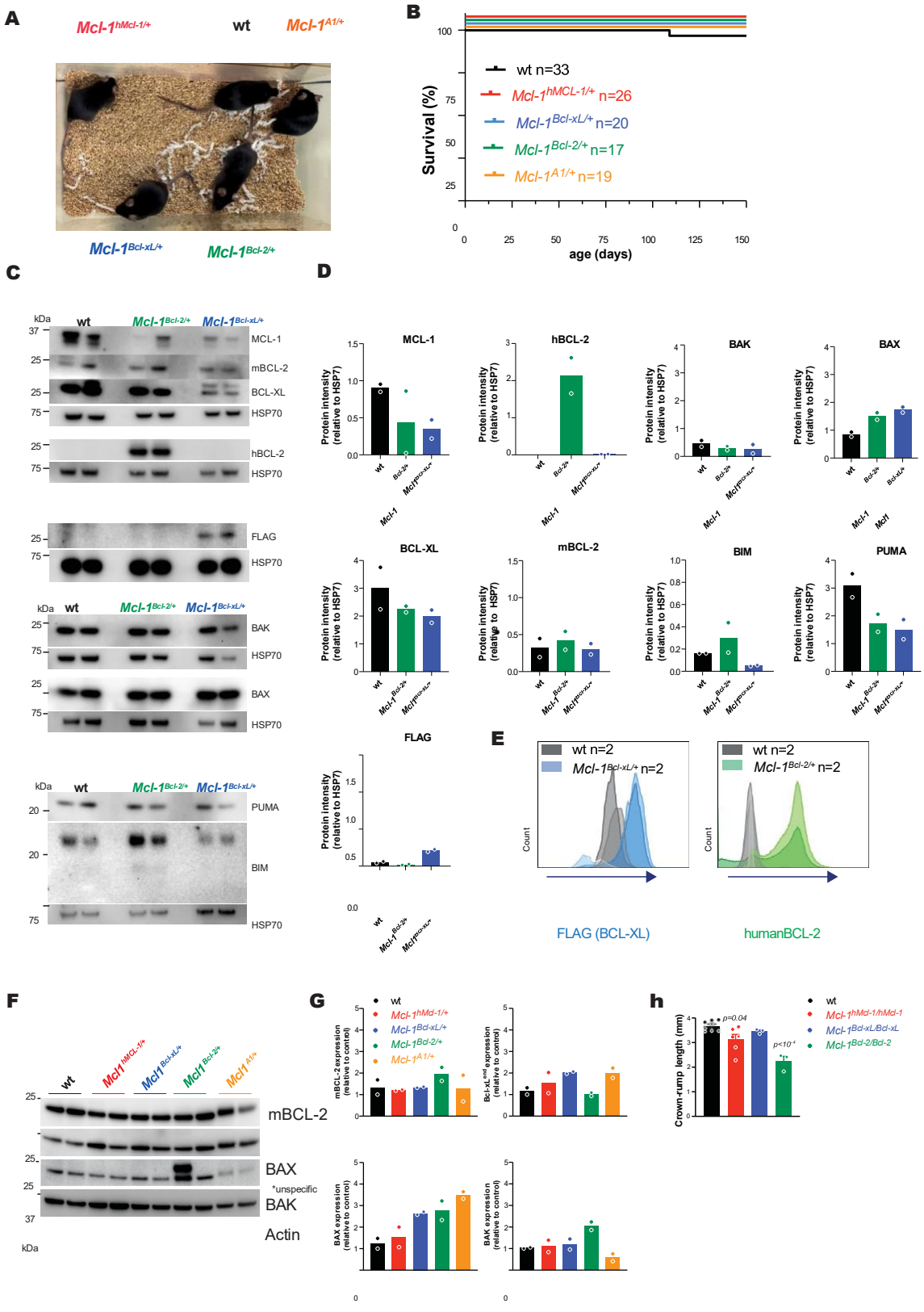

Fig. S2. Expression analysis of the knock-in proteins in cells from heterozygous mice. (A)

Fig S2 Representative image of heterozygous *Mcl-1*$^{hMcl\text{-}1/+}$, *Mcl-1*$^{Bcl\text{-}xL/+}$, *Mcl-1*$^{Bcl\text{-}2/+}$ and *Mcl-1*$^{A1/+}$ mice (female, age 50-70d). (**B**) Kaplan-Meyer survival curves for wild-type (n=33), *Mcl-1*$^{hMcl\text{-}1/+}$ (n=26), *Mcl-1*$^{Bcl\text{-}xL/+}$ (n=20), *Mcl-1*$^{Bcl\text{-}2/+}$ (n=17) and *Mcl-1*$^{A1/+}$ (n=19) mice. Log Rank (Mantle-Cox) test. No significant differences were observed. (**C**) Western blots of MEF lysates from E11.5 wild-type, *Mcl-1*$^{Bcl\text{-}xL/+}$ and *Mcl-1*$^{Bcl\text{-}2/+}$ embryos (n=2 per genotype, MEF isolates of individual embryos were loaded into individual lanes) detecting the indicated proteins. 6 protein

gels were run to allow the detection of proteins with the same protein size. Probing for HSP70 served as a protein loading control and is shown for individual membranes. (**D**) Densitometric quantification of the protein expression levels detected in the Western blots presented in (C). (**E**) Flow cytometric analysis of FLAG-BCL-XL and human BCL-2 expression in bone marrow cells from wild-type, *Mcl-1*$^{Bcl\text{-}xL/+}$ and *Mcl-1*$^{Bcl\text{-}2/+}$ mice using monoclonal antibodies detecting FLAG or human BCL-2, respectively (n=2 mice per genotype). (**F)** Western blot of E10.5 embryo lysates from wild-type (wt), *Mcl-1*$^{hMcl\text{-}1/+}$, *Mcl-1*$^{Bcl\text{-}xL/+}$, *Mcl-1*$^{Bcl\text{-}2/+}$ and *Mcl-1*$^{A1/+}$ embryos (n=2 per genotype) detecting the indicated proteins. (**G**) Densitometric quantification of the protein expression levels detected in the Western blots presented in (F) and densitometric quantification of endogenous BCL-XL expression detected in the Western blot presented in Fig. 1B. (**H**) Crown-rump length measurements of E10.5 wild-type (wt; n=8), *Mcl-1*$^{hMcl\text{-}1/hMcl\text{-}1}$ (n=6), *Mcl-1*$^{Bcl\text{-}xL/Bcl\text{-}xL}$ (n=3), *Mcl-1*$^{Bcl\text{-}2/Bcl\text{-}2}$ (n=3) embryos. Embryos were measured from snout to the base of the tail to assess developmental size at E10.5. One-way ANOVA with Dunnet's multiple comparison to wild-type; p-values shown.

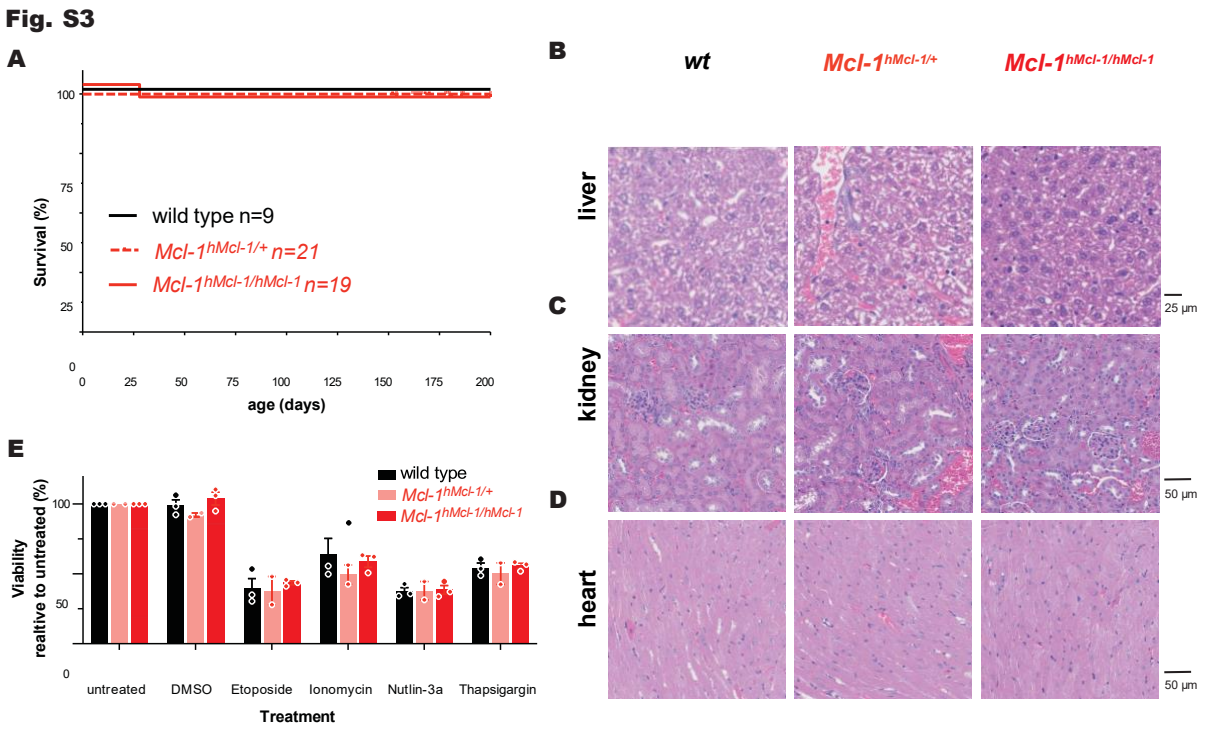

Fig. S3. *Mcl-1*$^{hMcl\text{-}1/hMcl\text{-}1}$ control mice are indistinguishable from wild-type mice. (**A**) Kaplan-Meyer survival curves for wild-type (n=9), *Mcl-1*$^{hMcl\text{-}1/+}$ (n=21) and *Mcl-1*$^{hMcl\text{-}1/hMcl\text{-}1}$ (n=19) mice. Log Rank (Mantle-Cox) test. No significant differences were observed. (**B-D**) Representative H&E-stained sections of the liver (**B**), kidney (**C**) and heart (**D**) from wild-type (left panel), *Mcl-1*$^{hMcl\text{-}1/+}$ (middle panel) and *Mcl-1*$^{hMcl\text{-}1/hMcl\text{-}1}$ (right panel) mice (50-60 days old). (**E**) Survival analysis (MTT assay) of primary murine embryonic fibroblasts (MEFs), generated from wild-type, *Mcl-1*$^{hMcl\text{-}1/+}$ and *Mcl-1*$^{hMcl\text{-}1/hMcl\text{-}1}$ E11.5 embryos (n=2 per genotype), treated with DMSO (ctrl), etoposide (20 µg/mL), ionomycin (2.5 µg/mL), the MDM2 inhibitor nutlin-3A (20 µM), thapsigargin (500 pM) for 48h. Data shown as mean ± SEM from ≥2 independent experiments, each performed in triplicates. Two-way ANOVA with Tukeys's multiple comparison. No significant differences were observed.

Fig. S4

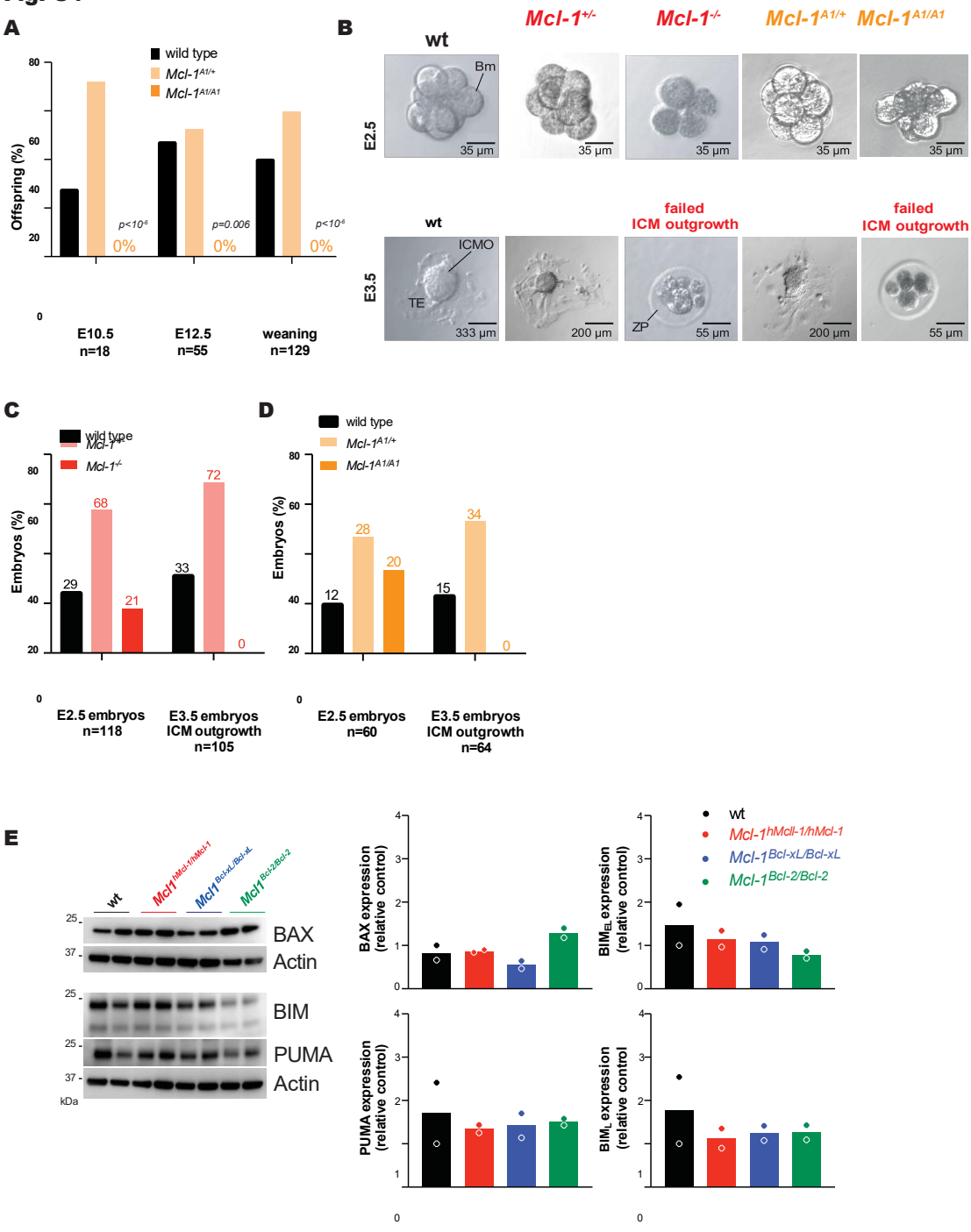
A
wild type
Mcl-1A1/+
Mcl-1A1/A1
Offspring (%)
p<10-6
0%
p=0.006
0%
p<10-6
0%
E10.5 n=18
E12.5 n=55
weaning n=129
B
wt
Mcl-1+/-
Mcl-1-/-
Mcl-1A1/+
Mcl-1A1/A1
E2.5
Bm
35 µm
E3.5
ICMO
TE
333 µm
200 µm
failed ICM outgrowth
ZP
55 µm
C
wild type
Mcl-1+/-
Mcl-1-/-
Embryos (%)
29
68
21
33
72
0
E2.5 embryos n=118
E3.5 embryos ICM outgrowth n=105
D
wild type
Mcl-1A1/+
Mcl-1A1/A1
12
28
20
15
34
0
E2.5 embryos n=60
E3.5 embryos ICM outgrowth n=64
E
wt
Mcl1hMcl-1/hMcl-1
Mcl1Bcl-xL/Bcl-xL
Mcl1Bcl-2/Bcl-2
kDa
BAX
Actin
BIM
PUMA
Actin
BAX expression (relative control)
BIMEL expression (relative control)
PUMA expression (relative control)
BIML expression (relative control)
wt
Mcl-1hMcl-1/hMcl-1
Mcl-1Bcl-xL/Bcl-xL
Mcl-1Bcl-2/Bcl-2
F
E12.5

Fig. S4

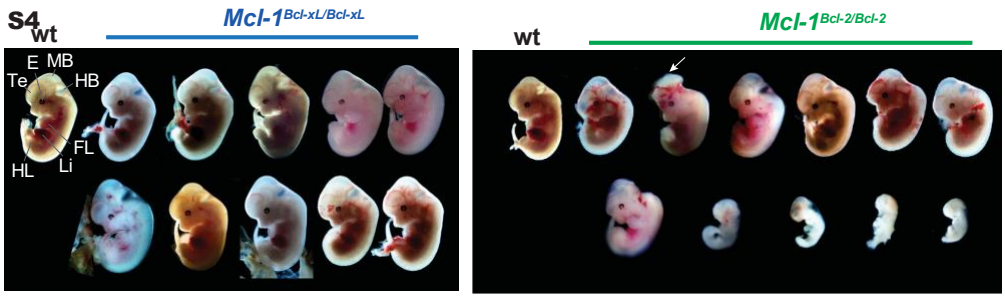

Fig. S4. Assessment of *Mcl-1*$^{A1/A1}$, *Mcl-1*$^{Bcl\text{-}xL/Bcl\text{-}xL}$ and *Mcl-1*$^{Bcl\text{-}2/Bcl\text{-}2}$ embryos. (**A**) Offspring genotype frequency at E10.5 (n=18), E12.5 (n=55) and weaning (n=129) from *Mcl-1*$^{A1/+}$ intercrosses (C57BL/6), analyzed using cumulative binomial probability (p-values and n indicated). E10.5 data from Fig. 1F are included for comparison. (**B**) Representative images showing wild-type, *Mcl-1*$^{+/-}$, *Mcl-1*$^{-/-}$, *Mcl-1*$^{A1/+}$ and *Mcl-1*$^{A1/A1}$ E2.5 embryos (FVBxBALB/cxC57BL/6, upper panels). Inner cell mass (ICM) outgrowth was imaged after 5 days of culture of E3.5 blastocysts (lower panel). (**C-D**) Offspring genotype frequencies at E2.5 and E3.5 and ICM outgrowths from E3.5 embryos from intercrosses of (**C**) *Mcl-1*$^{+/-}$ and (**D**) *Mcl-1*$^{A1/+}$ mice (FVBxBALB/cxC57BL/6), analyzed using cumulative binomial probability (p-values and n indicated). (**E**) Western blot of E10.5 embryo lysates from wild-type, *Mcl-1*$^{hMcl\text{-}1/hMcl\text{-}1}$, *Mcl-1*$^{Bcl\text{-}xL/Bcl\text{-}xL}$ and *Mcl-1*$^{Bcl\text{-}2/Bcl\text{-}2}$ embryos (n=2 per genotype, one embryo lysate per lane) detecting the indicated proteins (left) and densitometric quantification of protein expression (right). (**F**) Representative images showing wild-type (n=2), *Mcl-1*$^{Bcl\text{-}xL/Bcl\text{-}xL}$ (n= 10) and *Mcl-1*$^{Bcl\text{-}2/Bcl\text{-}2}$ (n= 11) embryos at embryonic day E12.5. **Labeling**: E, eye; e, ear; FL, forelimb (forelimb bud, E11.5 and E12.5); HB, hindbrain; HL, hindlimb bud; Li, liver; MB, midbrain; PA, pharyngeal arches; Te, telencephalon. Arrowhead indicates collapsed telencephalic vesicle. Arrows indicate exencephaly.

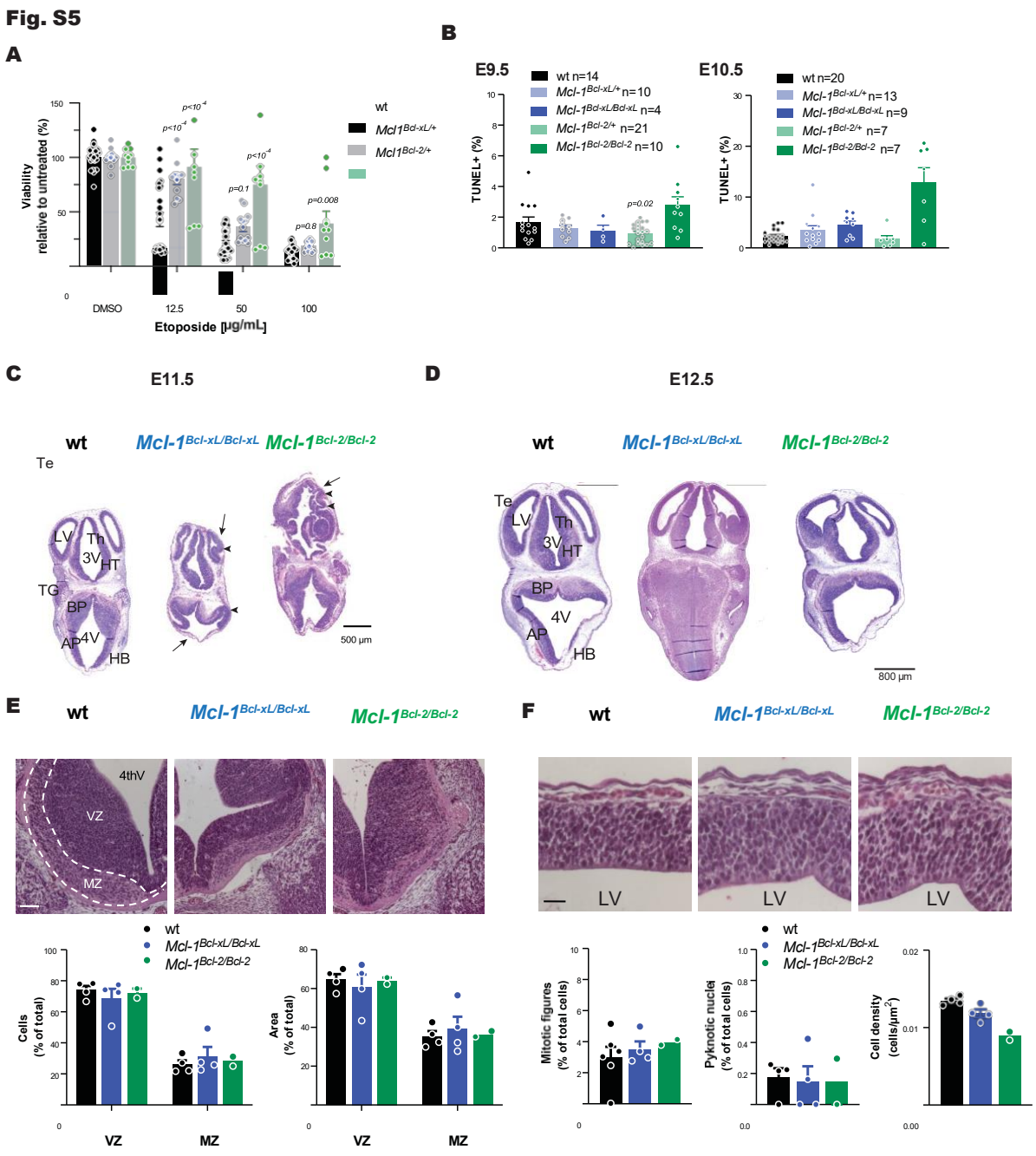

Fig. S5. Apoptosis analysis in *Mcl-1*$^{Bcl\text{-}xL}$ and *Mcl-1*$^{Bcl\text{-}2}$ embryos. (**A**) Survival analysis (MTT assay) of primary murine embryonic fibroblasts (MEFs) generated from wild-type, *Mcl-1*$^{hMcl\text{-}1/+}$ and *Mcl-1*$^{hMcl\text{-}1/hMcl\text{-}1}$ E11.5 embryos (n=2 per genotype) treated with etoposide for 48h. Data shown as mean ± SEM, ≥2 experiments in triplicates. Two-way ANOVA with Tukey's multiple comparison; p-values shown. (**B**) Percentages of TUNEL+ cells in E9.5 (left panel) and E10.5 embryos (right panel) of the indicated genotypes and n numbers. Data shown as mean ± SEM. One-way ANOVA with Dunnet's multiple comparison; p-values (when significant) and n numbers shown. (**C-D**) Representative H&E-stained serial sections of the head at the forebrain/hindbrain level of *Mcl-1*$^{Bcl\text{-}xL/Bcl\text{-}xL}$ and *Mcl-1*$^{Bcl\text{-}2/Bcl\text{-}2}$ embryos at embryonic day (**C**) E11.5 and (**D**) E12.5, with wild-type littermates for comparison. (**E**) Representative hindbrain

sections from wild-type, *Mcl-1*$^{Bcl\text{-}xL/Bcl\text{-}xL}$ and *Mcl-1*$^{Bcl\text{-}2/Bcl\text{-}2}$ E11.5 embryos (top rows). Percentage of cells (bottom left) and area (bottom right) of the ventricular and marginal zones were quantified in wild-type (n=4), *Mcl-1*$^{Bcl\text{-}xL/Bcl\text{-}xL}$ (n=3) and *Mcl-1*$^{Bcl\text{-}2/Bcl\text{-}2}$ (n=2) E11.5 embryos. Data shown as mean ± SEM except for the *Mcl-1*$^{Bcl\text{-}2/Bcl\text{-}2}$ data where error bars cannot be

displayed due to n=2. One-way-ANOVA with Dunnett's multiple comparison test. No significant differences were observed between wild-type (n=4) and *Mcl-1*$^{Bcl\text{-}xL/Bcl\text{-}xL}$ (n=3). (**F**) Representative images of the dorsal telencephalon, the developing cerebral cortex, in cranial sections of wild-type, *Mcl-1*$^{Bcl\text{-}xL/Bcl\text{-}xL}$ and *Mcl-1*$^{Bcl\text{-}2/Bcl\text{-}2}$ E11.5 embryos (top). Quantification of mitotic figures (bottom left), pyknotic nuclei (bottom middle), and cell density (bottom right) was performed as in (E). One-way-ANOVA with Dunnett's multiple comparison test. No significant differences were observed between wild-type (n=4) and *Mcl-1*$^{Bcl\text{-}xL/Bcl\text{-}xL}$ (n=3). **Labeling**: 3V, third ventricle; 4V, mesencephalic vesicle (future 4th ventricle); AP and BP, alar and basal plate of the hindbrain; Ctx, developing cortes; E, eye; HB, hindbrain; Hi, developing hippocampus; HT, hypothalamus (diencephalon); LV, telencephalic vesicle or lateral ventricle; MC, mouth cavity; **MZ**, **marginal zone**; NC, nasal cavity; PS, palatal shelf, here elevated; St, striatum; TG, trigeminal ganglion; Th, thalamus (diencephalon); Te, telencephalon; To, tongue. **VZ**, **Ventricular Zone.** Arrows indicate collapsed telencephalic and mesencephalic vesicles. Arrowheads indicate neuroepithelial folds that would appear as ridges when external morphology was examined.

Fig. S6

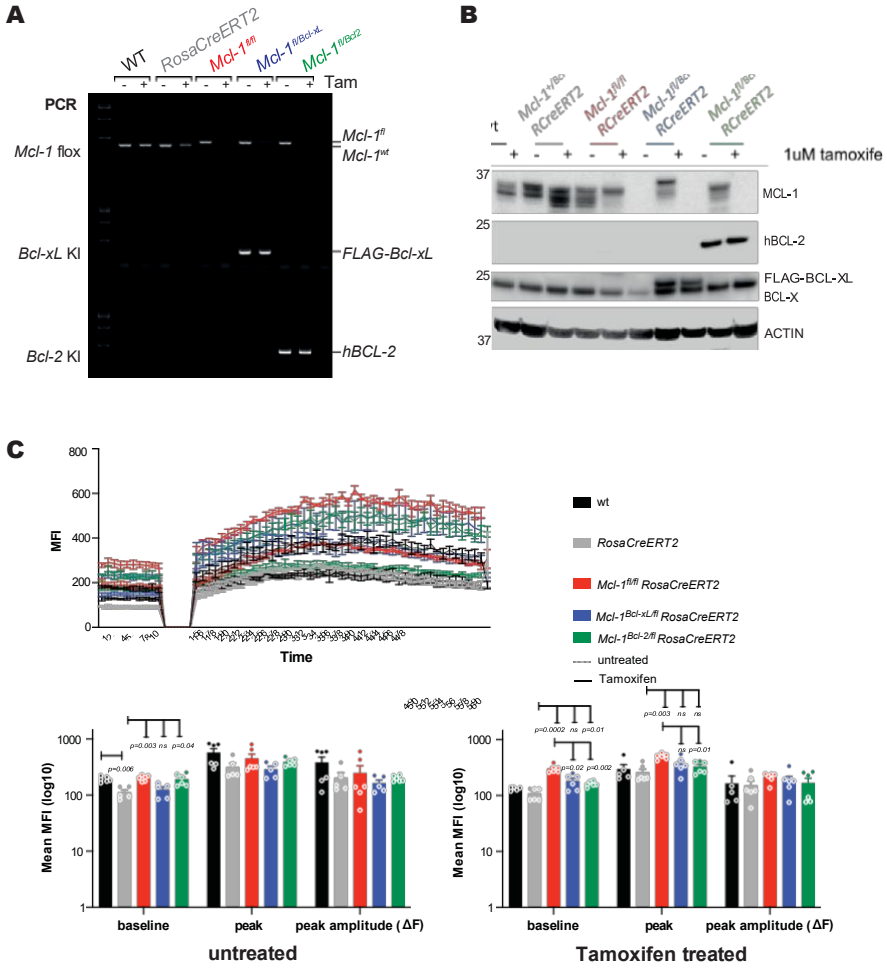

Fig. S6 Conditional CreERT2-inducible MEFs. Representative PCR analysis (**A**) and Western blot analysis (**B**) of *Mcl-1*^{fl} deletion upon treatment with 4-Hydroxytamoxifen (Tam, 1 µM, 72 h) in MEFs of the indicated genotypes. (**C**) Calcium flux analysis in MEFs of the indicated genotype performed by flow cytometry. Cells were treated with ionomycin (4 ng/mL) to release calcium storage 10 sec after start of recording (top panel). Baseline levels, peak levels and peak amplitude were calculated in MEFs of the indicated genotypes, either left untreated (bottom left) or treated with 4-Hydroxytamoxifen (1 µM) and cultured as "del" lines for >1 week (bottom right). Data are presented as mean ±SEM from 2 independent experiments, each performed in triplicates. Two-way ANOVA with Tukey's multiple comparison; p-values shown.

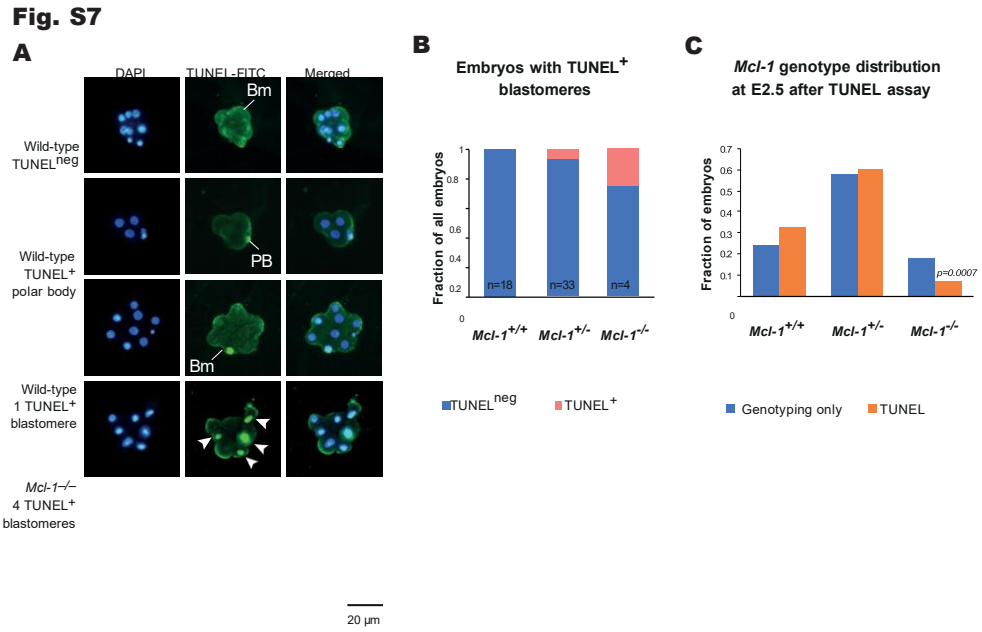

Fig. S7. *Mcl-1*$^{-/-}$ E2.5 embryos (FVBxBALB/cxC57BL/6 background) die due to increased apoptosis. (**A)** Immunofluorescence images of TUNEL$^+$ cells in *Mcl-1*$^{+/+}$ and *Mcl-1*$^{-/-}$ E2.5 embryos (FVBxBALB/ cxC57BL/6) counterstained with DAPI (blue). Embryos were genotyped post imaging. 1st row, negative, background signal (dull green, non-nuclear); 2nd row, TUNEL$^+$ polar body (bright green, small, no cytoplasm); 3rd row, embryo with a single TUNEL$^+$ blastomere (bright green, large with cytoplasm compared to polar body); 4th row, *Mcl-1*$^{-/-}$ embryo with four TUNEL$^+$ blastomeres. (**B**), Offspring genotype frequency at E2.5 embryos from intercrosses of *Mcl-1*$^{+/-}$ mice (FVBxBALB/cxC57BL/6), either directly after recovery (genotyping only) or after TUNEL staining (TUNEL), analyzed computing the cumulative binomial probability; p-values and n shown. Loss of *Mcl-1*$^{-/-}$ embryos compared to the direct genotyping (p=0.0007) suggests that *Mcl-1*$^{-/-}$ embryos failed to adhere to slides during TUNEL procedure. (**C**) Embryo fraction with TUNEL$^+$ blastomeres among *Mcl-1*$^{+/+}$ (n=18), *Mcl-1*$^{+/-}$ (n=33) and *Mcl-1*$^{-/-}$ (n=4) embryos (FVBxBALB/cxC57BL/6). **Labeling**: Bm, blastomere; ICMO, inner cell mass outgrowth; TE, trophectoderm; ZP, zona pellucida; PB, polar body. Arrowheads indicate TUNEL+ blastomeres in the *Mcl-1*$^{-/-}$ embryo.

Fig. S8

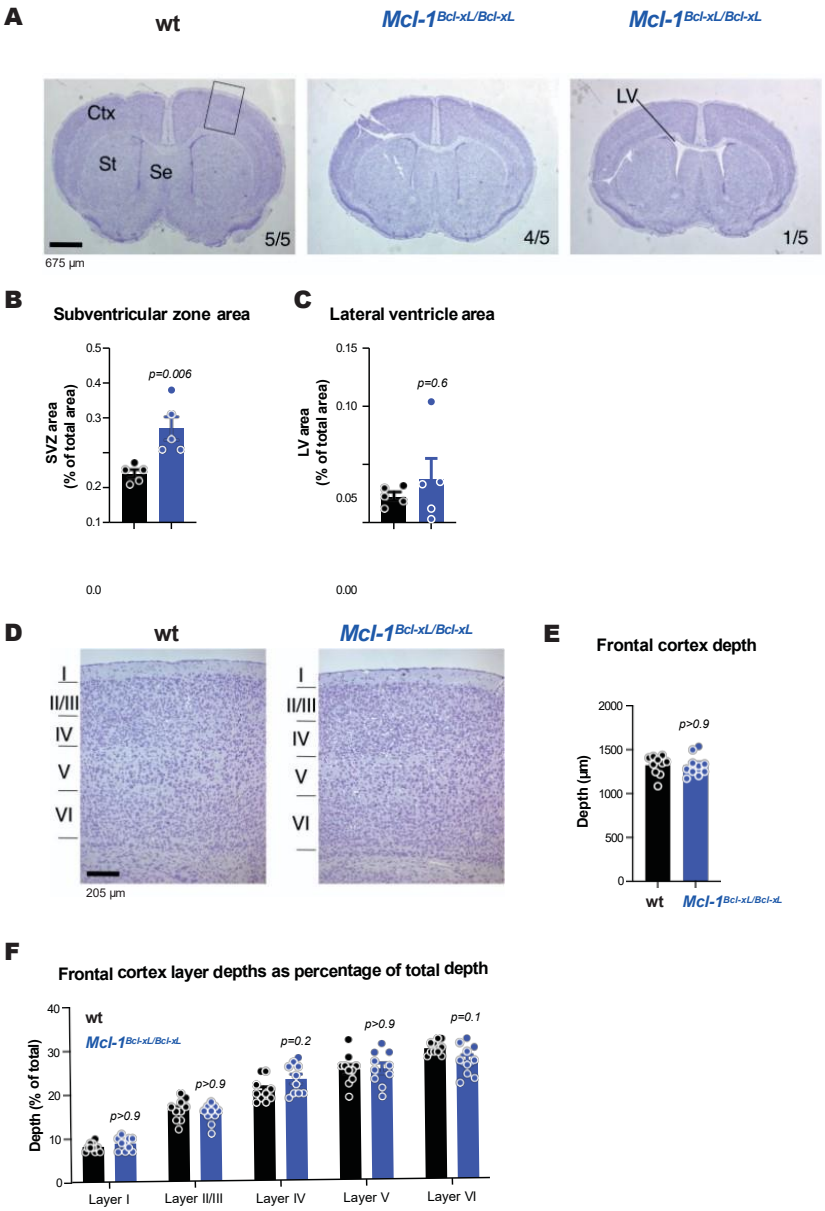

Fig. S8. Enlarged forebrain subventricular zone neurogenic region in *Mcl-1*$^{Bcl\text{-}xL/Bcl\text{-}xL}$ early postnatal mice. (**A-G**) Cresyl violet-stained forebrain sections (**A,D**) and morphometric analysis (**B,C,E,F**) of the forebrains at the level of the frontal cortex of wild-type (wt) and *Mcl-1*$^{Bcl\text{-}xL/Bcl\text{-}xL}$ pups (FVBxBALB/cxC57BL/6). (**A**) Cresyl violet-stained forebrain sections of wild-type and *Mcl-1*$^{Bcl\text{-}xL/Bcl\text{-}xL}$ pups. One of five *Mcl-1*$^{Bcl\text{-}xL/Bcl\text{-}xL}$ pups had enlarged lateral ventricles (right panel), while the others were similar to wt (middle panel). (**B**) Size of the subventricular zone neurogenic region. (**C**) Area of the lateral ventricles. Note, one *Mcl-1*$^{Bcl\text{-}xL/Bcl\text{-}xL}$ is an outlier. This pup displayed enlarged lateral ventricles, also shown in **(**A**).** The lateral ventricle size of the other 4 *Mcl-1*$^{Bcl\text{-}xL/Bcl\text{-}xL}$ pups (FVBxBALB/cxC57BL/6) did not differ from the 5 wt controls**.** (**D**) Magnifications of frontal cortical layers I-VI, as indicated in forebrain sections (A). (**E**) Total depth of the cerebral cortex. (**F**) Depth of the cortical layers as percentage of the total depth of wild-type (n=5) and *Mcl-1*$^{Bcl\text{-}xL/Bcl\text{-}xL}$ (n=5) pups (ages 15 to 23 days old;

F1 x B6 (BALB/cxC57BL/6). Data shown as mean ± SEM. Circles represent individual pups (B,C) or two hemispheres each of 5 individual pups per genotype (E,F). Two-tailed Student's t-test (B,C) and one-way-ANOVA with Dunnett's multiple comparison test (F). p-values shown.

Labeling: I to VI, cortical layers | to VI. Ctx, cortex; LV, lateral ventricle; Se, septum, St, striatum. Scale bar = 675 μm (A) and 205 μm (E).

Fig. Se

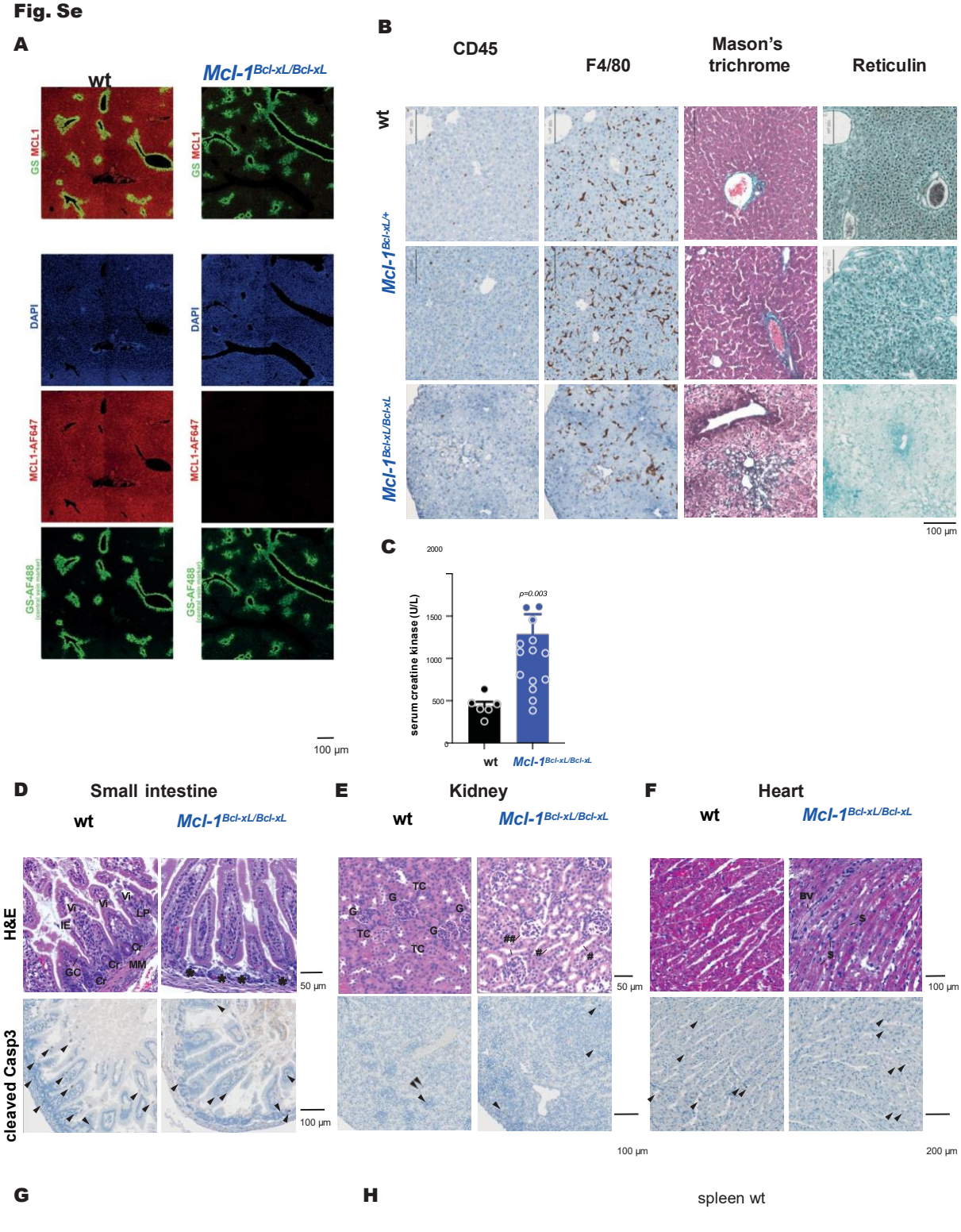
A
wt
Mcl-1Bcl-xL/Bcl-xL
GS MCL1
DAPI
MCL1-AF647
GS-AF488
100 µm
B
CD45
F4/80
Mason's trichrome
Reticulin
wt
Mcl-1Bcl-xL/+
Mcl-1Bcl-xL/Bcl-xL
100 µm
C
serum creatine kinase (U/L)
p=0.003
2000
1500
1000
500
0
wt
Mcl-1Bcl-xL/Bcl-xL
D
Small intestine
wt
Mcl-1Bcl-xL/Bcl-xL
H&E
cleaved Casp3
Vi
LP
IE
Cr
GC
MM
50 µm
100 µm
E
Kidney
wt
Mcl-1Bcl-xL/Bcl-xL
TC
G
50 µm
100 µm
F
Heart
wt
Mcl-1Bcl-xL/Bcl-xL
BV
S
100 µm
200 µm
G
Liver
Heart
H
wt
Mcl-1Bcl-xL/Bcl-xL
spleen wt
positive ctrl

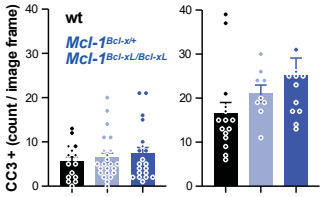
wt
Mcl-1Bcl-x/+
Mcl-1Bcl-xL/Bcl-xL
CC3+ (count / image frame)
0
10
20
30
40

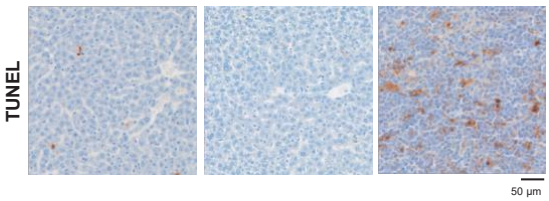
TUNEL
50 µm

Fig S9. *Mcl-1*$^{Bcl\text{-}xL/Bcl\text{-}xL}$ pups present with damage to multiple organs. (**A**) Representative immunofluorescent images of liver sections from wild-type (wt) and *Mcl-1*$^{Bcl\text{-}xL/Bcl\text{-}xL}$ pups (FVBxBALB/cxC57BL/6, 21-day-old), stained for MCL-1 (red), Central vein, expressing glutamine synthetase (GS) (green); and DAPI (blue). (**B**) Representative liver sections from wild-type (wt, left panel), *Mcl-1*$^{Bcl\text{-}xL/+}$ (middle panel) and *Mcl-1*$^{Bcl\text{-}xL/Bcl\text{-}xL}$ (bottom panel) pups (FVBxBALB/cxC57BL/6) stained for reticulin, Masson's Trichrome, F4/80 (macrophages) and CD45 (leukocytes). (**C**) Serum concentrations of creatine kinase from wt (n=6) and *Mcl-1*$^{Bcl\text{-}xL/Bcl\text{-}xL}$ (n=14) pups (FVBxBALB/cxC57BL/6). Data shown as mean ± SEM. Welch's t-test with; p-values shown. (**D-F**) Representative H&E- (top row) and cleaved (activated) caspase3 (cleaved Casp3)-stained sections (bottom row) from wt (left panel) and *Mcl-1*$^{Bcl\text{-}xL/Bcl\text{-}xL}$ pups (right panel) (FVBxBALB/cxC57BL/6) of the small intestine (**D**), kidney (**E**) and heart myocardium (**F**). Black arrowheads: apoptotic (cleaved caspase-3 positive) cells. # enlarged renal tubule lumina enclosed by degenerating renal tubular cells. ## degenerating glomeruli. $ degenerating cardiomyocytes. (**G**) Quantification of histological sections stained for cleaved Caspase 3 (CC3) in the liver (left panel) and heart (right panel) of wild-type (wt), *Mcl-1*$^{Bcl\text{-}xL/+}$ and *Mcl-1*$^{Bcl\text{-}xL/Bcl\text{-}xL}$ pups (FVBxBALB/cx C57BL/6). (**H**) Representative images of TUNEL stained liver sections from wt and *Mcl-1*$^{Bcl\text{-}xL/Bcl\text{-}xL}$ pups (FVBxBALB/cxC57BL/6, 21-day-old). Wt spleen section used as positive control, showing TUNEL^{+} cells. **Labeling**: BV, blood vessel; Cr, crypts, also termed glands; IE, intestinal epithelium; G, glomeruli; GC, goblet cell; LP, lamina propria; MM, muscularis mucosae; TC, tubular cells; Vi, villi.

Fig. S10

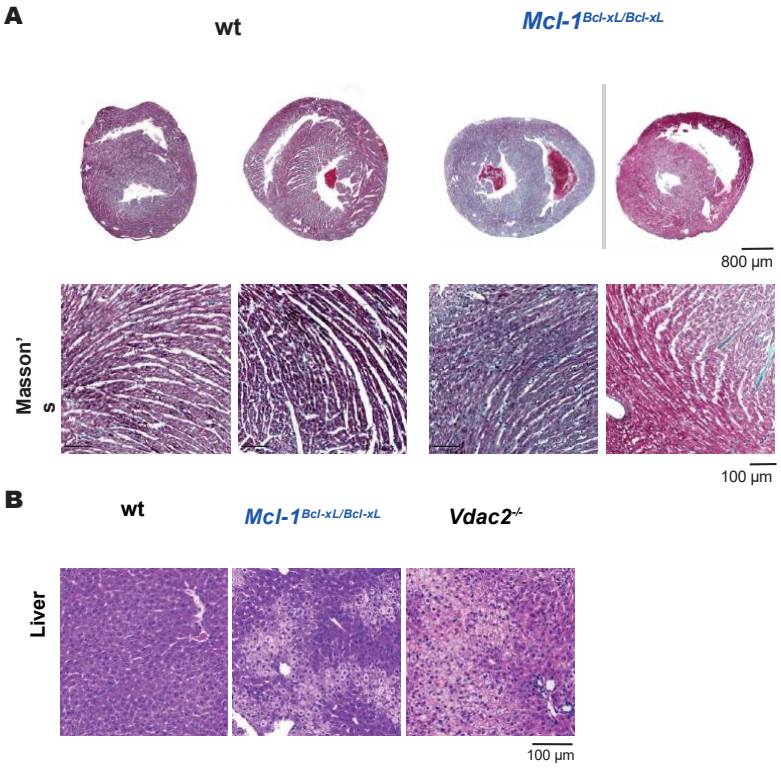

Fig S10. *Mcl-1*$^{Bcl\text{-}xL/Bcl\text{-}xL}$ pups present with severe organ damage. (**A**) Representative Mason's trichrome-stained heart sections (myocardium) from wild-type (wt, n=2, left panels) and *Mcl-1*$^{Bcl\text{-}xL/Bcl\text{-}xL}$ (n=2, right panels) pups (FVBxBALB/cxC57BL/6, 21-day-old). (**B**) Representative H&E-stained liver sections from wt (left panel), *Mcl-1*$^{Bcl\text{-}xL/Bcl\text{-}xL}$ (middle panel) and *Vdac2*$^{-/-}$ pups (right panel).

Fig. S11

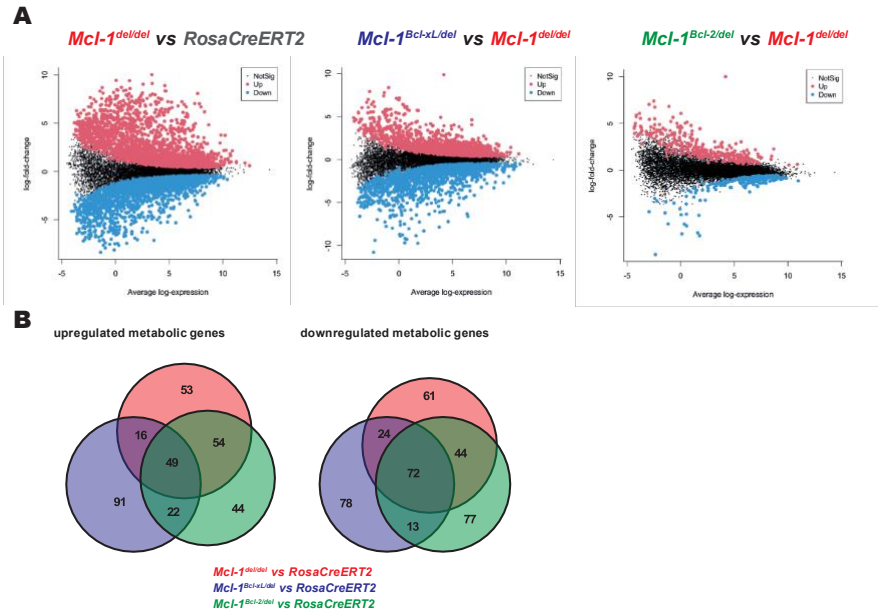

Fig S11. The regulation of metabolic genes is more similar between *Mcl-1*$^{del/del}$ MEFs and *Mcl-1*$^{Bcl-2/del}$ MEFs than between *Mcl-1*$^{del/del}$ MEFs and *Mcl-1*$^{Bcl-xL/del}$ MEFs. (**A,B**) RNAseq analysis performed in *Mcl-1*$^{del/del}$, *Mcl-1*$^{Bcl-xL/del}$, *Mcl-1*$^{Bcl-2/del}$ and control *RosaCreERT2* MEFs (n=5 each genotype). (**A**) MA-plot showing differentially expressed (DE) genes when comparing *Mcl-1*$^{del/del}$ MEFs with *RosaCreERT2*, *Mcl-1*$^{Bcl-xL/del}$ or *Mcl-1*$^{Bcl-2/del}$ MEFs, as indicated. (**B**) Venn diagram showing the overlap of DE genes in the metabolic pathway as identified by KEGG analysis in *Mcl-1*$^{del/del}$ MEFs, *Mcl-1*$^{Bcl-xL/del}$ and *Mcl-1*$^{Bcl-2/del}$ MEFs, each compared to *RosaCreERT2* MEFs. Gene IDs are presented in table S2.

Fig. S12

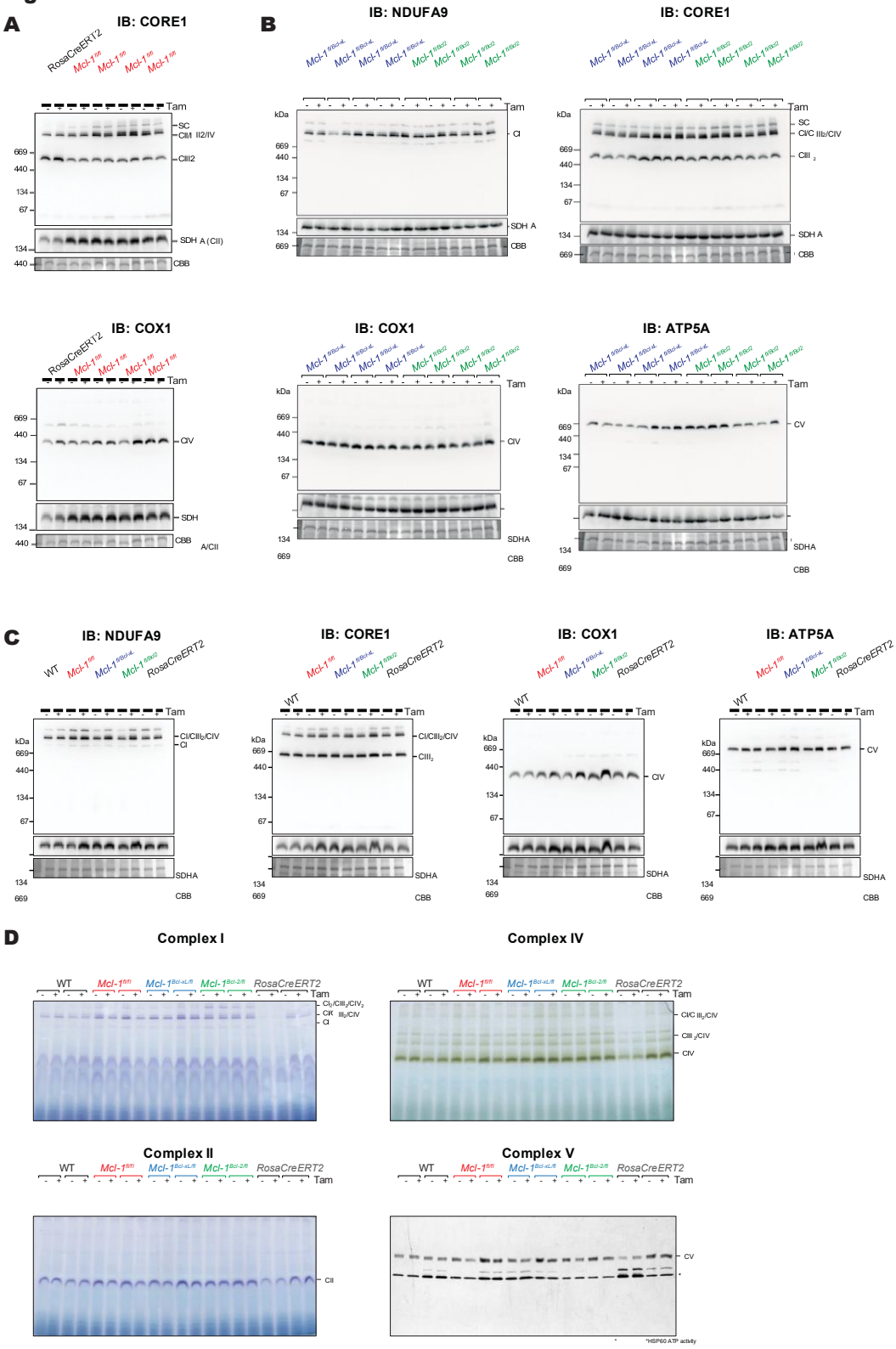
A
IB: CORE1
RosaCreERT2
Mcl-1fl/fl
Tam
SC
CIII2/IV
CIII2
SDH A (CII)
CBB
B
IB: NDUFA9
IB: CORE1
Mcl-1fl/Bcl-xL
Mcl-1fl/Bcl-2
CI
SDH A
IB: COX1
IB: ATP5A
CIV
CV
SDHA
A/CII
C
IB: NDUFA9
IB: CORE1
IB: COX1
IB: ATP5A
WT
CI/CIII2/CIV
CIII2
D
Complex I
Complex IV
Complex II
Complex V
CII
CV
*HSP60 ATP activity
E
IB:NDUFA9
IB:CORE1
IB:COX1
IB:ATP5A
wt
Mcl-1Bcl-xL/Bcl-xL
Mcl-1-/-
CI/II
CII

Fig. S12

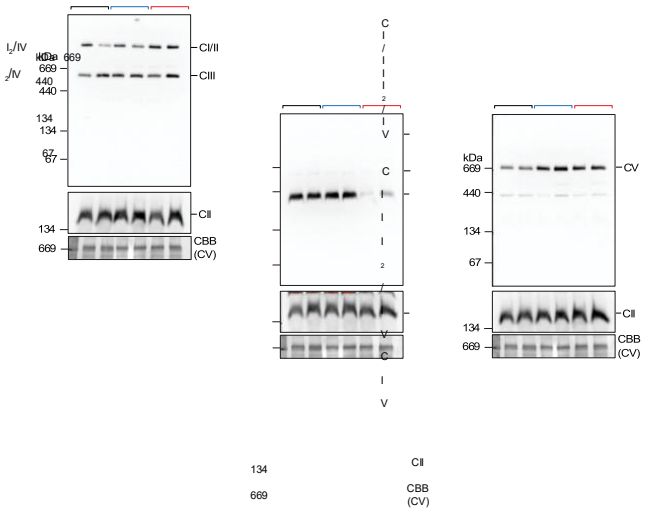

Fig S12. BCL-XL but not BCL-2 can substitute for the function of MCL-1 in OXPHOS. (**A-C**) Blue native PAGE and immunoblot analysis for respiratory complexes (using antibodies to COX1, NDUFA9, CORE1, ATP5A or SDHA on isolated mitochondria from (**A**) *RosaCreERT2* (n=1) and *Mcl-1*$^{fl/fl}$*RosaCreERT2* (n=4) as well as (**B**) *Mcl-1*$^{Bcl\text{-}xL/fl}$*RosaCreERT2* (n=4) and *Mcl-1*$^{Bcl\text{-}2/fl}$*RosaCreERT2* (n=4) MEFs that had been left untreated or treated with 4-Hydroxytamoxifen (TAM, 1µM, t=96h) and (**C**) wild type (wt), *RosaCreERT2, Mcl-1*$^{fl/fl}$*RosaCreERT2*, *Mcl-1*$^{Bcl\text{-}xL/fl}$*RosaCreERT2* and *Mcl-1*$^{Bcl\text{-}2/fl}$*RosaCreERT2* MEFs that had been left untreated or treated with TAM (1 µM) and cultured as *Mcl-1*^{del} lines for >1 month. Coomassie-stained complex V (CV) serves as a loading control. (**D**) In-gel activity assays of mitochondrial electron transport chain complexes I, II, IV, V. Mitochondrial proteins (50 µg per lane) were isolated from wild type (WT), *RosaCreERT2, Mcl-1*$^{fl/fl}$*RosaCreERT2*, *Mcl-1*$^{Bcl\text{-}xL/fl}$*RosaCreERT2* and *Mcl-1*$^{Bcl\text{-}2/fl}$*RosaCreERT2* MEFs (n=2 each genotype) that had been left untreated or treated with TAM (t=96h, 1 µM). The activity of Complex I was assessed using NADH and nitroblue tetrazolium (NBT). Complex II activity was detected using succinate and phenazine methosulfate (PMS), while Complex IV activity was assessed using a diaminobenzidine (DAB) staining method. Complex V activity (ATP synthase) was detected by coupling ATP hydrolysis to the precipitation of lead phosphate using a Pb(NO3)2 staining method. (**E**) Blue native PAGE and immunoblot analysis for respiratory complexes (using antibodies to COX1, NDUFA9, CORE1, ATP5A or SDHA (SDHA shown in lower box labelled CII)) on isolated mitochondria from wild-type, *Mcl-1*$^{-/-}$ and *Mcl-1*$^{Bcl\text{-}xL/Bcl\text{-}xL}$ MEFs (n=2 each genotype). Note, *Mcl-1*$^{Bcl\text{-}xL/Bcl\text{-}xL}$ MEFs have been generated from E12.5 *Mcl-1*$^{Bcl\text{-}xL/Bcl\text{-}xL}$ embryos in the absence of MCL-1. *Mcl-1*$^{-/-}$ MEFs have been generated by viral CRE transduction of *Mcl-1*$^{fl/fl}$ MEFs and puromycin selection of vector transduced cells. *Mcl-1*$^{-/-}$ MEFs were cultured for a prolonged time prior to this experiment (>2 years). Coomassie-stained complex V (CV) serves as a loading control.

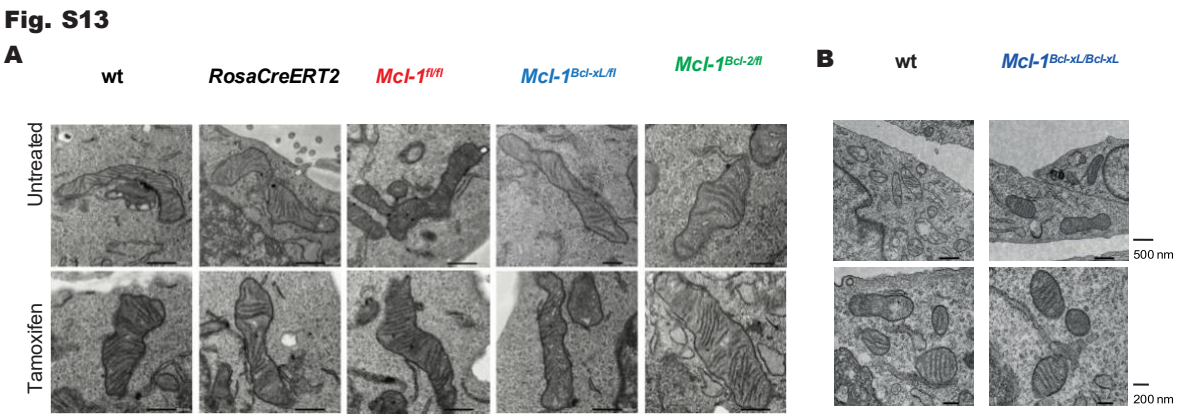

Fig S13. BCL-XL but not BCL-2 can substitute for the function of MCL-1 in mitochondrial morphology. (**A**) Representative transmission electron microscopy (TEM) images in MEFs of the indicated genotypes that were either left untreated (top panel) or had been treated with 4-Hydroxytamoxifen (TAM, 1μM) to delete the floxed *Mcl-1* allele(s) and cultured as "del" lines for >1 week (bottom panel). (**B**) Representative transmission electron microscopy (TEM) images from wild-type and *Mcl-1*$^{Bcl\text{-}xL/Bcl\text{-}xL}$ MEFs, at either 10,000x (top panel) or 20,000x magnification (bottom panel).

Fig. S14

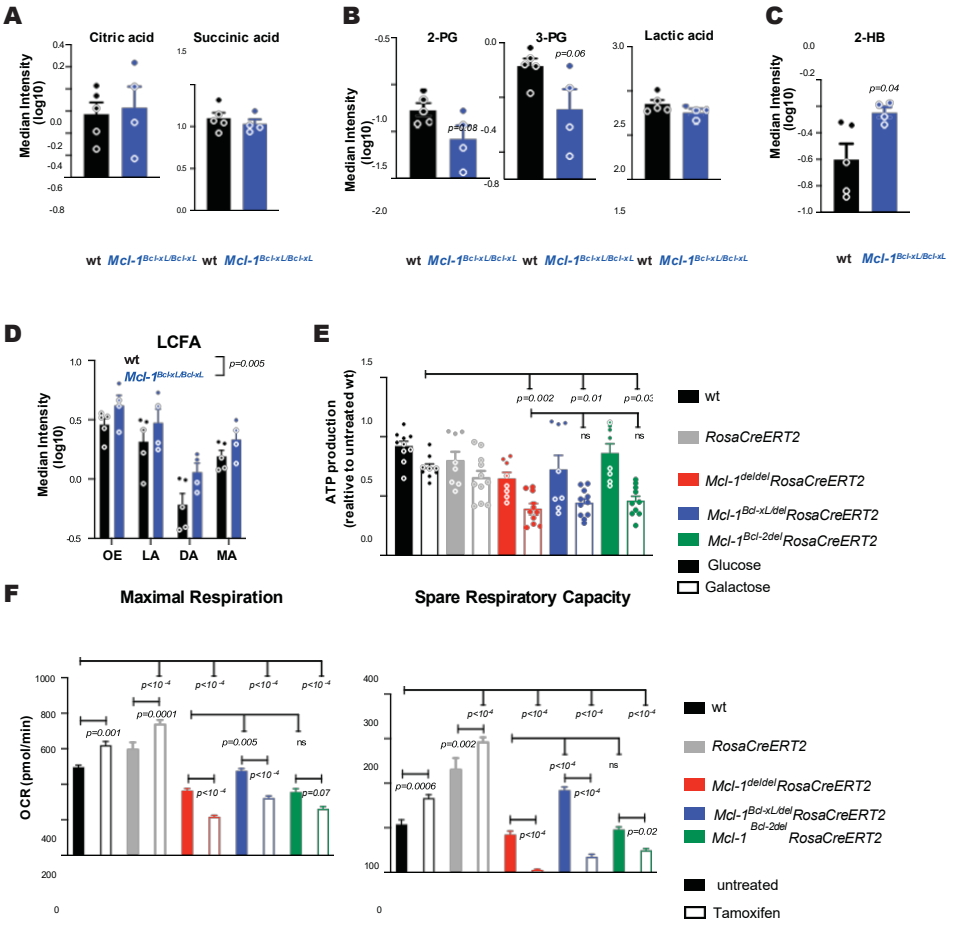

Fig S14. ***Mcl-1*$^{Bcl\text{-}xL/Bcl\text{-}xL}$ pups present with defects in FAO**. (**A-C**) Metabolomic analysis of liver extracts from wild-type (n=5) and homozygous *Mcl-1*$^{Bcl\text{-}xL/Bcl\text{-}xL}$ (n=4) pups (FVBxBALB/cxC57BL/6 mixed genetic background). Metabolite abundance of (**A**) TCA cycle intermediates citric acid and succinic acid, (**B**) glycolytic intermediates 2-phosphoglycerate (2PG), 3-phosphoglycerate (3PG) and lactic acid and (**C**) 2-hydroxybutyrate (2-HB) are presented as mean ± SEM. Two-tailed t-test; p-values shown. (**D**) Metabolite levels of oleic acid (OA), linoelic acid (LA), dodecanoic acid (DA), mysteric acid (MA). Statistical significance of variation amongst genotypes was tested using two-way ANOVA; p-values shown. (**E**) Cell titre glow ATP production analysis in MEFs of the indicated genotypes cultured for 48 h in medium containing glucose (filled bars) or galactose (hollow bars). Data shown as mean ± SEM from 3 independent experiments, performed in triplicates. Two-way ANOVA with Tukey's multiple comparison; p-values shown. (**F**) Representative Seahorse analysis in MEFs of the indicated genotypes in the absence (filled bars) or presence (hollow bars) of 4-Hydroxytamoxifen (TAM, 1µM), indicating maximal respiration (left panel) and spare capacity (right panel). Data shown as mean ± SEM from n=6 replicates. Two-way ANOVA with Tukey's multiple comparison; p-values shown.

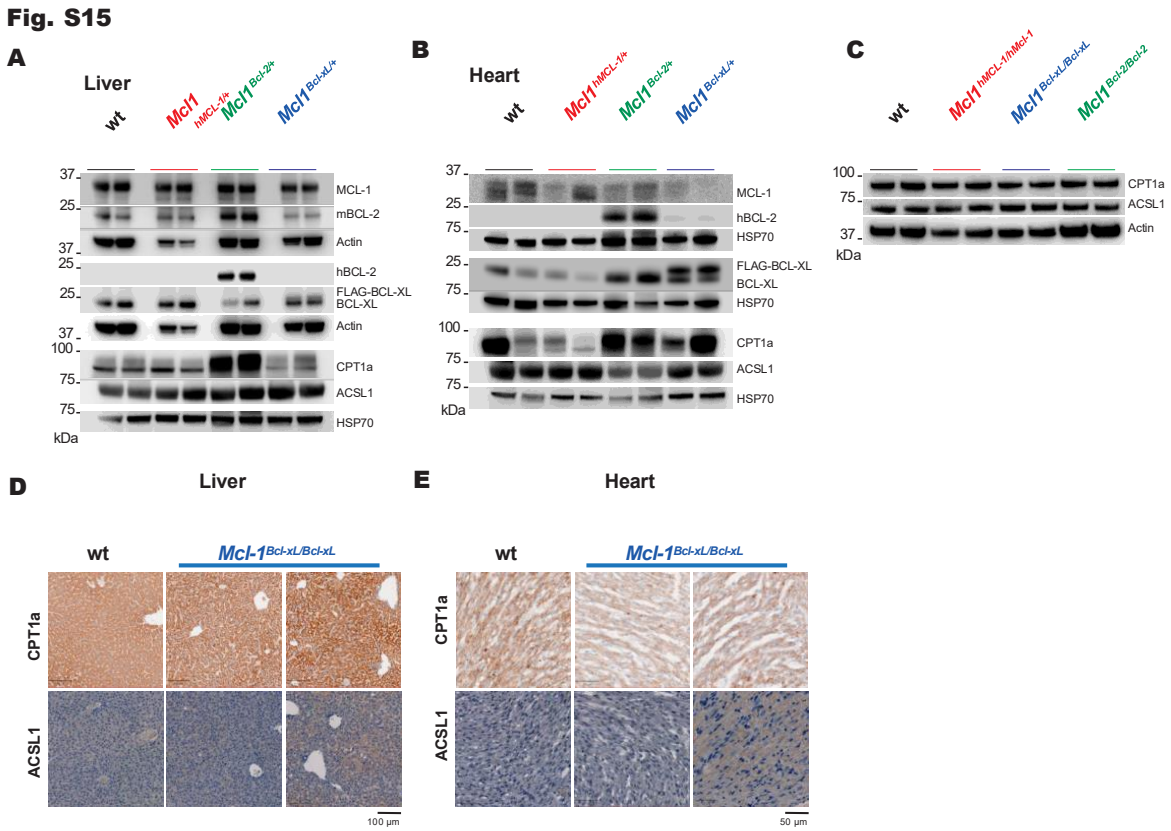

Fig. S15. (A-C) Western blot of liver **(A)** and heart **(B)** lysates from wild-type, *Mcl-1*$^{hMcl-1/+}$, *Mcl-1*$^{Bcl-2/+}$ and *Mcl-1*$^{Bcl-xL/+}$mice (C57BL/6, aged 50-70 days, n=2 per genotype, one lysate per lane) as well as (**C**) E10.5 wild-type, *Mcl-1*$^{hMcl-1/hMcl-1}$, *Mcl-1*$^{Bcl-xL/Bcl-xL}$, *Mcl-1*$^{Bcl-2/Bcl-2}$ embryos lysates (C57BL/6, n=2 per genotype, one lysate per lane) detecting the indicated proteins. Although human MCL-1 (hMCL-1) and mouse MCL-1 (mMCL-1) differ slightly in molecular weight (~2–3 kDa), mMCL-1 and hMCL-1 were not resolved in liver and heart samples. High metabolic activity and stress signaling in these tissues may promote differential phosphorylation and/or other post-translational modifications of mMCL-1 and hMCL-1, causing mMCL-1 and hMCL-1 band overlap on SDS-PAGE, unlike what we observed for lysates from embryos (Fig 1B,G). Phosphorylation pathways such as MAPK/ERK, PI3K/Akt, JNK, GSK-3β, and AMPK are highly active in both liver and heart, potentially contributing to the observed shifts in MCL-1 migration. **(D-E)** Representative histological sections stained for CPT1a (top) and ACSL1 (bottom) from wild-type (wt, left panel) and *Mcl-1*$^{Bcl-xL/Bcl-xL}$ pups (n=2, right panel) (FVBxBALB/cxC57BL/6) of the liver (**D**) and heart myocardium (**E**).

	Wild type E11.5	*Mcl-1*$^{Bcl\text{-}xL/Bcl\text{-}xL}$ E11.5	*Mcl-1*$^{Bcl\text{-}2/Bcl\text{-}2}$ E11.5	Wild type E12.5	*Mcl-1*$^{Bcl\text{-}xL/Bcl\text{-}xL}$ E12.5	*Mcl-1*$^{Bcl\text{-}2/Bcl\text{-}2}$ E12.5
Total # of assessed embryos	**37**	**13**	**26**	**36**	**17**	**18**
Normal	**34**	**4**	**6**	**36**	**16**	**6**
Small, normal	**2**	**2**	**0**	**0**	**0**	**0**
Small, abnormal	**1**	**1**	**3**	**0**	**1**	**2**
Small, dead	**0**	**1**	**14**	**0**	**0**	**7**
Exencephaly	**0**	**3**	**0**	**0**	**0**	**1**
Other cranial abnormalities	**0**	**0**	**3**	**0**	**0**	**1**
Blood accumulations	**1**	**5**	**1**	**0**	**0**	**1**

Table S1. Anomalies in homozygous embryos. Anomalies were assessed in wild-type, *Mcl-1*$^{Bcl\text{-}xL/Bcl\text{-}xL}$ and *Mcl-1*$^{Bcl\text{-}2/Bcl\text{-}2}$ and embryos at embryonic stages E11.5 and E12.5 as indicated. Total number of embryos assessed are indicated (top row). Embryos were assessed for each of the criteria independently and may have been counted positive more than 1 criteria (e.g. cranial abnormalities & blood accumulations).

: Mcl-1 del/del
y Mcl-1 Bcl-:L/del
z Mcl-1 Bcl-2/del

Downregulated metabolic genes

:yz	:y	:z	yz	:	y	z
ID: Pgap1	ID: Ac:1	ID: Eprs1	ID: Adcy9	ID: Gp:4	ID: Inpp4a	ID: Atp6v1h
ID: Cyp27a1	ID: Pcbd1	ID: Ado	ID: Pde7a	ID: Shnt2	ID: Idh1	ID: Mgat4a
ID: Npl	ID: Ddc	ID: Aldh1l2	ID: Setd7	ID: Uqcrq	ID: Gnppa	ID: Gls
ID: Man1a	ID: Afnid	ID: Gdpd1	ID: Prune1	ID: Sptlc2	ID: Pfkfb2	ID: Pign
ID: Acsl6	ID: Gnpr	ID: Acot2	ID: Pde5a	ID: Pfkp	ID: Aldh9a1	ID: Prd:6
ID: Aldoc	ID: Neu1	ID: Pck2	ID: Fktn	ID: He:b	ID: Ppo:	ID: Bpnt1
ID: Pycr1	ID: Mocs1	ID: Rrn2b	ID: Gfpt1	ID: Mpst	ID: Snpd2	ID: Snyd2
ID: Crppa	ID: Large2	ID: Cpo:	ID: Eno2	ID: Ndufa6	ID: Gant	ID: Mthfd1l
ID: Aldh6a1	ID: Gstn2	ID: Prdn9	ID: Inpp5f	ID: Arsa	ID: Ugp2	ID: Hddc2
ID: Aldh5a1	ID: Galnt12	ID: Asrgl1	ID: Lpcat2	ID: Atp5nc2	ID: Sat2	ID: Sirt1
ID: Ogdhl	ID: H6pd	ID: Psat1	ID: Xylb	ID: Atp6v0c	ID: Acadvl	ID: R:ylt1
ID: Cnbl	ID: C1galt1	ID: Rfk	ID: Rgn	ID: Ndufb10	ID: Srr	ID: Mars1
ID: St6gal1	ID: Aass	ID: Nnrk1	ID: Tnlhe	ID: Nne3	ID: Atp6v0a1	ID: Pigl
ID: B4galt4	ID: Dguok	ID: Aldh18a1		ID: Ndufa7	ID: Dnnt3a	ID: Pfas
ID: St3gal6	ID: Nagk	ID: Got1		ID: Enpp4	ID: Rdh12	ID: Pafah1b1
ID: Gbe1	ID: Setnar	ID: Chac1		ID: Co:7a2l	ID: O:sn	ID: Pigw
ID: Knt5b	ID: Mtnr14	ID: Then4		ID: Ndufa2	ID: Thtpa	ID: B4galnt2
ID: Gcnt1	ID: Anpep	ID: Phgdh		ID: B4gat1	ID: St3gal1	ID: Coasy
ID: Aldh1a1	ID: Hddc3	ID: Cept1		ID: Co:8a	ID: Oplah	ID: Aoc2
ID: Aldh1a7	ID: Me3	ID: Ahcyl1		ID: Pgan1	ID: Pfkn	ID: Odc1
ID: Gda	ID: Galnt18	ID: Pla2g12a		ID: Ndufb8	ID: Synj1	ID: Dld
ID: Pip5k1b	ID: Hsd3b7	ID: Kyat3		ID: Gsto2	ID: Hsd17b8	ID: L2hgdh
ID: Entpd1	ID: Nnnt	ID: Cth		ID: Atp5f1e	ID: Aldh3b1	ID: Gphn
ID: Pfkfb3	ID: Aldh1a2	ID: Coq3		ID: Car13	ID: Tn7sf2	ID: Ak6
ID: Ptgs1		ID: Atp6v1g1		ID: Ndufc1	ID: Papss2	ID: Mocs2
ID: Galnt3		ID: Ak4		ID: Atp5pb	ID: Plce1	ID: Gnpnat1
ID: B3galt1		ID: Car6		ID: Gstn5	ID: Scd2	ID: Gch1
ID: Sord		ID: Acot7		ID: Grhpr	ID: Plcb1	ID: Dgkh
ID: Plcb4		ID: Pi4k2b		ID: Aldh1b1	ID: Ggt7	ID: Adsl
ID: Ptgis		ID: Gpat3		ID: Nans	ID: Acss2	ID: Hagh
ID: Gyg1		ID: Psph		ID: Pgn1	ID: Uckl1	ID: Carnnt1
ID: Pld1		ID: Asns		ID: Ndufs5	ID: Selenbp1	ID: Sgns1
ID: Mccc1		ID: Akr1b7		ID: Ak2	ID: Gstn7	ID: Pank1
ID: Glt28d2		ID: Hk2		ID: Prdn16	ID: Gstn1	ID: Nt5c2
ID: Selenbp2		ID: Mthfd2		ID: Hpse	ID: Ndst4	ID: Gpan
ID: Fno5		ID: Suclg2		ID: Cds1	ID: Acadn	ID: Suv39h2
ID: Gstn4		ID: Agpat5		ID: Co:6a1	ID: Bpnt2	ID: Uap1l1
ID: Any1		ID: Alg11		ID: Atp6v1f	ID: Galt	ID: Uck1
ID: Agl		ID: Gsr		ID: Ndufb2	ID: Pigo	ID: Crls1
ID: Hadh		ID: Asah1		ID: Nt5c3	ID: Car9	ID: Pik3ca
ID: B4galt1		ID: Mri1		ID: Atp6v1e1	ID: Elovl1	ID: Plch1
ID: Alad		ID: Gpt2		ID: Ndufa3	ID: Pigv	ID: Slc33a1
ID: Hacd4		ID: Tk2		ID: Ethe1	ID: Pafah2	ID: Gnps
ID: Alg6		ID: Mtn1		ID: Pafah1b3	ID: Man1c1	ID: Flad1
ID: Pde4b				ID: Bckdha	ID: Prdn2	ID: Pip5k1a
ID: Gp:7				ID: Sirt2	ID: Dhrs3	ID: Cers2
ID: Atp6v0b				ID: Gys1	ID: Ahcyl2	ID: Dbt
ID: Hngcl				ID: Fut1	ID: Ggc:	ID: Dpyd
ID: Akr1b10				ID: Echs1	ID: Suclg1	ID: Gcln
ID: Tpk1				ID: Cbr4	ID: Itpkc	ID: Ugcg
ID: Ezh2				ID: Msno1	ID: Gpi1	ID: Ctps1
ID: Atp6v0e2				ID: Ndufa13	ID: Bcat2	ID: Trit1
ID: Hibadh				ID: Isyna1	ID: Aldh1a3	ID: Mecr
ID: Ggct				ID: Gcdh	ID: Idh2	ID: Srn
ID: Snyd1				ID: Atp6v0d1	ID: Fah	ID: Selenoi
ID: Mgll				ID: Aprt	ID: Neu3	ID: Cd38
ID: Tpi1				ID: Galns	ID: Inppl1	ID: Gnpda2
ID: Mgst1				ID: Ntpcr	ID: Rrn1	ID: Ppat
ID: Cnas				ID: Pigyl	ID: Gdpd3	ID: Gatc
ID: Cyp2s1				ID: Ndufb11	ID: Acadsb	ID: Mdh2
ID: Dhdh				ID: Pgk1	ID: Uros	ID: Tigar
ID: Man2a2					ID: Inpp5a	ID: Bcat1
ID: P4ha3					ID: Ptdss2	ID: Tnen86b
ID: Pde3b					ID: Nadsyn1	ID: Pgn2l1
ID: Hgsnat					ID: Dhcr7	ID: Uqcrc2
ID: Mtnr7					ID: Cers4	ID: Cdipt
ID: Atp6v1b2					ID: Acp5	ID: Dctd
ID: Large1					ID: St3gal4	ID: Galnt7
ID: Snpd3					ID: Hykk	ID: Dhodh
ID: Plod2					ID: Ppcdc	ID: Adpgk
ID: Nnnat3					ID: He:a	ID: Glce
ID: Renbp					ID: Gsta4	ID: Elovl4
					ID: Pccb	ID: Pik3cb
					ID: Hyal1	ID: Inpdh2
					ID: Ant	ID: Maoa
					ID: Plcd1	ID: Prps1
					ID: Entpd3	ID: Acsl4
					ID: Ocrl	

Upregulated metabolic genes

:yz	:y	:z	yz	:	y	z
ID: Chst10	ID: Inpp1	ID: Rdh10	ID: Pla2g4a	D: Pikfyve	ID: Co:5b	ID: Idh1
ID: Pik3c2b	ID: Vnn1	ID: Ugt1a7c	ID: And2	I :Atic	ID: Mgat4a	ID: Etnk2
ID: Ptgs2	ID: Chpt1	ID: Dsel	ID: Acly	I :Kdsr	ID: Ndufb3	ID: Hk1
ID: Dse	ID: Nanpt	ID: Mgat5	ID: Nnt	I :Gstt2	ID: Rpe	ID: Ugp2
ID: Mgat1	ID: Uqcrfs1	ID: Mgst3	ID: Dad1	I :Pip5k1c	ID: Sdy	ID: Mdh1
ID: St6galnac	ID: Idnk	ID: Enpp1	ID: Pnn1	I :Suo:	ID: Prd:6	ID: Dc:r
ID: Rrn2	ID: Gp:8	ID: Enpp3	ID: Pgp	I :Pgan2	ID: Mthfd1l	ID: Cbr2
ID: Cnpk2	ID: Pnp2	ID: Ggt5	ID: Ggta1	ID: Ogdh	ID: And1	ID: Ckb
ID: Rdh11	ID: B3gnt5	ID: Gstt3	ID: Agps	I :Mgat4b	ID: Aldh1l2	ID: Idi1
ID: Dglucy	ID: Mocos	ID: Gstt1	ID: Gatn	ID: Galnt10	ID: Ndufa12	ID: Hngcr
ID: Lpcat1	ID: Tcirg1	ID: P4ha2	ID: Adh7	ID: Acaca	ID: Gns	ID: Hngcs1
ID: Sdha	ID: Plaat3	ID: Mtnr4	ID: Pisd	ID: Nt5c	ID: Shnt2	ID: Nudt13
ID: Arsb	ID: Pde1a	ID: Pip4k2b	I :Aacs	ID: Tk1	ID: Ptges3	ID: E:t1
ID: Gcnt4	ID: Hdc	ID: Aoc3	II :Aadat	ID: Prps1l3	ID: Upp1	ID: Csad
ID: Plpp1	ID: Cyp51	ID: Lpin1	I :Me1	ID: Arg2	ID: Aspa	ID: Hno:2
ID: Pnp	ID: Ugdh	ID: Mgat2	I :Alg13	ID: Srd5a1	ID: Co:11	ID: Cbr3
ID: Cryl1	ID: Atp5ne	ID: Pde4d		ID: Elovl7	ID: Nne2	ID: Acat2
ID: O:ct1	ID: Co:6a1	ID: Btd		ID: E:tl3	ID: Nne1	ID: Atp6v0e
ID: Sqle	ID: Ndufa1	ID: Adcy4		ID: Gart	ID: Nt5c3b	ID: Pde9a
ID: A4galt	ID: Co:7b	ID: Atp12a		ID: Synj2	ID: Pgs1	ID: Fads2
ID: Hacd2	ID: Gla	ID: Enpp2		ID: Acsbg3	ID: Adi1	ID: Scd2
ID: Pde10a	ID: Sat1	ID: Pcyt1a		ID: Cndp2	ID: Acp1	ID: Scd1
ID: Man2a1		ID: Acat3		ID: Sephs1	ID: Dld	ID: Galnt5
ID: Xdh		ID: Cdo1		ID: Dpn2	ID: Acot2	ID: Galk2
ID: Ndst1		ID: Carns1		ID: Acp2	ID: Pcbd2	ID: Fdps
ID: Lipg		ID: Pten		ID: Sno:	ID: Dhfr	ID: Gstn6
ID: Cyp26a1		ID: St6galnac6		ID: Plcb1	ID: Aco:2	ID: Gstn1
ID: Dolk		ID: Dhrs9		ID: Gss	ID: Glud1	ID: Ppt1
ID: Ass1		ID: E:t2		ID: Pigt	ID: Gnpnat1	ID: G6pd2
ID: Ak1		ID: Sqor		ID: Gucy1b1	ID: Gn45935	ID: Ndufb2
ID: Galnt13		ID: Lpin3		ID: Bpnt2	ID: Setdb2	ID: Aldh1l1
ID: Hsd17b12		ID: Ada		ID: Car9	ID: Sucla2	ID: Ndufa3
ID: Rpn2		ID: B4galt5		ID: Pgd	ID: Esd	ID: Idh2
ID: Mecon		ID: Gucy1a1		ID: Cad	ID: Dgkh	ID: Vkorc1
ID: B3galnt1		ID: Ndst4		ID: Mthfd2l	ID: Nadk2	ID: Oat
ID: Ndst3		ID: Elovl6		ID: Setd1b	ID: Co:6c	ID: Nat2
ID: Npr2		ID: Cda		ID: Atp6v0a2	ID: Atp6v1c1	ID: Hsd11b2
ID: Cyp2j6		ID: Plod1		ID: Bpgn	ID: Cyc1	ID: Sc5d
ID: Plpp3		ID: Chpf2		ID: Co:6b2	ID: Pnn2	ID: Gsta4
ID: Hsd17b11		ID: Plb1		ID: Chsy1	ID: Prodh	ID: Co:7a2
ID: Nudt9		ID: Aco:3		ID: Acer3	ID: Unps	ID: Pccb
ID: Aldh2		ID: Cyp26b1		ID: Anpd3	ID: Co:17	ID: Glb1
ID: Plod3		ID: Cers4		ID: Xylt1	ID: Cpo:	ID: Plcd1
ID: Etnk1		ID: Csgalnact1		ID: Acsl1	ID: Atp6v0c	ID: Nsdhl
ID: Pde8a		ID: Inpp4b		ID: Galnt7	ID: Fahd1	
ID: Pik3c2a		ID: Nqo1		ID: Plcg2	ID: Enpp4	
ID: Nt5e		ID: Gucy1a2		ID: Knt2a	ID: Eno1b	
ID: Maob		ID: Cyp1a1		ID: Pafah1b2	ID: Atp5f1a	
ID: Prps2		ID: Pkn		ID: Mpi	ID: Chka	
		ID: Car12		ID: Gclc	ID: Psat1	
		ID: Gnppb		ID: ND2	ID: Gldc	
		ID: Stt3b		ID: CYTB	ID: Minpp1	
		ID: Ids		ID: Ctps2	ID: Aldh18a1	
		ID: G6pd:			ID:Elovl3	
					ID: Gsto1	
					ID:St6galnac4	
					ID: Ndufa8	
					ID:Cers6	
					ID: Itpa	
					ID: Crls1	
					ID: Ahcy	
					ID: Ak5	
					ID: Cth	
					ID: Ugcg	
					ID: Alpl	
					ID: Eno1	
					ID: Tyns	
					ID: Selenoi	
					ID: Lap3	
					ID: Coq2	
					ID: Hpse	
					ID: Gpat3	
					ID: Gatc	
					ID: Knt5a	
					ID: Galnt17	
					ID: Akr1b8	
					ID: Pde1c	
					ID: Mogs	
					ID: Bcat1	
					ID:Pla2g4c	
					ID: Co:6b1	
					ID: Hno:1	
					ID: Idh3a	
					ID: Hngcll1	
					ID: Dgkh	
					ID: C1galt1c1	
					ID: Gk	
					ID: Pgk1	
					ID: Prps1	
					ID: Hsd17b10	
					ID: Sns	

Table S2. Overlap of DE metabolic genes in MEFs

sgRNA guide sequences:

sgRNA1: *ggtgaagatctttggtggac*
sgRNA2: *atagccttgtgagtgcaata*

targeting vector sequences:

hMcl-1 to *mMcl-1*

ggttttcttccactcccgctgctcatgagaggtctctctctttctgagtttggtttggttttaatgtgtttggctattttggtttttgagacagaaactcatggtagcccaggctggcctcagagtcattatgtaatagtgacggaagatggccttggactcctgccctgctgcctaacaagcactgg
cggagtccagggataagtcaccctctctagcaccagcatttgttttttgttttgttttgttctgagagacagagactctctctgtgacttaggctagcttggatgttgaaacccgggtcttcattattctgggcttacagctatgcacactacagccatccagaacattatgacttgactacctgta
ctgcaggagactcagctattcctttgtctctagtcccctctgttgattcatcctaaccccacaattagtaatgaaactgaattagaacgtacatcatggtgctcagtgtcctgtttcccaactgctacgtgagtccaaacccatatgaggtctgtgggggcaacctggaagaaacaggaga
attaattagctcaaggctatcctcagctacacagcaagttcaagaccagccaaggctacatgtgatcctgtctctcaaagcattaaaaggggtggccagatggttcaggggtcaagctagcaggctgctcttccagagaaccccaagttcagtttccagcacctaagctagctgcctc
acaggcctctgacttccagatgcatctgcacacatgcacatcatttaaagtgatttttttaagtccatgctgaatctgcagctggtgtcctgactgtaagaatgcagccaggccgaggcaggaagatggcttccaattggggaccaacctgggcaaacctttctcttccataaagctttcct
ataggtcatcaaacacaaatgaattctgctgctcggttacaacatgtcattcatatatatatatatatatatatatatatatatatatatatatatatatatatatatgtctcccatctcagattgtggttacttgttttgggattaaaagttcctacagaaatattttagtcactacaactgcaaaatgcttctctccatactc
cctgccacatcctataaactaggattttagatcttctcctacaaaataatcatatggttccctgtctcctcttactactgtagtttaatgtttatctatttatatcaggcagtggtggtgcatgccttttaattctaatactttgggaggcagaagcaggcagatctctgtgagttcaaggccagcttggtcta
cagaacaagttccagagcagctggggctacacagagtaacccctgtctctaaaaactgaaacaaaaatgtatagatttaatgcatatgtggatgtcaggaacagtggttaggagcccgtttcttccctccagcacatgggttccagggtttggcagcaattgtctttacttgctggacc
atcatctatctccccatgtcttttgttttgagcctcccaagttctggaactgaaggtatgcagccaatttacagggttttaaaccccaaggttttatgttaggcaagcattctccaagtaagccacatttccagcttgccacttacttatctatctatctatctatctatctatctatctggtttgagacag
ggtctcaacctttaaccctggctgatgggcgcttcctatgtagaccaagtgtcttagtttgggtctctgttgctatggcaaagcaccacaaccaaaagcagcttgggagaaaagggttcattgggctagcttgcttccacattactgttcatcactgaaggacatcaggacaggaactc
aaacggggcaggaacctagaggcagaggccatgggcaggagctgctaactggcttgtttcccatggcttgctcagcctgttttcttacagaacccaggaccgccagtccatggaattccagcttgtgtcaagttgatattaagtctaacAagtccaccaaagatcttcaccgttttatat
ggtgctgggcatcaacccaggacttctacaagggtaggcaaattctctaccaactgagttactcccgtaaccatccttgttaatttgagcagcaggctcatcatgtagccaaaaatgagtttaaattgagtctctgcctcccccaggcctgggcgaccaagcaaaaagcacaagttccgtccgcg
ctataggcctagccaccataaatggctcatattttagacttttactgtttggggataggtagggagctaggctcttctggcagccagaggtcaactctggaaagtggtctcactcctcattgttaggtgggttctgtgtattgaactcaggtctttagggctgggtttcaggagcctttcacca
gttgaatctttcacaggctccacataaataacccctaatagctgtccatgaaaagtcattttggccaggcagtgtggggcacgcctttaattccagcactcgggaggcagaggcaggaggatttctgagtttgaggccagcctgatctacagagtgagttccagtgcagccagggct
acacagagaaacctgtctcgaaaaacaaaaaaacaaaaacaaaaaacaaaaaacaaaaaaacaaaaaaacggaacggaaagtcattttggaacacagggagtgagggctcacagtagaaaaatgacagagcaggactccccctaacttttaagcaaatcaatggttaatattc
ctttgtgtatgagactggagatgccctccctggtttgctcttccagggtttaactcccagcacccacctggaggcaggcacacaaccacaaatacacacaaacaaaaaagttgtttaagactggtatgttataaaaaacacagcaggtagtgcaacgagaaaggctaaggcaggact
gcctaacgttaggaccagcctgggctatgcagagttccagggcagttcgaaattcaaaaacgcacacagatcagcaggcgttcccgagcaggaacctcccgggaagccaagcactggccgggctgagagttgtaccggacaaaaagcacaatccgtccgcg
agccaaggccaggtaccgcgctccgccaaccgtagccgcggaagccgcgagagcgctccggccggaagaggcgcggagtggccgggccagccctccggaaacgcccgccccttcccctttacGGGAAGTCCTCGCCTGCGTCAGCACGGCCCT
AAGGCGGCGGCAGGGAACGGCCTTCCTCACTCCTGACTTCCGCCTGCCTCCGGTCTGGAGTCGCGGCCTTCCCCGCTCCTTCCCCTCAGCCTGCGGCGTCCGACCATGTTTGGCCTCAAA
AGAAACGCGGTAATCGGACTCAACCTCTACTGTGGGGGGGCCGGCTTGGGGGCCGGCAGCGGCGGCGCCACCCGCCCGGGAGGGCGACTTTTGGCTACGGAGAAGGAGGCCTCGGCC
CGGCGAGAGATAGGGGGAGGGGAGGCCGGCGCGGTGATTGGCGGAAGCGCCGGCGCAAGCCCCCGTCCACCCTCACGCCAGACTCCCGGAGGGTCGCGCGGCCGCCGCCCATTGG
CGCCGAGGTCCCCGACGTCACCGCGACCCCCGCGACCCCTGCTTTCTTCGCGCCCACCCGCCGCGCGGCGCCGCCTGAGGAGATGGAAGCCCCGGCGCCATCATGTCGCCC
GAAGAGGAGCTGGACGGGTACGAGCCGGAGCCTCTCGGGAAGCGGCCGGCTGTCCTGCCGCTGCTGGAGTTGGTCGGGGAATCTGGTAATAACACCAGTACGGACGGGTCACTACCCTC
GACGCCGCCGCCAGCAGAGGAGGAGGAGGACGAGTTGTACCGGCAGTCGCTGGAGATTATCTCTCGGTACCTTCGGGAGCAGGCCACCGGCGCCAAGGACACAAAGCCAATGGGCAGG
TCTGGGGCCACCAGCAGGAAGGCGCTGGAGACCTTACGACGGGTTGGGGATGGCGTGCAGCGCAACCACGAGACGGCCTTCCAAGGCATGCTTCGGAAACTGGACATCAAAAACGAAGA
CGATGTGAAATCGTTGTCTCGAGTGATGATCCATGTTTTCAGCGACGGCGTAACAAACTGGGGCAGGATTGTGACTCTCATTTCTTTTGGTGCCTTTGTGGCTAAACACTTGAAGACCATAAA
CCAAGAAAGCTGCATCGAACCATTAGCAGAAAGTATCACAGACGTTCTCGTAAGGACAAAACGGGACTGGCTAGTTAAACAAAGAGGCTGGGATGGGTTTGTGGAGTTCTTCCATGTAGAGG
ACCTAGAAGGTGGCATCAGGAATGTGCTGCTGGCTTTTGCAGGTGTTGCTGGAGTAGGAGCTGGTTTGGCATATCTAATAAGATAGCCTTGTGAGTGCAATAGtGGACTCTTAAAGCTCCAG
CCACCAAACTACATGCATCTGTGAAAACATGTGTATTTATGAAGGTGGACTTGAAGCTGCCCAGGATTTTAACAGTCCAGTTCTACTGTAGCAACATAGCAAAAAGAAAGTGGCTACAGGATT
GTGGCTAACAAGAATAAATACATGGGAAAAGTGCTCCCCCTGGAAGAGTCACTGTCTGAATGAAGCAAAGTTCCCTCTCAGCAAACACTGAGAGGCCATGGAGAAGGACTTCTAGAATGAAT
GAAAGGGGTGGATGGAAAGGTTTGATTTCCTATCTAGAGATGGAAGAGGGGCCAGTCATCAGGCTAGTCACAAAGCTCAATAAATATCCATTACTCTGCTCAGAGTGTTGAGAGAGAAGCCC
TAATTAACAACGTTGGTGACTTGTGTAAAATGGATTTGTAACCTACAAGTCACCAAACGATGACTAGAAGCTGCAGTGCTGTACAGGAATGTGAAGGTGGAGGCCTCTGAGCAGTCCAGGGTGT
GCTTGACAAAGTCCCAAGTGCTCAGGACTTTTAGCCCTGTCTACTTTGGCTTGGTTTGGATGATTCTTAAGTTTATTAGCCTAGTGATGGGCCAAAAAGTACTTGACTTAAGGTTCACTAATTAG
TTACAAAACTGAACAGCCTCGATTTTTAAGAAAATTTATGAAATGTATTTGTCTGTAAAAATTGTATATATTTTTACAGAAAGTCTATTTCTTTGAACATAAGAGGGAAGTCTTGGATTTAGTTTTT
TTCCATACCCTTTTGAAATTTGCAGCTTCTCTAGTTAGAAATGTATTTCTTACAGCTTTTTAAGACTTTGTCATCCGTTCTAGTGTATATGCAGAGCCTGTTGTGTGTGGACTGGTTATAGATT
TATAACTATGCAGGGTTAATTATCCAATCTTTTTTTTTTGTATTTAAAGATCACAGGTAGATAGATGTAAGACATTTGATCCCCTGTTGACTTACAAAATTGTAAATGGTAAAGCAGGCTAGAGTC
TTAACCATGGTGCTATTCACTGGGTTTACTTGTTTAACACAAGTTTATACCTGGTGTCAATAAAACAAATATGTATTTCTTGTCTACTAAGGATTGCCAAGCTTTGTTTTGAATTTCTGTATTGGT
CTCTAGGTGTAGCCTTTACTTCCTTTACTGTTGGCGTGTTATGCTCCCAGTTCCCCTATAGAGTCGTCTACACTTCCTCCCTGTGCTCTTCACTGGCCATTTTAGTTATCTGCATTAGAACTCTC
ACCCCAACCCCCCCAAAACTTTGAACCTAAATAACCCCTCCCCCATCCTAATCAGAGTCAGCACAGCTTTCCTGTCAGAGGATAGGAACACTTGCTCTTTGAGCCCCGTGACCGACAGTGAC
CAGGGATTGGCATTCTTGGATTGGCATGCTTTCCATTGTTACTTTGTCTATTTTGGTAAGAAAAACATCAAAGGTCCCCTTGGGAATTTCAAAGGTTGGAAATTATACGTTTATACTTTTATTAG
TTTGCTCCAAGTATGACTGTGTTCACTTAAGTTTAGAGAAACACTGGGTTTTGCTAAACTCGGTTAACAAAAGCCACTGGTAACTGAAGGTATTTAAGCTAGGGTCATTTGAAAGCTTCAGCCT
CAGAATGTGACCTTTAGTCAGGGCTGCAGATAAAAATAGGCAGGAATCAAATGACTAAGAATGTAATAGGGAAGAAGTGCCCTGCCTGCCAGCTTGGGAGTGATTTGTACCTGTGTATTTATC
CTTGATCATAGTTTGCTTATTTATGTTTAACTCTTCGGACTTCAGAGCACTTTATGTAGTTGAATAAACCCTAGAGGTTGAGGTGACTAAAAGGTTAGCCTCTCATAACCCAGCCATGGAAGTTT
TGTTTACTAGGAGCCTGACTTCCCAGCTCACAAAGGGTGAAATGAAAGCTGAAGTACAGACAGGATCTTAGTAGGTATTTTAGGTCCAGGGCCATGAAGACTTGGAGAGCGCAGTGGCTGG

mBcl2a1b to *mMcl-1*

tggcctggactcctgccctgctgcctaacaagcactggcggagtccagggataagtcacccctcctagcaccagcatttgttttgttttgttttgttctgagagacagagactctctctgtgacttaggctagctttggatgttgaaacccgggtcttcattattctgggcttacagctatgca
cactacagccatccagaacattatgacttgactacctgactgcaggagactcagctattcctttgtctctagtcccctctgttgattcatcctaaccccacaattagtaatgaaactgaattagaacgtacatcatggtgctcagtgtcctgtttcccaactgctacgtgagtccaaacccat
atgaggtctgtgggggcaacctggaagaaacaggagaattaattagctcaaggctatcctcagctacacagcaagttcaagaccagccaaggctacatgtgatcctgtctctcaaagcattaaaaggggtggccagatggttcaggggtcaagctagcaggctgctcttccagag
aacccaagttcagtttccagcacctaagctagctgcctcacaggcctctgacttccagatgcatctgcacacatgcacatcatttaaagtgatttttttaagtccatgctgaatctgcagctggtgtcctgactgtaagaatgcagccaggccgaggcaggaagatggcttccaattgggg
accaacctgggcaaacctttctcttccataaagctttcctataggtcatcaaacacaaatgaattctgctgctcggttacaacatgtcattcatatatatatatatatatatatatatatatatatatatatatatatatatatatatatatatatatgtctcccatctcagattgtggttacttgttttgggattaaaagttccttacagaaat
attttagtcactacaactgcaaaatgcttctctccatactccctgccacatcctataaactaggattttagatcttctcctacaaataatcatatggttccctgtctcctcttactactgtagtttaatgtttatctatttatatcaggcagtggtggtgcatgccttttaattctaatactttgggaggcagaa
gcaggcagatctctgtgagttcaaggccagcttggtctacagaacaagttccagagcagctggggctacacagagtaaccctgtctctaaaaactgaaacaaaaatgtatagatttaatgcatatgtggatgtcaggaacagtggttaggagccccgtttcttccctccagcacatg
ggttccagggtttggcagcaattgtctttacttgctggacatcatctatctccccatgtctttgttttgagcctcccaagttctggaactgaaggtatgcagccaatttacagggttttaaaccccaaggttttatgttaggcaagcattctccaagtaagccacatttccagcttgccacttacta
tctatctatctatctatctatctatctgttgagacagggtctcaacctttaaccctggctgatgggcgcttcctatgtagaccaagtgtcttagtttgggtctctgttgctatggcaaagcaccacaaccaaaagcagcttgggagaaaagggttcattgggctagcttgcttccacat
tactgttcatcactgaaggacatcaggacaggaactcaaacgggcaggaactctagaggcagaggccatgggcaggagctgctaactggcttgtttcccatggcttgctcagcctgttttcttacagaacccaggaccgccagtccatggaattccagcttgtgtcaagttgatattaag
agtctaacAagtccaccaaagatcttcaccgttttatatggtgctgggatcaacccaggacttctacaagggtaggcaaattctctaccaactgagttactcccgtaaccatccttttgttcatttagacagcaggctcatcatgtagccaaaaatgagttttaaattgagtctctgcctct
gcctcccaggcctgggcaagctcttctgccaattgagctatagcctagccctaaatggctcatattttagacttttactgtttggggatagggtagggagctaggctcttctggcagccagaggtcaactctggaaagtggtctcactccttcattgttaggtgggttctgtgtattga
actcaggtctttagggctgggtttcaggagcctttcaccagttgaatctttcaccagttcacaggctccacatataataccccttaatagctgtccatgaaaagtcattttggccaggcagtgtggggcacgcctttaattccagcactcgggaggcagaggcaggaggatttctgagtttgaggcca
gcctgatctacagagtgagttccagtgcagccagggctacacagagaaaccctgtctcgaaaaacaaaaaaacaaaaacaaaaaacaaaaaacaaaaaacaaaaaaacggaacggaaagtcattttggaacacagggagtgagggctcacagtagaaaaatgacagagcag
gactcccctaacttttaagcaaatcaatggttaatattcctttgtgtatgagactggagatgccctccctggtttgctcttccagggtttaactcccagcacccacctggaggcaggcacacaaccacaaatacacacaaacaaaaaagttgtttaagactggtatgttataaaaacaca
gcaggtagtgcaacgagaaaggctaaggcaggactgcctaacgttaggaccagcctgggctatgcagagttccagggcagcttgaaattcaaaaacgcacacagatcagcaggcgttcccgagcaggaaccattcccgggaagccaagcacttggccagccgggctga
gagttgtaccggacaaaaaagcacaatccgtccgcgagccaaggccaggtaccgcgctccgccaaccgtagccgcggaagccgcgagagcgctccggccggaagaggcgcggagtggccgggccagccctccggaaacgcccgccccttcccctttacGGGAAG
TCCTCGCCTGCGTCAGCACGGCCCTAAGGCGGCGGCAGGGAACGGCCTTCCTCACTCCTGACTTCCGCCTGCCTCCGGTCTGGAGTCGCGGCCTTCCCCGCTCCTTCCCCTCAGCCTGC
GGCGTCCGACCATGGACTACAAAGACGATGACGACAAGGGATCTGCTGAGTACGAGTTCATGTATATCCACTCCCTGGCTGAGCACTATCTTCAGTATGTGCTACAGGTACCCGCCTTTGAG
TCGGCTCCAAGCAAAGCATGCAGAGTGCTACAAAGAGTTGCTTCTCCGTTCAGAAGGAAGTTGAAAAGAATCTGAAGTCATACTTGGATGACTTTCACGTGGAATCCATAGATACCGCCAGA
ATAATATTCAACCAAGTGATGGAAAAAGAGTTTGAAGATGGCATCATTAACTGGGGAAGGATTGTGACTATATTTGCCTTTGGGGGTGTTCTCCTCAAAAAACTTCCGCAAGAGCAGATTGCC
CTGGATGTAGGTGCTTACAAACAAGTTTCCAGTTTTGTGGCAGAATTCATAATCAATGAACAGGAGAATGGATACGGCGGAATGGAGGTTGGGAAGATGGCTTCATAAAGAAGTTTGAACCC
AAATCTGGCTGGCTGACTTTTCTGCAGATGACAGGACAGTTCTGGGAAATGCTCTTTCTCCTCAAGTAACCTTGTGAGTGCAATAGtGGACTCTTAAAGCTCCAGCCACCAAACTACATGCATC
TGTGAAAACATGTGTATTTATGAAGGTGGACTTGAAGCTGCCCAGGATTTTAACAGTCCAGTTCTACTGTAGCAACATAGCAAAAAGAAAGTGGCTACAGGATTGTGGCTAACAAGAATAAAT
ACATGGGAAAAGTGCTCCCCCTGGAAGAGTCACTGTCTGAATGAAGCAAAGTTCCCTCTCAGCAAACACTGAGAGGCCATGGAGAAGGACTTCTAGAATGAATGAAAGGGGTGGATGGAAA
GGTTTGATTTCCTATCTAGAGATGGAAGAGGGGCCAGTCATCAGGCTAGTCACAAAGCTCAATAAATATCCATTACTCTGCTCAGAGTGTTGAGAGAGAAGCCCTAATTAACAACGTTGGTGA
CTTGTGTAAAATGGATTTGTAACCTACAAGTCACCAAACGATGACTAGAAGCTGCAGTGCTGTACAGGAATGTGAAGGTGGAGGCCTCTGAGCAGTCCAGGGTGTGCTTGACAAAGTCCCAAGT
GCTCAGGACTTTTAGCCCTGTCTACTTTGGCTTGGTTTGGATGATTCTTAAGTTTATTAGCCTAGTGATGGCCAAAAAGTACTTGACTTAAGGTTCACTAATTAGTTACAAAACTGAACAGCCTC
GATTTTTAAGAAAATTTATGAAATGTATTTGTCTGTAAAAATTGTATATATTTTTACAGAAAGTCTATTTCTTTGAACATAAGAGGGAAGTCTTGGATTTAGTTTTTTTCCATACCCTTTTGAAATTT
GCAGCTTCTCTAGTTAGAAATGTATTTCTTACAGCTTTTTAAGACTTTGTCATCCGTTCTAGTGTATATGCAGAGCCTGTTGTGTGTGGACTGGTTATAGATTTATAACTATGCAGGGTTAAT
TATCCAATCTTTTTTTTTTTGTATTTAAAGATCACAGGTAGATAGATGTAAGACATTTGATCCCCTGTTGACTTACAAAATTGTAAATGGTAAAGCAGGCTAGAGTCTTAACCATGGTGCTATTCAC
TGGGTTTACTTGTTTAACACAAGTTTATACCTGGTGTCAATAAAACAAATATGTATTTCTTGTCTACTAAGGATTGCCAAGCTTTGTTTTGAATTTCTGTATTGGTCTCTAGGTGTAGCCTTTACT
TCCTTTACTGTTGGCGTGTTATGCTCCCAGTTCCCCTATAGAGTCGTCTACACTTCCTCCCTGTGCTCTTCACTGGCCATTTTAGTTATCTGCATTAGAACTCTCACCCCAACCCCCCCAAAAC
TTTGAACCTAAATAACCCCTCCCCCATCCTAATCAGAGTCAGCACAGCTTTCCTGTCAGAGGATAGGAACACTTGCTCTTTGAGCCCCGTGACCGACAGTGACCAGGGATTGGCATTCTTGG
ATTGGCATGCTTTCCATTGTTACTTTGTCTATTTTGGTAAGAAAAACATCAAAGGTCCCCTTGGGAATTTCAAAGGTTGGAAATTATACGTTTATACTTTTATTAGTTTGCTCCAAGTATGACTGT
GTTCACTTAAGTTTAGAGAAACACTGGGTTTTGCTAAACTCGGTTAACAAAAGCCACTGGTAACTGAAGGTATTTAAGCTAGGGTCATTTGAAAGCTTCAGCCTCAGAATGTGACCTTTAGTCA

GGGCTGCAGATAAAAATAGGCAGGAATCAAATGACTAAGAATGTAATAGGGAAGAAGTGCCCTGCCTGCCAGCTTGGGAGTGATTTGTACCTGTGTATTTATCCTTGATCATAGTTTGCTTAT
TTATGTTTAACTCTTCGGACTTCAGAGCACTTTATGTAGTTGAATAAACCCTAGAGGTTGAGGTGACTAAAAGGTTAGCCTCTCATAACCCAGCCATGGAAGTTTTGTTTACTAGGAGCCTGAC
TTCCCAGCTCACAAAGGGTGAAATGAAAGCTGAAGTACAGACAGGATCTTAGTAGGTATTTTAGGTCCAGGGCCATGAAGACTTGGAGAGCGCAGTGGCTGG

hBcl-2 to *mMcl-1*

tggccttggactcctgccctgctgcctaacaagcactggcggagtccagggataagtcaccctcctagcaccagcatttgtttttgttttgttttttgtttctgagagacagagactctctctgtgacttaggctagctttggatgttgaaacccgggtcttcattattctgggcttacagctatgca
cactacagccatccagaacattatgacttgactaccgtactgcaggagactcagcattctctttgtctctagtcccctctgttgattcatcctaacccacaattagtaatgaaactgaattagaacgtacatcatggtgctcagtgtcctgtttcccaactgctacgtgagtctcaaacccat
atgaggtctgtggggcaaccttggaagaaacaggagaattaattagctcaaggctatcctcagctacacagcaagttcaagaccagccaaggctacatgtgatcctgtctctcaaagcattaaaaggggtggccagatggttcaggggtcaagctagcaggctgctcttccagag
aacccaagttcagtttccagcacctaagctagctgcctcacaggcctctgacttccagatgcatctgcacacatgcacatcatttaaagtgatttttttaagtccatgctgaatctgcagctggtgtcctgactgtaagaatgcagcaggccgaggcaggaagatggcttccaattgggg
accaacctgggcaaacctttctcttccataaagctttcctataggtcatcaaacacaaatgaattctgctgctcggttacaacatgtcattcatatatatatatatatatatatatatatatatatatatatatatatatctccatctcagattgtggttacttgttttggattaaaagttccttacagaaat
attttagtcactacaactgcaaaatgcttctctccatactccctgccacatcctataaactaggatttagatcttctcctacaaataatcatatggttccctgtctccttactactgtagtttaatgtttatctatttatatcaggcagtggtggtgcatgccttttaattctaatactgggaggcagaa
gcaggcagatctctgtgagttcaaggccagcttggtctacagaacaagttccagagcagctggggctacacagagtaaccctgtctctaaaaactgaaacaaaaatgtatagatttaatgcatatgtggatgtcaggaacagtggttaggagccccgtttctttcccttccagcacatg
ggttccagggtttggcagcaattgtctttacttgctggaccatcatctatctccccatgtctttgttttgagccctccaagttctggaactgaaggtatgcagccaatttacagggttttaaaccccaaggttttatgttaggcaagcattctccaagtaagccacatttccagcttgccacttactta
tctatctatctatctatctatctatctggtttgagacagggtctcaacctttttaaccctggctgatgggcgcttcctatgtagaccaagtgtcttagtttgggtctctgttgctatggcaaagcaccacaaccaaaagcagctgggagaaaaaggttcattgggctagcttgcttccacat
tactgttcatcactgaaggacatcaggacaggaactcaaacggggcaggaacctagaggcagaggccatgggcaggagctgctaactggcttgtttcccatggcttgctcagcctgttttcttacagaacccaggaccgccagtccatggaaattccagcttgtgtcaagttgatatta
agtctaacAagtccaccaaagatcttcaccgttttatatggtgctggggatcaacccaggacttctacaaggggtaggcaaattctctaccaactgagttactcccgtaaccatcctttgttcattttagacagcaggctcatcatgtagccaaaaatgagttttaaattgagtctcttgcctct
gcctcccaggcctgggcaagctcttctgccaattgagctatagccctagccgagcaaaggtcccgagcgctccgccaaccgtagccgcggaagcgccgcgagagcgctccggccggaagaggcgcggagtggccgggccagccctccggaaacgcccgccccttcccctttacGGGAAG
TCCTCGCCTGCGTCAGCACGGCCCTAAGGCGGCGGCAGGGAACGGCCTTCCTCACTCCTGACTTCCGCCTGCCTCCGGTCTGGAGTCGCGGCCTTCCCCGCTCCTTCCCCTCAGCCTGC
GGCGTCCGACCATGGCGCACGCTGGGAGAACAGGGTACGATAACCGGGAGATAGTGATGAAGTACATCCATTATAAGCTGTCGCAGAGGGGCTACGAGTGGGATGCGGGAGATGTGGGC
GCCGCGCCCCCGGGGGCCGCCCCCGCACCGGGCATCTTCTCCTCCCAGCCCGGGCACACGCCCCATCCAGCCGCATCCCGGGACCCGGTCGCCAGGACCTCGCCGCTGCAGACCCCG
GCTGCCCCCGGCGCCGCCGCGGGGCCTGCGCTCAGCCCGGTGCCACCTGTGGTCCACCTGACCCTCCGCCAGGCCGGCGACGACTTCTCCCGCCGCTACCGCCGCGACTTCGCCGAGA
TGTCCAGCCAGCTGCACCTGACGCCCTTCACCGCGCGGGGACGCTTTGCCACGGTGGTGGAGGAGCTCTTCAGGGACGGGGTGAACTGGGGGAGGATTGTGGCCTTCTTTGAGTTCGGT
GGGGTCATGTGTGTGGAGAGCGTCAACCGGGAGATGTCGCCCCTGGTGGACAACATCGCCCTGTGGATGACTGAGTACCTGAACCGGCACCTGCACACCTGGATCCAGGATAACGGAGG
CTGGGATGCCTTTGTGGAACTGTACGGCCCCAGCATGCGGCCTCTGTTTGATTTCTCCTGGCTGTCTCTGAAGACTCTGCTCAGTTTGGCCTGTGGGAGCCTTGCATCACCCTGGGTGCC
TATCTGGGCCACAAGTGACCTTGTGAGTGCAATAGTGGACTCTTAAAGCTCCAGCCACCAAACTACATGCATCTGTGAAAACATGTGTATTTATGAAGGTGGACTTGAAGCTGCCCAGGATTT
TAACAGTCCAGTTCTACTGTAGCAACATAGCAAAAAGAAAGTGGCTACAGGATTGTGGCTAACAAGAATAAATACATGGGAAAAGTGCTCCCCCTGGAAGAGTCACTGTCTGAATGAAGCAAA
GTTCCCCTCTCAGCAAACACTGAGAGGCCATGGAGAAGGACTTCTAGAATGAATGAAAGGGGTGGATGGAAAGGTTTGATTTCCTATCTAGAGATGGAAGAGGGGCCAGTCATCAGGCTAGT
CACAAAGCTCAATAAATATCCATTACTCTGCTCAGAGTGTTGAGAGAGAAGCCCTAATTAACAACGTTGGTGACTTGTGTAAAATGGATTTGTAACCTACAAGTCACCAAACGATGACTAGAAG
CTGCAGTGCTGTACAGGAATGTGAAGGGAGGCCTCTGAGCAGTCCAGGGTGTGCTTGACAAAGTCCCAAGTGCTCAGGACTTTTAGCCCTGTCTACTTTGGCTTGGTTTGGATTGAACTTA
GTTTATTAGCCTAGTGATGGCCAAAAAGTACTTGACTTAAGGTTCACTAATTAGTTACAAAACTGAACAGCCTCGATTTTTAAGAAAATTTATGAAATGTATTTGTCTGTAAAAATTGTATATATT
TTTACAGAAAGTCTATTTCTTTGAACATAAGAGGGAAGTCTTGGATTTAGTTTTTTTCCATACCCTTTTGAAATTTGCAGCTTCTCTAGTTAGAAATGTATTTCTTACAGCTTTTTAAGACTTTGTC
ATCCGTTCTAGTGTATATGCAGAGCCTGTTGTGTGTGGACTGGTTATAGATTTATAACTATGCAGGGTTAATTATCCAATCTTTTTTTTTTTGTATTTAAAGATCACAGGGTAGATAGATGTAAG
ACATTTGATCCCCTGTTGACTTACAAAATTGTAAATGGTAAAGCAGGCTAGAGTCTTAACCATGGTGCTATTCACTGGGTTTACTTGTTTAACACAAGTTTATACCTGGTGTCAATAAAACAAAT
ATGTATTTCTTGTCTACTAAGGATTGCCAAGCTTTGTTTTGAATTTCTGTATTGGTCTCTAGGTGTAGCCTTTACTTCCTTTACTGTTGGCGTGTTATGGCCTGTTCACCTATAGAGTCGTCT
ACACTTCCTCCCTGTGCTCTTCACTGGCCATTTTAGTTATCTGCATTAGAACTCTCACCCCAACCCCCCCAAAACTTTGAACCTAAATAACCCCTCCCCCATCCTAATCAGAGTCAGCACAGCT
TTCCTGTCAGAGGATAGGAACACTTGCTCTTTGAGCCCCGTGACCGACAGTGACCAGGGATTGGCATTCTTGGATTGGCATGCTTTCCATTGTTACTTTGTCTATTTTGGTAAGAAAAACATC
AAAGGTCCCCTTGGGAATTTCAAAGGTTGGAAATTATACGTTTATACTTTATTAGTTTGCTCCAAGTATGACTGTGTTCACTTAAGTTTAGAGAAACACTGGGTTTTGCTAAACTCGGTTAACA
AAAGCCACTGGTAACTGAAGGTATTTAAGCTAGGGTCATTTGAAAGCTTCAGCCTCAGAATGTGACCTTTAGTCAGGGCTGCAGATAAAAATAGGCAGGAATCAAATGACTAAGAATGTAATA
GGGAAGAAGTGCCCTGCCTGCCAGCTTGGGAGTGATTTGTACCTGTGTATTTATCCTTGATCATAGTTTGCTTATTTATGTTTAACTCTTCGGACTTCAGAGCACTTTATGTAGTTGAATAAACC
CCTAGAGGTTGAGGTGACTAAAAGGTTAGCCTCTCATAACCCAGCCATGGAAGTTTTGTTTACTAGGAGCCTGACTTCCCAGCTCACAAAGGGTGAAATGAAAGCTGAAGTACAGACAGGAT
CTTAGTAGGTATTTTAGGTCCAGGGCCATGAAGACTTGGAGAGCGCAGTGGCTGG

mBcl2l1 to *mMcl-1*

ggtttctttccactcccgctgctcatgagaggtctctctctttctgagtttggtttggttttaatgtgtttggctatttttgtttttgagacagaaactcatggtagcccaggctggcctcagagtcattatgtaatagtgacggaagatggccttggactcctgccctgctgcctaacaagcactgg
cggagtccagggataagtcaccctcctagcaccagcatttgtttttgtttgttttttgtttctgagagacagagactctctctgtgacttaggctagctttggatgttgaaacccgggtcttcattattctgggcttacagctatgcacactacagccatccagaacattatgacttgactaccgta
ctgcaggagactcagctattccttgtctctagtcccctctgttgattcatcctaacccacaattagtaatgaaactgaattagaacgtacatcatggtgctcagtgtcctgtttcccaactgctacgtgagtctcaaacccatatgaggtctgtggggcaacctggaagaaacaggaga
attaattagctcaaggctatcctcagctacacagcaagttcaagaccagccaaggctacatgtgatcctgtctctcaaagcattaaaaggggtggccagatggttcaggggtcaagctagcaggctgctcttccagagaacccaagttcagtttccagcacctaagctagctgcctc
acaggcctctgacttccagatgcatctgcacacatgcacatcatttaaagtgatttttttaagtccatgctgaatctgcagctggtgtcctgactgtaagaatgcagcaggccgaggcaggaagatggcttccaattggggaccaacctgggcaaacctttctcttccataaagctttcct
ataggtcatcaaacacaaatgaattctgctgctcggttacaacatgtcattcatatatatatatatatatatatatatatatatatatatatatatatatatatatctccatctcagattgtggttacttgttttgggattaaaagttccttacagaaatattttagtcactacaactgcaaaatgcttctctccatactc
cctgccacatcctataaactaggatttagatcttctcctacaaatatcatatggttccctgtctctcttactactgtagtttaatgtttatctatttatatcaggcagtggtggtgcatgccttttaattctaatactgggaggcagaagcaggcagatctctgtgagttcaaggccagcttggtcta
cagaacaagttccagagcagctggggctacacagagtaacccgtctctaaaaactgaaacaaaaatgtatagatttaatgcatatgtggatgtcaggaacagtggttaggagcccgtttctttccctccagcacatgggttccaggggtttggcagcaattgtctttacttgctggacc
atcatctatctccccatgtctttgttttgagcctcccaagttctggaactgaaggtatgcagccaatttacagggttttaaaccccaaggttttatgttaggcaagcattctccaagtaagccacatttccagcttgccacttacttatctatctatctatctatctatctatctggtttgagacag
ggtctcaacctttaaccctggctgatgggcgcttcctatgtagaccaagtgtcttagtttgggtctctgttgctatggcaaagcaccacaaccaaaagcagcttgggagaaaaggttcattgggctagcttgcttccacattactgttcatcactgaaggacatcaggacaggaactc
aaacggggcaggaacctagaggcagaggccatgggcaggagctgctaactggcttgtttcccatggcttgctcagcctgttttcttacagaacccaggaccgccagtccatggaattccagcttgtgtcaagttgatattaagtctaacAagtccaccaaagatcttcaccgttttatat
ggtgctggggatcaacccaggacttctacaaggggtaggcaaattctctaccaactgagttactcccgtaaccatcctttgttcattttagacagcaggctcatcatgtagccaaaaatgagttttaaattgagtctcttgcctctgcctccccaggcctgggcaagctcttctgccaattgag
ctataggcctagccaccataaatggctcatattttagactttgttgggagtagggtagggagctaggctcttctggcagccagaggtcaactctggaaagtggtctcactcctcattgttagggtgggttctgtgtattgaactcaggtctttagggctgggtttcaggagcctttcacca
gttgaatctttcacaggctccacataaataacccctaataagctgtccatgaaaagtcattttggccaggcagtgtggggcacgcctttaattccagcactcggggaggcagaggcaggaggatttctgagtttgaggccagcctgatctacagagtgagttccagtgcagccagggct
acacagagaaacccctgtctcgaaaaacaaaaaaacaaaaacaaaaaacaaaaaacaaaaaaccggaacggaaagtcattttggaacacaggggagtgagggctcacagtagaaaaatgacagagcaggactccccctaacttttaagcaaatcaatggttaatattc
ctttgtgtatgagactggagatgcccctcctggtttgctcttcaggggtttaactcccagcacccacctggaggcaggcacacaaccacaaatacacacaaacaaaaaagtgtttaagactggtatgttataaaaacacagcaggtagtgcaacgagaaaggctaaggcaggact
gcctaacgttaggaccagcctgggctatgcagagttccagggcagcttgaaattcaaaaacgcacacagatcagcaggcgttcccgagcaggaaccattcccgggaagccaagcacttggccagccgggctga
agccaaggccaggtaccgcgctccgccaaccgtagccgcggaagcgccgcgagagcgctccggccggaagaggcgcggagtggccgggccagccctccggaaacgcccgccccttcccctttacGGGAAGTCCTCGCCTGCGTCAGCACGCCCT
AAGGCGGCGGCAGGGAACGGCCTTCCTCACTCCTGACTTCCGCCTGCCTCCGGTCTGGAGTCGCGGCCTTCCCCGCTCCTTCCCCTCAGCCTGCGGCGTCCGACCATGGACTACAAAGAC
GATGACGACAAGGGATCTTCTCAGAGCAACCGGGAGCTGGTGGTCGACTTTCTCTCCTACAAGCTTTCCCAGAAAGGATACAGCTGGAGTCAGTTTAGTGATGTCGAAGAGAATAGGACTGA
GGCCCCAGAAGAAACTGAAGCAGAGAGGGAGACCCCCAGTGCCATCAATGGCAACCCATCCTGGCACCTGGCGGATAGCCCGGCCGTGAATGGAGCCACTGGCCACAGCAGCAGCTTTGG
ATGCGCGGGAGGTGATTCCCATGGCAGCAGTGAAGCAAGCGCTGAGAGAGGCAGGCGATGAGTTTGAACTGCGGTACCGGAGAGCGTTCAGTGATCTAACATCCCAGCTTCACATAACCC
CAGGGACCGCGTATCAGAGCTTTGAGCAGGTAGTGAATGAACCTTTCGGGATGGAGTAAACTGGGGTCGCATCGTGGCCTTTTTCTCCTTTGGCGGGGCACTGTGCGTGGAAAGCGTAGA
CAAGGAGATGCAGGTATTGGTGAGTCGGATTGCAAGTTGGATGGCCACCTATCTGAATGACCACCTAGAGCCTTGGATCCAGGAGAACGGCGGCTGGGACACTTTTGTGGATCTCTACGGG
AACAATGCAGCAGCCGAGAGCCGGAAAGGCCAGGAGCGCTTCAACCGCTGGTTCCTGACGGGCATGACTGTGGCTGGTGTGGTTCTGCTGGGCTCACTCTTCAGTCGGAAGTGACCTTGT
GAGTGCAATAGtGGACTCTTAAAGCTCCAGCCACCAAACTACATGCATCTGTGAAAACATGTGTATTTATGAAGGTGGACTTGAAGCTGCCCAGGATTTTAACAGTCCAGTTCTACTGTAGCAA
CATAGCAAAAAGAAAGTGGCTACAGGATTGTGGCTAACAAGAATAAATACATGGGAAAAGTGCTCCCCCTGGAAGAGTCACTGTCTGAATGAAGCAAAGTTCCCTCTCAGCAAACACTGAGA
GGCCATGGAGAAGGACTTCTAGAATGAATGAAAGGGGTGGATGGAAAGGTTTGATTTCCTATCTAGAGATGGAAGAGGGGCCAGTCATCAGGCTAGTCACAAAGCTCAATAAATATCCATTA
CTCTGCTCAGAGTGTTGAGAGAGAAGCCCTAATTAACAACGTTGGTGACTTGTGTAAAATGGATTTGTAACCTACAAGTCACCAAACGATGACTAGAAGCTGCAGTGCTGTACAGGAATGTGA
AGGGAGGCCTCTGAGCAGTCCAGGGTGTGCTTGACAAAGTCCCAAGTGCTCAGGACTTTTAGCCCTGTCTACTTTGGCTTGGTTTGGATGATTCTTAAGTTTATTAGCCTAGTGATGGCCAAA
AAGTACTTGACTTAAGGTTCACTAATTAGTTACAAAACTGAACAGCCTCGATTTTTAAGAAAATTTATGAAATGTATTTGTCTGTAAAAATTGTATATATTTTTACAGAAAGTCTATTTCTTTGAAC
ATAAGAGGGAAGTCTTGGATTTAGTTTTTTTCCATACCCTTTTGAAATTTGCAGCTTCTCTAGTTAGAAATGTATTTCTTACAGCTTTTTAAGACTTTGTCATCCGTTCTAGTGTATATGCAGAGC
CTGTTGTGTGTGGACTGGTTATAGATTTATAACTATGCAGGGTTAATTATCCAATCTTTTTTTTTTGTATTTAAAGATCACAGGGTAGATAGATGTAAGGACATTTGATCCCCTGTTGACTTACAA
AATTGTAAATGGTAAAGCAGGCTAGAGTCTTAACCATGGTGCTATTCACTGGGTTTACTTGTTTAACACAAGTTTATACCTGGTGTCAATAAAACAAATATGTATTTCTTGTCTACTTAAGGATTG
CCAAGCTTTGTTTTGAATTTCTGTATTGGTCTCTAGGTGTAGCCTTTACTTCCTTTACTGTTGGCGTGTTATGCTCCCAGTTCCCCTATAGAGTCGTCTACACTTCCTCCCTGTGCTCTTCACTG
GCCATTTTAGTTATCTGCATTAGAACTCTCACCCCAACCCCCCCAAAACTTTGAACCTAAATAACCCCTCCCCCATCCTAATCAGAGTCAGCACAGCTTTCCTGTCAGAGGATAGGAACACTT
GCTCTTTGAGCCCCGTGACCGACAGTGACCAGGGATTGGCATTCTTGGATTGGCATGCTTTCCATTGTTACTTTGTCTATTTTGGTAAGAAAAACATCAAAGGTCCCCTTGGGAATTTCAAAG
GTTGGAAATTATACGTTTATACTTTTATTAGTTTGCTCCAAGTATGACTGTGTTCACTTAAGTTTAGAGAAACACTGGGTTTTGCTAAACTCGGTTAACAAAGCCACTGGTAACTGAAGGTATT
TAAGCTAGGGTCATTTGAAAGCTTCAGCCTCAGAATGTGACCTTTAGTCAGGGCTGCAGATAAAAATAGGCAGGAATCAAATGACTAAGAATGTAATAGGGAAGAAGTGCCCTGCCTGCCAG
CTTGGGAGTGATTTGTACCTGTGTATTTATCCTTGATCATAGTTTGCTTATTTATGTTTAACTCTTCGGACTTCAGAGCACTTTATGTAGTTGAATAAACCCTAGAGGTTGAGGTGACTAAAAGG
TTAGCCTCTCATAACCCAGCCATGGAAGTTTTGTTTACTAGGAGCCTGACTTCCCAGCTCACAAAGGGTGAAATGAAAGCTGAAGTACAGACAGGATCTTAGTAGGTATTTTAGGTCCAGGGC
CATGAAGACTTGGAGAGCGCAGTGGCTGG

Table S3. *sgRNA* guide, targeting vector and oligonucleotide sequences used for genotyping

Primers to detect *hMcl-1* knock- in
fw CACCCTCACGCCAGACTC
rev TGCCAAACCAGCTCCTACTC
Primers to detect *FLAG-Bcl-xL* knock-in
fw GCCTTCCTCACTCCTGACTTC
rev CAGGATGGGTTGCCATTGATG
Primers to detect *hBcl-2* knock-in
fw GGATAACGGAGGCTGGGATG
rev GACAGTGACTCTTCCAGGGG
Primers to detect *FLAG-A1* knock-in
fw GAACGGCCTTCCTCACTCC
rev TCCACGTGAAAGTCATCCAAG
Primers to detect *Mcl-1* wt
fw TTTCTTTCGGTGCCTTTGTG
rev ACCTACCACCTACAACGACC
Primers to detect *RosaCre* knock-in and *Rosa26* wt
fw GCCAATGCTCTGTCTAGGGGTTGG
rev1 CTTGCTCTCCCAAAGTCGCTCTGAG
rev2 TCGTTGCATCGACCGGTAATGCAGGC

Table S4. Oligonucleotide sequences used for genotyping

Antibodies used for immunoblotting		
rabbit anti-MCL-1; mouse specific (polyclonal)	Rockland,	#600-401-394
rat anti-MCL-1 (polyclonal)	Abcam	#ab243136
hamster anti-BCL-2; mouse specific (clone 3F11)	in house	N/A
mouse anti-BCL-2; human specific (clone Bcl-2-100)	in house	N/A
rabbit anti-BCL-XL (cloneE18)	Abcam	#ab32370
mouse anti-FLAG (clone M2)	Sigma-Aldrich	#F1804
rat anti-A1; mouse specific (clone 6D6)	in house	N/A
mouse anti-beta-ACTIN (clone AC-40)	Sigma-Aldrich	#A4700
rabbit anti-PUMA (mouse, human and other species) (polyclonal)	Abcam	#ab9645
rat anti-BIM; mouse, human and several other species (clone 3C5)	in house	N/A
rabbit anti-BAX (polyclonal)	Millipore	#ABC11
rabbit anti-BAK (polyclonal)	Sigma	#ABC12
mouse anti-HSP-70 (mouse, human and several other species) **(clone N6)**	in house	N/A
mouse anti-SDHA (clone **2E3GC12FB2AE2)**	Abcam	#ab14715
mouse anti-UQCRC1 (CORE1) (clone 16D10AD9AH5)	Thermo Fisher Scientific	#459140
mouse anti-COX1 (clone COX 111)	Thermo Fisher Scientific	#35-8100
rabbit anti-NDUFA9 (polyclonal)	In house	N/A
mouse anti-ATP5A (clone 15H4C4)	Abcam	#ab14748

Antibodies used for immunohistochemistry		
rabbit anti-cleaved caspase-3 (Asp175) (polyclonal)	Cell Signaling	#9661

Antibodies used for immunofluorescence		
rat anti MCL-1-A647 (clone 19C4-15)	in house	N/A
mouse anti CD31/PCAM1-PE (clone C31.7)	Abcam	#ab215753
mouse anti-Glutamine Synthetase (clone 6GS)	BD Biosciences	#610518; RRID: AB_397880
rabbit anti-MCL-1 (clone D2W9E)	Cell Signaling	#94296
donkey anti-mouse IgG secondary antibody, AlexaFluor plus 488	ThermoFisher Scientific	#A32766
donkey anti-rabbit IgG secondary antibody, AlexaFluor plus 647	ThermoFisher Scientific	#A32795

Table S5. List of primary antibodies

Movie S1-S3.

Representative movies of wild-type **(Movie S1),** homozygous *Mcl-1*$^{Bcl\text{-}xL/Bcl\text{-}xL}$ **(Movie S2)** and homozygous *Mcl-1*$^{Bcl\text{-}2/Bcl\text{-}2}$ **(Movie S3**) E12.5 embryos (C57BL/6 background) after whole mount embryo staining and clearing (iDISCO (*67*)). The vasculature is marked by CD31/PCAM1 staining (red) and blood cells are marked in green due to their inherent autofluorescence.